PB88-113253

Experimental and Modeling Study of the Photochemical Reactivity of Heatset Printing Oils

California Univ., Riverside

Prepared for

Environmental Protection Agency
Research Triangle Park, NC

Oct 87

U.S. Department of Commerce
National Technical Information Service
NTIS

PB88-113253

EPA/600/3-87/033
October 1987

AN EXPERIMENTAL AND MODELING STUDY OF THE PHOTOCHEMICAL REACTIVITY OF HEATSET PRINTING OILS

by

William P. L. Carter

Statewide Air Pollution Research Center
University of California
Riverside, California 92521

Cooperative Agreement No. CR810214-01

Project Officer

Joseph J. Bufalini

Chemistry and Physics Division
Atmospheric Sciences Research Laboratory
Research Triangle Park, NC 27711

ATMOSPHERIC SCIENCES RESEARCH LABORATORY
OFFICE OF RESEARCH AND DEVELOPMENT
U. S. ENVIRONMENTAL PROTECTION AGENCY
RESEARCH TRIANGLE PARK, NORTH CAROLINA 27711

REPRODUCED BY
U.S. DEPARTMENT OF COMMERCE
NATIONAL TECHNICAL
INFORMATION SERVICE
SPRINGFIELD, VA. 22161

TECHNICAL REPORT DATA

(Please read Instructions on the reverse before completing)

1. REPORT NO. EPA/600/3-87/033	2.	3. RECIPIENT'S ACCESSION NO. PB88 113253/AS
4. TITLE AND SUBTITLE AN EXPERIMENTAL AND MODELING STUDY OF THE PHOTOCHEMICAL REACTIVITY OF HEATSET PRINTING OILS		5. REPORT DATE October 1987
		6. PERFORMING ORGANIZATION CODE
7. AUTHOR(S) William P. L. Carter		8. PERFORMING ORGANIZATION REPORT NO.
9. PERFORMING ORGANIZATION NAME AND ADDRESS Statewide Air Pollution Research Center University of California Riverside, California 92521		10. PROGRAM ELEMENT NO. A101/B/63/20 – 2044 (FY-87)
		11. CONTRACT/GRANT NO. CR810214-01
12. SPONSORING AGENCY NAME AND ADDRESS Atmospheric Sciences Research Laboratory-RTP, NC Office of Research and Development U.S. Environmental Protection Agency Research Triangle Park, North Carolina 27711		13. TYPE OF REPORT AND PERIOD COVERED Final
		14. SPONSORING AGENCY CODE EPA/600/09

15. SUPPLEMENTARY NOTES

NO_x

16. ABSTRACT

A series of chamber experiments and computer model simulations were carried out to assess the atmospheric ozone formation potential of the heatset printing oils Magie-47 and Magie-470 relative to that of ethane. n-Pentadecane, a representative major constituent of these oils, was also studied. The results showed that n-pentadecane and the printing oils tend to slow down the initial rate of ozone formation in NO_x-air irradiations, but they also caused higher final ozone yields in some surrogate-NO_x-air experiments. The model was used to estimate the reactivities of ethane and n-pentadecane for several idealized model scenarios representing urban air pollution episodes. The predicted atmospheric reactivities of n-pentadecane and the printing oils relative to ethane were found to be highly dependent on the conditions of the model scenario. Thus, decisions on whether regulation of emissions of printing oils is beneficial in reducing atmospheric ozone must take into account the range of conditions of the air sheds into which they are emitted.

17. KEY WORDS AND DOCUMENT ANALYSIS

a. DESCRIPTORS	b. IDENTIFIERS/OPEN ENDED TERMS	c. COSATI Field/Group

18. DISTRIBUTION STATEMENT RELEASE TO PUBLIC	19. SECURITY CLASS (This Report) UNCLASSIFIED	21. NO. OF PAGES 137
	20. SECURITY CLASS (This page) UNCLASSIFIED	22. PRICE PC A07/MF A01

EPA Form 2220-1 (9-73)

NOTICE

The information in this document has been funded by the United States Environmental Protection Agency under Cooperative Agreement No. CR810214 with the Statewide Air Pollution Research Center, University of California at Riverside. It has been subjected to the Agency's peer and administrative review, and it has been approved for publication as an EPA document. Mention of trade names or commercial products does not constitute endorsement or recommendation for use.

ABSTRACT

A series of chamber experiments and computer model simulations were carried out to assess the atmospheric ozone formation potential of the heatset printing oils Magie-47 and Magie-470 relative to that of ethane. n-Pentadecane, a representative major constituent of these oils, was also studied. The results showed that n-pentadecane and the printing oils tend to slow down the initial rate of ozone formation in NO_x-air irradiation, but they also caused higher final ozone yields in some surrogate-NO_x-air experiments. The model was used to estimate the reactivities of ethane and n-pentadecane for several idealized model scenarios representing urban air pollution episodes. The predicted atmospheric reactivities of n-pentadecane and the printing oils relative to ethane were found to be highly dependent on the conditions of the model scenario. Thus, decisions on whether regulation of emissions of printing oils is beneficial in reducing atmospheric ozone must take into account the range of conditions of the air sheds into which they are emitted.

SUMMARY

A series of environmental chamber experiments and computer model simulations have been carried out to assess the atmospheric ozone formation potential of two representative heatset printing oils, relative to that of ethane. The experiments were carried out in the SAPRC 6400-liter indoor Teflon chamber, and consisted of NO_x-air irradiations of the printing oils Magie-47 and Magie-470, the representative printing oil constituent n-pentadecane, and ethane, both by themselves and when added to a simplified urban organic surrogate mixture. The results showed that while the printing oils decreased the initial rate of ozone formation in NO_x-air irradiations due to inhibition of radical levels, they caused higher final ozone yields in some surrogate-NO_x-air experiments. Magie-47 was observed to be very similar in reactivity to pure n-pentadecane, while Magie-470 was more reactive than n-pentadecane when irradiated by itself in NO_x-air mixtures, but not significantly different from n-pentadecane or Magie-47 in the surrogate-NO_x-air irradiations.

The results of these experiments were used to test current models for the reactivities of ethane and n-pentadecane. The predictions of the ethane model fit the experimental data within the uncertainties. Although the mechanism for the photooxidation of n-pentadecane is not totally understood, a reaction mechanism was developed by extrapolating models previously adjusted to fit the reactivities of C_6-C_9 n-alkanes, and this mechanism was able to simulate most of the results of the experiments with n-pentadecane and Magie-47. A few discrepancies in the model simulations of some of those experiments were observed, but it is unclear, without carrying out further experiments, whether this reflects problems with the mechanism or experimental difficulties.

The model was then used to predict the reactivities of ethane and n-pentadecane for several idealized model scenarios representative of air pollution episodes. It was found that the predicted atmospheric reactivities of n-pentadecane (and, by implication, the printing oils) are highly dependent on the conditions of the model scenario, particularly the ROG/NO_x ratio and the composition of the surrogate used to represent base case ROG emissions. Thus, decisions on whether regulation of emissions of printing oils is beneficial in reducing atmospheric ozone must take into account the range of conditions of the airsheds into which they are emitted. However, if it is assumed that a surrogate similar to that recommended by the EPA as the default ROG composition in EKMA calculations is appropriate, then the n-pentadecane mechanism predicts that the printing oils will be approximately twice as reactive as ethane under the ROG/NO_x conditions which are the most favorable for ozone formation.

However, the uncertainties in the n-pentadecane reaction mechanism used to represent the reactions of the printing oils, and the fact that their predicted reactivities are extremely sensitive to airshed conditions, means that the predictions of this model regarding the atmospheric reactivities of the printing oils are highly uncertain. Further research concerning the details of the atmospheric reaction mechanisms of the higher alkanes, and the factors which influence predictions of atmospheric reactivities, are required before definitive conclusions can be made.

TABLE OF CONTENTS

Abstract iii
Summary iv
List of Figures vii
List of Tables viii
Acknowledgements ix

I. INTRODUCTION 1

II. EXPERIMENTAL 5

A. Environmental Chamber 5
B. Experimental Procedures and Materials 5
C. Analytical Techniques 9
1. Gas Chromatographic Analyses 9
2. Formaldehyde Analysis 13
3. Continuous Monitoring Instruments 14
4. Light Intensity Determination 16
5. Analysis of Printing Oils 18

III. EXPERIMENTAL RESULTS 19

A. Summary of Chamber Runs and Characterization Results 19
B. Results of Single Component-Tracer-NO_x-Air Irradiations 25
C. Results of the Incremental Reactivity Experiments 27

IV. MODEL CALCULATIONS 38

A. Chemical Mechanism Employed 38
1. Ethane and Base Case Surrogate Mechanism 38
2. n-Pentadecane Reaction Mechanisms 39
B. Simulations of the Chamber Experiments 43
1. Chamber Effects Model and Simulations of Characterization Runs 43
2. Results of Simulations of the Single Component Organic-NO_x-Air Irradiations 45
3. Results of Simulations of Ozone yields Observed in the Mini-Surrogate Runs 47
4. Results of Simulations of the Experimental Incremental Reactivities 48
C. Simulations of Incremental Reactivities for Idealized Airshed Scenarios 50
1. Principles and Model Scenarios Employed 50
2. Results of the Airshed Reactivity Simulations 55

V. CONCLUSIONS 63

VI. REFERENCES 67

TABLE OF CONTENTS
(continued)

APPENDIX A A-1

Preliminary Report on Computer Modeling of the Battelle Chamber Data

APPENDIX B

Computer Tape Containing Detailed Data Tabulations from the Chamber Experiments B-1

APPENDIX C

Listing of the Chemical Kinetic Model Used in the Reactivity Simulations C-1

LIST OF FIGURES

Figure Number	Title	Page
1	The SAPRC indoor Teflon chamber with associated analytical instruments	6
2	Experimental and calculated concentration-time profiles for ozone, NO, and NO_2 observed in a representative standard "mini-surrogate"-NO_x-air irradiation used in the incremental reactivity determinations	30
3	Plots of experimental and calculated incremental reactivities of ethane against amounts of ethane added in the ITC "mini-surrogate"-NO_x-air experiments	34
4	Plots of experimental and calculated incremental reactivities of n-pentadecane and the printing oils Magie-47 and Magie-470 against amounts of test substance added in the ITC "mini-surrogate"-NO_x-air experiments	35

LIST OF TABLES

Table Number	Title	Page
1	Chronological Summary of Environmental Chamber Experiments Carried out in the Printing Oil Reactivity Study	20
2	Summary of Results of the Single Component-NO_x-Air Runs Carried Out in the Printing Oil Reactivity Study	26
3	Summary of the Average Initial Reactant Concentrations Measured in the Standard "Mini-Surrogate"-NO_x-Air Experiments Used in the Incremental Reactivity Determinations	29
4	Summary of Ozone Yields Observed in the Incremental Reactivity Runs	31
5	Experimental Incremental Reactivities Derived From the t = 1-, 2-, 3- and 6-Hour Ozone Yields Observed in the Mini-Surrogate-NO_x-Air Irradiations With and Without Added Test Compounds	33
6	Summary of Chamber-Dependent Input Parameters Used in the Model Simulations of the ITC Chamber Runs Carried Out in This Study	44
7	Summary of Conditions and Input Data Employed in the Airshed Scenarios Used for Reactivity Assessments	52
8	Compositions of the Surrogate Mixtures Used to Represent Base-Case ROG Emissions	55
9	Summary of Conditions, Input Data and Values of Chamber-Dependent Parameters Employed in the Model Simulations of the ITC, Surg-4 Scenario	56
10	Calculated Daily Maximum Ozone Yields Observed for the Base-Case Simulations for the Airshed and ITC Scenarios	57
11	Calculated Incremental Reactivities for Ethane and n-Pentadecane for the Airshed and ITC Scenarios	58
12	Ratios of Calculated Incremental Reactivities for n-Pentadecane to Those for Ethane for the Airshed and ITC Scenarios	59

ACKNOWLEDGMENTS

We wish to gratefully acknowledge the following people at SAPRC for their contributions to this program and in the preparation of this report: Mr. William D. Long and Ms. Li Li N. Parker for major efforts in carrying out the environmental chamber experiments, Ms. Sara M. Aschmann for assistance in the GC analyses, Ms. Minn P. Poe and Mr. Bret M. McMillan for assistance in the data processing, Ms. Minn P. Poe for assistance in preparation of the figures used in this report, and Ms. Christy J. LaClaire for carrying out the word processing tasks involved in preparation of this report. We also wish to acknowledge the EPA Contract Officer, Dr. Joseph J. Bufalini, and Dr. Basil Dimitriades of the EPA for helpful discussions and guidance in planning this study.

I. INTRODUCTION

Web-offset printing operations can result in the emission of printing oils into the atmosphere, and these vaporized oils may undergo photochemical reactions which contribute to the formation of atmospheric ozone. Since ozone is a major air quality problem in many urban areas, the precursors to ozone formation are subject to regulatory control under State Implementation Plans. To determine whether controls of printing oil emissions need to be included in such plans, it is necessary to establish whether the presence of these oils in the atmosphere can contribute significantly to ozone formation, i.e., to establish whether these oils can be considered to be "reactive" relative to ozone formation.

To be considered to be "reactive", an organic compound or mixture must (1) be sufficiently volatile so that it can react in the gas phase, (2) react in the atmosphere sufficiently rapidly that its reactions can be of significance, and (3) react in such a manner that it contributes to ozone formation. In many cases it is obvious whether or not a compound or mixture can be considered to be reactive or unreactive. If a compound has a negligible volatility or is essentially inert in the atmosphere, it can be considered to be unreactive. If, however, relatively low concentrations of a compound cause significant ozone formation when irradiated in the presence of NO_x in environmental chambers, then it is clearly reactive. In cases when a compound or mixture is either marginally volatile, reacts in the atmosphere but does so relatively slowly, or reacts in such a way that it is not clear whether or not its reactions enhance or suppress ozone formation, then it is not immediately obvious whether to classify this compound or mixture as reactive or unreactive. In these cases, the current regulatory policy is to use the reactivity of ethane to define the borderline between reactive and unreactive organic compounds.

In order to obtain the data necessary to assess whether heatset printing oils must be considered to be reactive, the Environmental Conservation Board of the Graphic Arts Technical Foundation contracted Battelle, Columbus, Laboratories to determine the volatilities of representative printing oils and to study their photochemical reactivities in environmental chamber irradiations. The results of these Battelle studies are reported elsewhere (Battelle 1982, 1983, 1984). In summary, they determined that these oils are sufficiently volatile that "virtually all of the oil constituents are available to participate in gas phase photochemical reactions" (Battelle 1983), and thus they cannot be considered to be unreactive on the basis or volatility. However, the results of the environmental chamber experiments are more ambiguous with regard to whether they react in a manner which promotes ozone formation. Some experiments indicated that the printing oils studied are somewhat more reactive than ethane, while others indicated that they were less reactive. Therefore, these printing oils appear to be on the borderline of reactivity, and the data from the Battelle study did not, by themselves, clarify whether regulation of these oils as ozone precursors is appropriate.

A significant amount of this uncertainty arises from the problems of interpreting environmental chamber data when used to study relatively unreactive compounds. This arises because the conditions under which environmental chamber experiments are carried out are not the same as those in the ambient atmosphere, and these differences become highly significant when comparing relatively unreactive substances such as ethane and printing oils. In particular, chamber effects have a significant influence on the result of environmental chamber irradiations of less reactive mixtures (Bufalini et al. 1977), and this must be taken into account in interpreting the results of such experiments. In addition, it is rarely practical to use environmental chamber experiments to attempt to simulate the full range of reaction conditions which occur in the atmosphere, and which affect the relative reactivity of the substances being compared.

In principle, computer model simulations, where the chemical mechanism used in the model is tested by comparing its predictions against the available environmental chamber data, can be employed to predict reactivities under atmospheric conditions. In this way the computer model is used to correct for chamber effects and to make extrapolations from conditions of environmental chamber experiments to those in urban airsheds. However, in order for this procedure to be scientifically credible and thus appropriate as a basis for control decisions, it is necessary that the model employed be consistent with our current understanding of atmospheric chemistry in general, and with our knowledge of the atmospheric reactions of the major constituents of the printing oils. Heatset printing oils consist primarily of saturated alkanes with an average molecular weight of approximately 205, which corresponds to that of n-pentadecane (n-$C_{15}H_{32}$). While the high molecular weight alkanes react relatively rapidly with the hydroxyl radical (the primary mode of reaction of saturated compounds in the atmosphere), they also react in a manner which removes radicals and NO_x from the system (Carter and Atkinson 1985). This latter characteristic tends to reduce their reactivity, and may even make them ozone inhibitors under some conditions. Computer model simulations may indicate whether this occurs under atmospheric conditions, provided the mechanism is adequately characterized and tested.

In order to determine whether our current understanding of the atmospheric reactions of the constituents of these printing oils is sufficient that computer model simulations can be reliably employed for assessing their reactivity under atmospheric conditions, we carried out a preliminary computer modeling study in which we compared the results of model simulations to the results of the Battelle chamber experiments. The report on this study is reproduced in Appendix A of this report. Although the model simulations were in qualitative agreement with the chamber data, the overall performance of the model in simulating these data was not satisfactory. Thus, the model did not fit the experimental maximum ozone yields and times in the NO_x-air irradiations employing the printing oils alone unless it was assumed that other classes of highly reactive compounds were present in these oils. The model also did not correctly simulate the ozone yields observed in the ethane-NO_x-air irradiations, suggesting that the chamber effects were not correctly taken into account. This was not unexpected, since the Battelle experiments were not carried out for the purpose of model validation, and the number of experiments carried out were limited. As a result of our preliminary study, it was concluded that the chemical mechanism employed in these calculations was not sufficiently well validated for use in airshed calculations of the type needed for control strategy calculations, and that further studies, both experimental and modeling, were required.

Because of this, the EPA contracted to the Statewide Air Pollution Research Center (SAPRC) of the University of California at Riverside to carry out environmental chamber experiments to provide additional data for model testing, and to use these data as a basis for evaluating their atmospheric reactivities. The experiments were carried out in the SAPRC 6400-liter indoor Teflon chamber (ITC), which has been extensively employed previously for obtaining data for model testing purposes (e.g., Carter et al. 1984, 1985, 1986a), and which is therefore reasonably well characterized for this purpose. The experiments consisted of NO_x-air irradiations of the representative printing oils Magie-47 and Magie-470, of ethane, and of the representative printing oil constituent n-pentadecane, both by themselves (with trace amounts of propene present to test the effects of their reactions on radical levels), and when added to a standard "mini-surrogate"-NO_x-air mixture. This "mini-surrogate" consisted of four hydrocarbons (n-butane, propene, trans-2-butene, and m-xylene) designed to be a highly simplified representative of the mixture of organics emitted into polluted urban areas (Atkinson et al. 1983). The data obtained were used to evaluate the suitability of our chemical mechanisms for predicting the atmospheric reactivities of n-pentadecane and the printing oils. The results of these experiments and the model predictions of the atmospheric reactivities of ethane and n-pentadecane are discussed in this report.

Detailed tabulations of the data obtained in this study are available on a computer-readable data tape from the author of this report for the cost of duplication. (These data tabulations also include results of several acetylene-NO_x-air irradiations, which were carried out in conjunction with this study at the request of the EPA, and the discussion in the Experimental section of this report is also applicable to those runs.) These detailed data tabulations, and the format of the computer tape on which they are distributed, are described in Appendix B of this report.

II. EXPERIMENTAL

A. Environmental Chamber

The ~6400-liter SAPRC indoor Teflon chamber (shown schematically in Figure 1) was employed for all of the chamber experiments carried out in this study. The chamber consisted of a reaction bag which was constructed of 2-mil thick FEP Teflon panels heat-sealed together using a double-lap seam and externally reinforced with Mylar tape. The reaction bag was fitted inside an aluminum frame of dimensions of 8 ft x 8 ft x 4 ft. One edge was hinged to allow the bag to collapse to less than one-fifth of its maximum volume.

The light source for this indoor Teflon chamber consisted of two diametrically opposed banks of 40 Sylvania 40-W BL blacklamps backed by arrays of Alzak-coated reflectors. For all the runs reported here, the light intensity was held constant at 70% of its maximum. The light intensity corresponded to a NO_2 photolysis rate of 0.31 min^{-1}, which is approximately 60% of the theoretical value expected for a solar zenith angle of zero. The spectral distribution is reasonably representative of the solar spectrum in the actinic region, but falls off in intensity in the region above ~350 nm, relative to the solar spectrum. The intensity and spectral characteristics of this light source have been discussed by Carter et al. (1984, 1985, 1986a).

Pure air for these experiments was provided by an air purification system, which has been described in detail previously (Doyle et al. 1977). This system can produce both dry and humidified pure air, and reduced the hydrocarbon levels (as measured in the chamber) to ~800 ppb methane, <5 ppb of C_2 hydrocarbons and propane and <1 ppb of all higher hydrocarbons.

B. Experimental Procedures and Materials

Before each experiment, the chamber was flushed with purified air for at least three hours with the lights on and then for at least two hours with the lights off. For the final flush the purified air was humidified to ~50% relative humidity (RH). Prior to any reactant injections, background samples were analyzed using all of the gas chromatographic instruments to be employed during the run. NO, NO_2 and the various surrogate

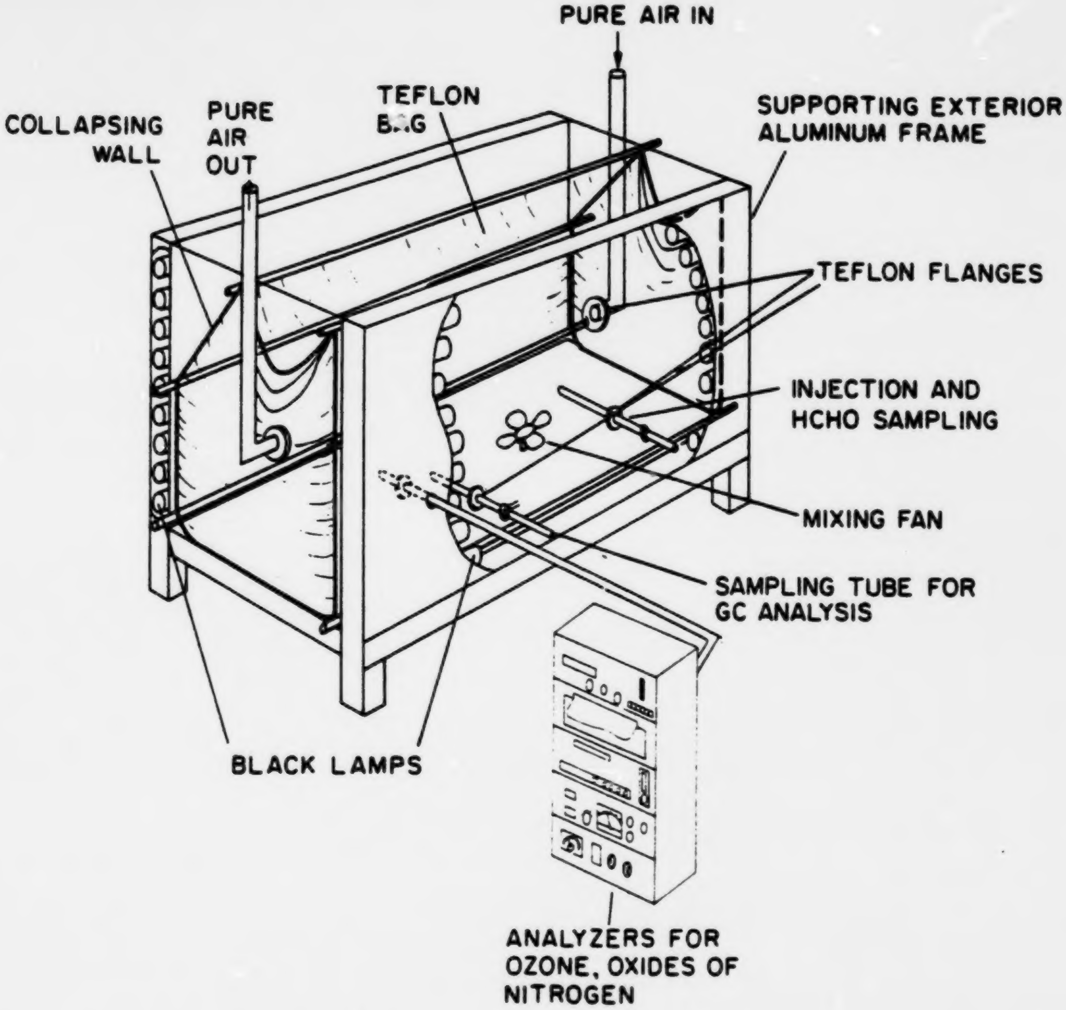
PURE AIR IN
COLLAPSING WALL
PURE AIR OUT
TEFLON BAG
SUPPORTING EXTERIOR ALUMINUM FRAME
TEFLON FLANGES
INJECTION AND HCHO SAMPLING
MIXING FAN
SAMPLING TUBE FOR GC ANALYSIS
BLACK LAMPS
ANALYZERS FOR OZONE, OXIDES OF NITROGEN

Figure 1. The SAPRC indoor Teflon chamber with associated analytical instruments.

components (n-butane, propene, trans-2-butene, and m-xylene) were then injected individually, as described below. Gas chromatographic (GC) samples were then taken on all instruments prior to the beginning of the irradiations.

Techniques used to inject the reactants depended on the type of reactant, and are as follows:

NO and NO_2. In the case of NO, the calculated volume of gaseous NO was taken from a cylinder of Matheson, C.P. grade nitric oxide with a 20-ml gas-tight, all-glass syringe (with a stainless steel tip), and diluted to 100-ml with N_2 using a separate 100-ml syringe. The NO_2 was prepared in a similar manner, except that the NO was diluted with an excess of O_2 to yield NO_2. The contents of these syringes were then injected into the chamber through the Pyrex tube running into the chamber through the injection and formaldehyde sampling port (see Figure 1), and then flushed into the chamber with N_2.

Gaseous Hydrocarbons. The gaseous hydrocarbon reactants employed in this study were ethane, propene, trans-2-butene (all CP grade), and acetylene (Matheson, 99.6% stated purity). These compounds were injected using 100 ml glass syringes and flushed into the chamber using the same general procedure as employed for NO. (In some experiments employing acetylene, the acetylene was passed through a dry ice/acetone trap to reduce the acetone impurity (see the chronological summary of runs given in the Results section, and the detailed data tabulations).

Volatile Liquid Reactants. The volatile liquid reactants used in this study consisted of acetaldehyde (Aldrich, 99% stated purity) and m-xylene (Mallinkrodt). The acetaldehyde was purified by vapor transfer before use. The desired amount of the liquid was injected, using a microsyringe, into a 5-liter Pyrex bulb equipped with stopcocks on each end and a port for the injection of the liquid. The port was then closed, and one end of the bulb was attached to the injection port of the chamber and the other to a nitrogen source. The stopcocks were then opened, and the vaporized contents of the bulb were flushed into the chamber for approximately 20 minutes.

n-Pentadecane. The n-pentadecane employed in this study (and the n-tetradecane used for GC calibration purposes) were from a "Qual Grade" sample kit from Poly Science, Co. In the first run employing n-pentadecane (run ITC-981), it was injected as described above for the volatile liquids, except that the bulb was flushed for ρ100 minutes (at 2 liter min^{-1}) while the bulb was heated with a heat gun. The estimated temperature of the bulb was 300°C. This did not result in all the n-pentadecane in the bulb being transferred into the chamber due to the low volatility of n-pentadecane. However, a sufficient amount was introduced into the chamber for a usable run to be carried out. In the subsequent experiments, the n-pentadecane was injected as described below for the printing oils.

Printing Oils. Samples of the printing oils Magie-47 and Magie-470 were obtained from Dr. Joseph J. Bufalini of EPA/ASRL. GC analyses indicated that these oils contained n-tetradecane, n-pentadecane, and a number of other compounds which were not identified (see below for the analysis technique employed). The injection technique described above for the volatile organics, and employed in the first run with the n-pentadecane, was not judged to be suitable for the printing oils because it did not result in complete volatilization of the material. (This was acceptable for n-pentadecane because it is a pure compound, but not for mixtures such as these oils, for which incomplete volatilization would result in a mixture being introduced in the chamber which was more volatile than the whole oil.) For the purpose of injecting the oil, the desired volume of the oil was placed in a small Pyrex bulb wrapped in heat tape, and the contents of the bulb, while being heated, were flushed with nitrogen at ρ0.5 liter min^{-1}. Prior to entering the chamber, but after leaving the heated area of the bulb, the output of the bulb was diluted with nitrogen at ρ2.4 liter min^{-1}, so that the flush gas entering the chamber would not be saturated with volatilized printing oil. This procedure was employed to minimize condensation of oil in the injection tube leading into the chamber, or on the chamber walls, and no visible condensation was employed. The same procedure was employed for n-pentadecane, except for run ITC-981 as discussed above.

The procedures during the irradiations were generally similar for most experiments. Data from the continous monitoring instruments (see below) were collected every 15 minutes using a computerized data acquisition system, and GC samples were taken at least hourly, and sometimes more frequently, depending on the type of experiment and compound being monitored. Irradiation time varied but most were of six-hour duration. The irradiation times, special procedures employed, and approximate initial reactant concentrations are given in the chronological listing of these runs given at the beginning of Section III. The detailed data tabulations described in Appendix B include comments giving the specific procedures employed for each run, as taken from the laboratory notebooks.

C. Analytical Techniques

In this section, the analytical procedures employed for each set of compounds and the physical parameters monitored in this program are described. In addition, the calibration techniques and estimated accuracy and precision levels are discussed. Except as indicated, the same technique and calibration procedure was employed for a given set of compounds or parameters for both the indoor and outdoor chamber experiments.

1. Gas Chromatographic Analyses

The organic reactants and products were monitored using six different gas chromatographic (GC) systems, each being suitable for a particular set of compounds. Samples for chromatographic analyses were withdrawn from the chamber using 100 ml gas-tight, all-glass syringes. The syringes were flushed at least three times with the chamber sample before the sample for analysis was taken. Depending on the gas chromatographic analysis system, the contents of the syringe were either (1) flushed through ρ2 ml stainless steel or ρ10 ml heated glass loops and subsequently transferred onto the GC column by turning a gas sample valve, (2) condensed in a trap cooled with liquid argon, and then transferred onto the column by simultaneously turning the gas sample valve and heating the loop with boiling water or ice water, or (3) flushed through a purged Tenax tube. The various gas chromatographic systems used, and the compounds they monitored, are briefly described below.

o Oxygenates such as acetaldehyde, acetone and 2-butanone, organic nitrates such as 2- and 3-pentyl nitrates and aromatic hydrocarbons such as toluene and m-xylene were monitored using the "C-600" gas chromatograph. This system consisted of a Varian 1400 GC with a flame ionization detector (FID) and a 10-ft x 0.125-in. stainless steel column packed with 10% Carbowax 600 on C-22 Firebrick (30/60 mesh). The flow through this column was set at 50 ml min^{-1} and, as was the case with all of the GC's, the carrier gas was nitrogen. The hydrogen flow was kept at 45 ml min^{-1}, and the oxygen flow used in the place of air to enhance sensitivity, was set at 250 ml min^{-1}. The detector was heated to 200°C, and the column was maintained at 75°C. Samples, of volume 100 ml, drawn from the chamber were trapped by pushing the gas sample through a 10-in. x 0.125-in. stainless steel tube packed with glass beads (80 mesh) and immersed in liquid argon. The sample was carried onto the column by then immersing the trap in boiling water and simultaneously actuating the gas sampling valve which was heated to 95°C to prevent adsorption of compounds.

- C_2-C_5 alkanes and alkenes were monitored using the "DMS" GC, which consisted of the electrometer and flame ionization detector from a Varian 1400 GC with a 34.5-ft x 0.125-in. stainless steel column packed with 10% 2,4-dimethylsulfolane on acid washed 60/80 mesh Firebrick. At the end of this column, before the detector, was a 2-ft x 0.125-in. stainless steel "soaker" column packed with 10% Carbowax 600 on Firebrick. The carrier nitrogen flow through these two columns was set at 50 ml min^{-1}, as was the hydrogen flow. The oxygen flow was 330 ml min^{-1}. The columns were maintained at 0°C and the detector was heated to 115°C. The 100-ml gas samples were trapped on a 10-in. x 0.125-in. stainless steel column packed with 10% 2,4-dimethylsulfolane on Firebrick, 60/80 mesh, immersed in liquid argon. The sample was then introduced to the column by simultaneously thawing the trap in ice water and turning the gas sampling valve.

- Methane, ethane, ethene and acetylene were monitored using the "PN" GC which consisted of a Varian 1400 GC with a flame ionization detector and a 5-ft x 0.125-in. stainless steel column packed with Porapak N, 80/100 mesh. The nitrogen carrier flow was set at 80 ml min^{-1}, the hydrogen flow at 60 ml min^{-1} and the oxygen flow at 400 ml min^{-1}. The column was maintained at 60°C, while the detector was heated to 180°C. When a sample was to be analyzed for methane, 100-ml of the sample was pushed through a 3-ml stainless steel loop. The sample in the loop was then transferred onto the column by actuating the gas sampling valve. Sampling for ethene, ethane and acetylene was accomplished by trapping the sample in a 11-in. x 0.125-in. stainless steel column packed with 10% Carbowax 400 on Firebrick, 30/60 mesh, immersed in liquid argon. The sample was thawed by immersing the trap in ice water and at the same time turning the valve so that the sample was transferred to the column.

The "PN" GC functioned erratically during the experiments carried out in this study, possibly due to a leak subsequently found in the sampling system. This was evidenced by the fact that the ethane concentrations in the experiments where it was injected were up to a factor of 2 higher than expected based on the amounts of ethane injected. For this reason, the "PN" ethane data taken during this program were subsequently judged to be invalid. For the purpose of carrying out model simulations of the runs with added ethane, the initial ethane concentrations were estimated based on the volume of ethane injected and the ratio of the measured initial concentrations of the other organic gases (i.e., propene, n-butane and trans-2-butene in the "mini-surrogate" experiments, or propene and n-butane in the tracer-NO_x-air runs) to the volumes of those gases injected. Based on the variabilities observed for the ratios of measured initial concentrations to amounts of organic gases injected into this chamber, the estimated initial ethane concentrations in these experiments are estimated to be uncertain by ~25%.

- C_{14} and C_{15} alkanes were monitored using the "SP-C-II" GC. This consisted of a Varian 1400 GC with a flame ionization detector, a 20-meter glass SuperPak II column made by Foxboro Analabs and a temperature programmer. The carrier nitrogen flow and the hydrogen flow were both set at 30 ml min^{-1}, and the oxygen flow was set at 260 ml min^{-1}. The detector was heated to 200°C, while the oven was temperature programmed from 80°C to 140°C at the rate of 8°C per minute. There were two different sampling procedures. For low concentrations, samples were drawn through a packed Tenax tube for 10 minutes with a pump at 1 liter min^{-1}, while for high concentrations (>100 ppb) a 100-ml syringe was used to draw a 100-ml sample through the Tenax tube. The Tenax tube was then attached to the nitrogen line, and the other end of the tube attached to the GC. The nitrogen flow was started, and a heating unit maintained at 250°C was attached to desorb the sample from the Tenax tube to the column. After two minutes, the oven temperature program was started.

- Peroxyacetyl nitrate (PAN) was monitored using an Aerograph gas chromatograph with electron capture detector (ECD). The detector was equipped with a standing current control, and since the response was directly influenced by the standing current, it was maintained to within 2% of a constant value during all experiments and calibrations. This GC used a 12-in. x 0.125-in. FEP Teflon column containing 5% Carbowax 400 on Chromosorb G (80/100 mesh) operating at room temperature with a nitrogen carrier flow of 75 ml min^{-1}.

Calibrations of all GC's were performed at approximately two- to three-month intervals, and, except for the gas chromatographs used to monitor PAN and the "SP C-II" GC, were carried in the same general manner. First, all gas flows were measured to verify that no changes had occurred (which would indicate previous measurements were erroneous). After measuring these flow rates, a calibration mixture was made up using one of two methods. The calibration mixture, composed of known quantities of various compounds, was then injected into the appropriate GC. The elution time and height of each peak was recorded. The height of each peak was multiplied by the attenuation and the response in millivolts was obtained.

For gaseous compounds, two calibrated ~2000-ml flasks were flushed with nitrogen for 20 minutes, and then 2 ml of each pure gas was injected into the first flask with a 5-ml syringe. This flask was allowed to mix for 20 minutes, and then 2 ml from this flask was transferred into the second flask. The contents of this second flask were allowed to mix for 20 minutes. This resulted in a concentration of ~1 ppm of the gas in the second flask. Loop calibrations were performed by connecting this second flask directly to the loop and flushing the loop with the contents of the flask. Trap calibrations were accomplished by diluting a 5-ml sample from the second flask with nitrogen in a 100-ml syringe, and passing the contents of the syringe through the trap. For a flask containing 1 ppm of the compound, this was equivalent to sampling 100-ml of gas containing 50 ppb of the compound.

Calibration of compounds that were liquid in a pure state at room temperature was carried out using an ~50-l all-glass carboy, which was first cleaned by being heated from the inside with a heat gun, then cooled using the heat gun with the heat off until the carboy reached room temperature, and finally flushed with nitrogen for one hour. The carboy was then dosed with 1 μl of each pure liquid to be calibrated using a 10-μl syringe. These were allowed to mix for one hour prior to any samples being taken. Trap and loop calibrations were both accomplished in the same way. A 1-ml sample was taken from the carboy with a 5-ml syringe and diluted with 99 ml of nitrogen. The samples were injected in the manner described previously. The exact concentration of each compound was calculated knowing the amount of liquid injected and its density.

Calibration of the compounds monitored by the "SP C-II" GC, e.g., n-tetradecane and n-pentadecane, was performed by diluting a known amount (by weight for solids and volume for liquids) of the compound in 5 ml of n-hexane. A sample of 1 microliter of this mixture was then placed in a purged Tenax tube. The samples were injected in the same procedure as described previously. The exact concentration of each compound was calculated knowing the amount of compound injected, its density and Avogadro's number.

Calibration samples of PAN were prepared in pressurized cylinders as described previously (Stephens et al. 1965), and the PAN concentration was determined from the infrared absorption of the 8.6μ) band [absorption cross-section = 13.9 x 10^{-4} ppm^{-1} (Stephens and Price 1973)]. The contents of the cylinder were diluted using a flow manifold with calibrated rotometers to yield PAN concentrations in the range 5-50 ppb, and 100-ml samples were taken directly from the flow manifold using gas-tight, all-glass syringes.

The expected accuracy and precision of concentration measurements of most of the compounds determined by the above systems were, with the exception of PAN and acetaldehyde, $\sim$5% or better. Due to varying peak widths, acetaldehyde concentrations were precise and accurate to $\sim$20%. Peroxyacetyl nitrate measurements were estimated to have $\sim$10% precision and $\sim$25% accuracy.

2. Formaldehyde Analysis

Formaldehyde was monitored using the chromatropic acid technique. Samples for analysis by this technique were obtained by drawing, at 1 liter min^{-1}, 20 liters of air from the chamber through a single bubbler containing 10 ml of doubly distilled water. The sample probe for the indoor chamber consisted of 0.5-in. Pyrex tube with the internal tip located 18 inches from the chamber wall. A metal bellows pump at the downstream end of the bubbler with a calibrated flow meter and needle valve was used to pull the sample through the bubbler. The samples were developed by adding 0.10 ml of chromatropic acid (4,5-dihydroxy-2,7-naphthalenedisulfonic acid disodium salt) to a 4.0 ml aliquot of the sample.

The solution was acidified by diluting it to 10.0 ml with concentrated sulfuric acid. The chromatropic acid solution was prepared by dissolving 0.10 g of the salt in 10.0 ml of doubly distilled water. The developed solutions had a purple color and the absorbances were measured at 580 nm by a Beckman Model 35 spectrophotometer, after initially zeroing the instrument with a prepared blank. Instrumental drift was also periodically checked during the measurements using the same blank.

Periodic calibrations of the spectrophotometer and flow meters were carried out. The spectrophotometer was calibrated by subjecting a known concentration of the developed product from the HCHO + chromatropic acid reaction to the same procedure as outlined above.

The accuracy and precision of this formaldehyde analysis technique depended upon a number of factors, including the calibration of the spectrometer and the efficiency of the bubbler in collecting formaldehyde from the air passing through it. In the past, the accuracy and precision of this technique had been quite variable, ranging from an optimum accuracy and precision of ~30%, to periods of anomalously low readings apparently due to problems with the bubbler, to periods of anomalously high and variable readings apparently due to contamination (Pitts et al. 1979). Although attempts had been made to improve the reliability of this technique for routine use, they have met with variable success.

3. Continuous Monitoring Instruments

Ozone, nitrogen oxides and temperature were monitored continuously using the instruments described below. Except as noted, samples for analysis by these systems were taken directly from a probe inserted ~18 inches into the chamber for the indoor chamber, using Teflon or Pyrex sampling lines.

- Ozone was monitored using a Dasibi Model 1003AH UV absorption ozone monitor, and for some experiments a Monitor Labs Model 8410 chemiluminescent ozone monitor was also employed. Although the two monitors gave comparable results, for maximum consistency the data used in the Results section of this report were taken from the Dasibi instrument. Calibrations were carried out every two months against a Dasibi Model 1003AH ozone monitor transfer standard which in turn was routinely calibrated by the California Air Resources Board. The ozone source was a Monitor Labs Calibrator Model 8500, with four different ozone concentrations, and the dilution gas was Liquid Carbonic Company Medical Air. The analyzer being calibrated was first zeroed using Medical Air, then the calibrator was turned on to produce the highest concentration of ozone, ρ0.3 ppm. Both analyzers were allowed to equilibrate before any readings were recorded. The ozone concentration was then reduced, and the output from both instruments was observed to verify that the response was linear, this being repeated at two lower ozone concentrations. If the response was not linear, then corrective action was taken. Finally, the analyzer being calibrated was again zeroed with Medical Air. The precision and accuracy were both better than 5%.

- Nitric oxide and total oxides of nitrogen (NO_x + organic nitrates) were monitored by a Columbia Scientific Instruments Series 1600 or by a Teco Model 14-B chemiluminescence oxides of nitrogen analyzer. The Columbia instrument was used for all runs in this study except for ITC-1005 and those following, and the Teco instrument was employed for all runs after ITC-998. It was discovered after most of the "mini-surrogate" runs were carried out that the Columbia Scientific Instruments analyzer had a serious zero drift problem, which resulted in a continual increase in the NO readings throughout the experiment. For this reason, the NO and total NO_x data taken during the runs with this instrument had no validity except for determining the initial concentrations. Because the instrument was zeroed at the start of every run, the Columbia data were considered to be valid in determining the initial NO concentrations. For runs ITC-999 and those following, only the data from the Teco instrument were used in the data analysis (though the detailed data tabulations described in Appendix B includes data from both instruments in runs where both were employed). The lack of valid NO data except for the initial concentrations for most of the "mini-surrogate" runs required a modification of the data analysis technique employed (see Discussion section).

Calibrations, using a Monitor Labs, Inc. Model 8500 calibrator as the dilution system, and a National Bureau of Standards cylinder of 97.4 ppm of NO in nitrogen, were performed bimonthly. The dilution gas was Liquid Carbonic Company Medical Air. The analyzer was first zeroed using Medical Air, then calibrated for NO by diluting the NO NBS mixture with Medical Air and measuring the flow of each gas with a bubble flowmeter.

The analyzer was allowed to equilibrate at each concentration for 30 minutes. The first concentration used was ρ0.30 ppm. The potentiometers in the analyzer were adjusted, if necessary, to match the NO output of the analyzer with the actual concentration. Two lower concentrations of NO were used to verify linearity of the analyzer. The converter efficiency was checked by setting up a NO concentration of about 0.30 ppm, and then reacting this with a lesser concentration of ozone. If the converter was operating properly, the NO_2 would equal the difference in NO. The linearity of the converter was verified by using three different concentrations of ozone. After this procedure was completed, the analyzer was re-zeroed with Medical Air. The accuracy and precision of this instrument in the absence of interfering nitrates (see below) was estimated to be comparable to those for the ozone monitors, i.e., better than 5%.

The analysis of NO_2 and NO_x is complicated by the fact that for such instruments the converters have been shown (Winer et al. 1974) to convert PAN, organic nitrates and HNO_3 to NO, and thus such species yield a positive interference in the NO_2 analysis cycle. (The NO data are unaffected.) Conversion of PAN and organic nitrates has been shown to be essentially quantitative (Winer et al. 1974) for the molybdenum converter employed in the Teco analyzer, but this has not been shown to be the case for the converter employed in the Columbia Scientific Industries instrument, and preliminary data from our laboratories have indicated that the conversion of PAN is not quantitative. No correction for this interference on the NO_2 data was attempted. However, the NO_2 readings could still be used to determine the initial NO_2 concentrations, since such interfering nitrogen-contaning species were not present initially.

- Temperature was monitored with an Analogic Model AN 2572 Digital thermocouple indicator using iron-constantan thermocouples. The thermocouple was installed in a probe inserted into the center of the chamber. This instrument was calibrated periodically using ice water as the source for 0°C and boiling water as the source for 100°C. The accuracy was better than 5%, and the precision was better than 1%.

4. Light Intensity Determination

The light intensity was measured periodically in separate experiments using the quartz tube NO_2 actinometry technique of Zafonte et al. (1977). Although only a single actinometry run was carried out in this study, the NO_2 photolysis rate obtained (0.31 min^{-1}) was in excellent agreement with the results of two previous determinations (0.316 and 0.309 min^{-1} for runs ITC-950 and ITC- 959, respectively). In general, except when the lights are new, the light intensity in this chamber does not change significantly with time (e.g., see Carter et al. 1985).

In this technique, the reactor cell consisted of a 100-cm segment of 25-mm (nominal) quartz tubing with 0.25-in. o.d. extensions at each end. The inside diameter of this tube was measured at both ends using calipers and had an average value of 21.44 mm.

The nitrogen dioxide for the indoor chamber was obtained from a Scott-Marrin, Inc. tank mixture of 1.5 ppm NO_2 in nitrogen, and was not diluted further. The NO_2 flow entered the reactor cell via 0.25-in. blackened FEP Teflon tubing, attached with a 0.25-in. stainless steel Cajon ultra-torr union. The exhaust from the cell was connected to the sampling line of the NO_x analyzer, and the excess was vented to the atmosphere via a "T". These sample lines were also blackened FEP Teflon tubing, of diameter 0.125-in. for the outdoor chamber and 0.25-in. for the indoor chamber.

Under typical conditions, the gas flow was set to 37 ml s^{-1}. With an exposed cell volume of 262 ml, a NO_2 residence time of 9.1 sec was established within the cell. This allowed a sufficient production of NO which could then be accurately measured.

NO and NO_2 were measured using a Teco Model 14-B chemiluminescence NO-NO_x monitor. NO and NO_2 were alternately measured on a 30-sec cycle. The maximum sensitivity for both gases was 5 ppb. During photolysis, NO concentrations generally ranged from 100-150 ppb. Nitrogen dioxide was measured by the NO_x mode of the instrument by subtracting the observed NO concentrations. Caution was exercised to ensure efficient operation of the reduction catalyst. The NO_x analyzer was calibrated bimonthly using the same procedure as for the NO_x analyzer described above for the chamber.

The precision of the NO_2 actinometry measurements was generally ~5-10%. This technique, as used, was inherently less precise and less capable of following rapid changes in light intensity than was the UV radiometric measurement technique. The accuracy of the NO_2 actinometry measurements were determined by a number of factors, including the accuracy of the NO_x analyzer, the extent to which plug flow conditions in the tube had been established, and whether the tube was placed in a location in which the light intensity and spectral distribution accurately reflected that in the chamber.

5. Analysis of Printing Oils

Although a comprehensive analysis of the composition of the printing oils Magie-47 and Magie-470 was not within the scope of this contract, some compositional analysis of these oils was necessary to quantify the amounts of oil injected into the chamber during the experimental runs. As indicated above, n-tetradecane and n-pentadecane were identified as constituents of both of these oils, and quantitative analyses of these two compounds were used for this purpose. These compounds were monitored using the "SP C-II" GC as indicated above. "Calibration" of the printing oils was carried out in the same manner as described above for the pure compounds monitored on that GC. A known volume of each oil was dissolved in n-hexane and injected onto the column via the Tenax tube, and the resulting peaks for n-tetradecane and n-pentadecane were measured. This yielded weight percents of n-tetradecane and n-pentadecane, respectively, of 9.0 and 10.8% for Magie-47 and 8.1 and 8.0% for Magie-470. The totals of the weight percents for these two compounds for each oil were then used to determine the amount of printing oil injected in the chamber runs from the analyzed gas phase concentrations of n-tetradecane and n-pentadecane, based on the assumption that these do not change when the oil is injected into the chamber. The total oil concentrations derived from the concentrations of n-tetradecane or of n-pentadecane alone agreed with those derived from the total of the two to within ±10%, indicating that this assumption is probably appropriate. (However, the estimated "ppmC" of oil for these runs used in the reactivity analysis discussed in the Results section must be considered to be somewhat more uncertain than the corresponding values for the pure compounds.)

III. EXPERIMENTAL RESULTS

A. Summary of Chamber Runs and Characterization Results

A total of 33 environmental chamber irradiations were carried out in this study, 10 runs for chamber characterization and conditioning purposes; eight runs in which ethane, n-pentadecane, or a printing oil was added to a standard "mini-surrogate"-NO_x mixture; eight control runs in which the standard "mini-surrogate"-NO_x mixture was irradiated with no test compound added; four runs in which ethane, n-pentadecane or a printing oil was irradiated in a radical tracer-NO_x-air mixture; and three acetylene-NO_x-air runs. (The acetylene runs are included at the request of the EPA; however, a discussion of the results, not pertinent to the experimental techniques employed, is not pertinent to the scope of this report.) Detailed tabulations of the data from all these runs are available in computer readable format, as discussed in Appendix B in this report. A chronological listing of the chamber runs, giving the major results of the characterization experiments, is given in Table 1.

It can be seen from Table 1 that several different types of runs were carried out for characterization and conditioning purposes. The purpose of these runs, and the results obtained as they apply to the interpretation and modeling efforts in this study, are briefly summarized below. More detailed discussions of the types of characterization runs carried out at SAPRC, and data interpretations are available elsewhere (Carter et al. 1984, 1985, 1986a). In general, the results of the characterization runs carried out in this study were consistent with results of previous such experiments carried out in this chamber.

- Propene-NO_x-Air Irradiations. These irradiations were carried out to both condition and evaluate the performance of the chamber. These runs were performed (1) immediately after a new reaction bag was installed at the start of this study, (2) in the middle of this study, after a series of runs were carried out in this chamber for another program and (3) after all the runs employing the printing oils have been carried out. Initial NO_x and propene were typically 0.5 ppm each, and the irradiations were carried out for six hours. Run results (see Table 1) were as expected.

Table 1. Chronological Summary of Environmental Chamber Experiments Carried Out in the Printing Oil Reactivity Study

ITC Run No.	Run Type	Comments and Results
		New reaction bag installed
975	Propene-NO_x	Conditioning run. Initial propene = 0.42 ppm, NO_x = 0.47 ppm. 0.42 ppm O_3 formed in 6 hours.
976	Tracer-NO_x	Characterization run. Initial NO_x = 0.10 ppm. Radical input rate = 0.08 ppb min^{-1}. NO oxidation rate = 0.04 ppb min^{-1}.
977	Mini-Surrogate	Standard control run for incremental reactivity determination. Results in Table 4.
978	Mini-Surrogate	Replicate standard run. Results in Table 4.
979	Mini-Surrogate + Ethane	7.45 ppm ethene added to standard surrogate run. Results in Table 4. Initial ethane estimated based on amount injected.
980	Mini-Surrogate	Replicate standard run. Results in Table 4. Ozone data obtained not consistent with results of the other standard mini-surrogate runs, and the results were not used in calculating the average ozone yields for the standard experiments.
981	Mini-Surrogate + n-C15	0.2 ppm n-pentadecane added to standard surrogate run. Results in Table 4.
982	Mini-Surrogate	Replicate standard run. Results in Table 4. Ozone yields in good agreement with other standard runs except for ITC-980 and 991.
983	Mini-Surrogate + Magie-47	Estimated 1.5 ppmC Magie-47 added to standard surrogate run. Results in Table 4.
984	Mini-Surrogate + Magie-470	Estimated 1.6 ppmC Magie-470 added to standard surrogate run. Results in Table 4.
985	Mini-Surrogate	Replicate standard run. Results in Table 4. Ozone yields in good agreement with other standard runs except for ITC-980 and 991.

(continued)

Table 1 (continued) - 2

ITC Run No.	Run Type	Comments and Results
986-989		(Runs carried out for another program. Experiments involved injections of biphenyl or naphthalene, methyl nitrite or N_2O_5 and NO_x into the chamber.)
990	Propene-NO_x	Conditioning run. Initial NO_x = 0.44 ppm, propene = 0.34 ppm. 0.44 ppm O_3 formed in 6 hours.
991	Mini-Surrogate	Replicate standard run. Results in Table 4. Ozone yields were consistently higher than the results of the other standard runs, and were not used in calculating the average standard ozone yields.
992	Mini-Surrogate + Ethane	14.9 ppm ethane added to standard surrogate run. Results in Table 4. Amount of ethane added estimated based in amount injected.
993	Mini-Surrogate + n-C15	0.3 ppm n-pentadecane added to standard surrogate run. Results in Table 4.
994	Mini-Surrogate	Replicate standard run. Results in Table 4. Ozone yields in good agreement with other standard runs except for ITC-980 and 991.
995	Mini-Surrogate + Magie-47	Estimated 6 ppmC Magie-47 added to standard surrogate run. Results in Table 4.
996	Mini-Surrogate + Magie-470	Estimated 6 ppmC Magie-470 added to standard surrogate run. Results in Table 4.
997	Mini-Surrogate	Replicate standard run. Results in Table 4. Ozone yields in good agreement with other standard runs except for ITC-980 and 991.
998	NO_2 Actinometry	k_1 = 0.310 min^{-1}, in good agreement with previous determinations.
999a	Tracer-NO_x	Characterization run. Initial NO_x = 0.08 ppm. Radical input rate = 0.07 ppb min^{-1}. NO oxidation rate = 0.03 ppb min^{-1}.

(continued)

Table 1 (continued) - 3

ITC Run No.	Run Type	Comments and Results
999b	Tracer-NO_x + Ethane	17.8 ppm ethane added at t = 2 hours in run ITC-999. 0.23 ppm O_3 formed in 4 hours. Results summarized in Table 2. Initial ethane estimated based on amount injected.
1000a	Tracer-NO_x	Characterization run. Initial NO_x = 0.10 ppm. Radical input rate = 0.07 ppb min^{-1}. NO oxidation rate = 0.14 ppb min^{-1}.
1000b	Tracer-NO_x + Acetylene	(This run was carried out on request of the EPA for another purpose. The results are included in the data tabulation, but are not discussed in this report.) 11.9 ppm acetylene added at t = 2 hours of run ITC-1000. 0.50 ppm O_3 formed in 4 hours.
1001	n-C15-NO_x	Initial NO_x = 0.13 ppm, n-C15 = 0.162 ppm. Essentially no ozone formed. Results are summarized in Table 2.
1002	Magie-47-NO_x	Initial NO_x = 0.11 ppm, estimated initial hydrocarbon = 3 ppmC. Essentially no ozone formed. Results are summarized in Table 2.
1003	Magie-470-NO_x	Initial NO_x = 0.11 ppm, estimated initial hydrocarbon = 3.3 ppmC. 0.08 ppm ozone formed. Results are summarized in Table 2.
1004	Tracer-NO_x	Characterization run. Initial NO_x = 0.10 ppm. Radical input rate = 0.06 ppb min^{-1}. NO oxidation rate = 0.12 ppb min^{-1}. Results summarized in Table 2.
1005	Propene-NO_x	Conditioning run. Initial NO_x = 0.5 ppm, propene = 0.56 ppm. 0.83 ppm ozone formed in 6 hours.
1006	Acetylene-NO_x	(This run was carried out on request of the EPA for another purpose. The results are included in the data tabulation, but are not discussed in this report.) Initial NO_x = 0.27 ppm, acetylene = 57.2 ppm, acetone (impurity) = 0.43 ppm. Maximum O_3 = 0.95 ppm at 2.5 hours.

(continued)

Table 1 (continued) - 4

ITC Run No.	Run Type	Comments and Results
1007	Acetylene-NO_x	(This run was carried out on request of the EPA for another purpose. The results are included in the data tabulation, but are not discussed in this report.) Acetylene was passed through dry ice trap to reduce the acetone impurity. Initial NO_x = 0.25 ppm, acetylene = 60 ppm, acetone = 0.05 ppm. Maximum O_3 = 0.87 ppm at 2.5 hours.
1008	Pure Air Irrad.	Characterization run. 0.087 ppm O_3 formed in 6.5 hours. Ozone yield in good agreement with prediction using chamber characterization model.
1009	Acetaldehyde-Air	Characterization run. 0.078 ppm O_3, and 8 ppb PAN formed in 6 hours. Ozone yield in good agreement with prediction using chamber characterization model.

- Tracer-NO_x-Air Irradiations. These were carried out for the purpose of characterizing the chamber radical source and excess NO oxidation caused by the presence of reactive organic contaminants. The purpose of these runs, and the details of how the results are analyzed are discussed elsewhere (Carter et al. 1982), and are not detailed here, except to note that they provide chamber characterization data needed for model simulations of the chamber experiments. These runs consisted of two-hour irradiations of 10 ppb each of propene and n-butane (whose relative rates of decay yield an estimate of the OH radical concentration, which reflects the magnitude of the chamber radical source), in NO_x-air mixtures. The initial NO_x levels were the same as those used in associated experimental runs, which was usually ~0.1 ppm. In some experiments, a test compound (e.g., ethane) was injected after two hours of the irradiation in order to obtain a direct indication of the effect of adding the compound to NO_x-air irradiations. In this case, the part of the irradiation following the addition of the test compound is classified as a test compound-NO_x-air run, whose results are discussed in the following section.

The chamber radical input rates and NO oxidation rates derived from the data from the tracer-NO_x-air runs are given in Table 1. The radical input rates varied from 0.06 to 0.08 ppb min^{-1} and the NO oxidation rates varied from 0.03 to 0.14 ppb min^{-1}. These results are typical for this chamber (Carter et al. 1986b), with the observed variability reflecting the inherent variabilities of the magnitude of the chamber radical source and levels of background reactive organics. The average radical input rates for these runs is 0.069 ± 0.007 ppb min^{-1}, which corresponds to a k_{RS} (radical input rate divided by the NO_2 photolysis rate [Carter et al. 1986b]) value of approximately 0.2. This was used in the model simulations of these runs (see Section IV).

- An Acetaldehyde-Air Irradiation (run ITC-1009) was carried out at the conclusion of this study for the purpose of measuring the rate of NO_x offgassing which occurs during chamber experiments, which also must be specified in model simulations of the chamber experiments. This experiment consisted of a six-hour irradiation of ~0.5 ppm acetaldehyde in air, and the formation of PAN and ozone which resulted was a direct indication of the rate of NO_x input into the chamber, presumably from NO_x offgassing from the walls. As shown on Table 1, the 6-hour ozone and PAN yields observed in this experiment were 78 and 8 ppb, respectively, in reasonable agreement with model predictions assuming the default NO_x offgassing rate established for this chamber for Carter et al. (1986b) (see Section IV).

- A single NO_2 Actinometry experiment (run ITC-998) was carried out around the middle of this study in order to verify that there were no changes in the light intensity from the normal value in this chamber. The yielded a NO_2 photolysis rate of 0.310 min^{-1}, in good agreement with results of previous determinations.

- A Pure Air Irradiation (run ITC-1008) was carried out around the end of this study to determine the ozone formation rate in the chamber in irradiations with the absence of added reactants. The 87 ppb of ozone formed in six hours was in good agreement with model predictions using the default NO_x offgassing rates and default background reactive organic levels (see Section IV).

B. Results of Single Component-Tracer-NO_x-Air Irradiations

One run each was carried out in which ethane, n-pentadecane, Magie-47 or Magie-470 was irradiated in NO_x-air mixtures with propene and n-butane tracers (~10 ppb each) being added to monitor radical levels. The purpose of these runs was primarily to provide data for model testing purposes and not to assess the atmospheric reactivities of these compounds directly, since the reactants present in these irradiations clearly cannot be considered to be representative of those in the atmosphere. These runs provide the data needed to test the model under a wider range of conditions than would otherwise be the case. Also model simulations of these experiments are affected by the least number of uncertainties.

A summary of the initial concentrations and results of these single component runs carried out is given in Table 2. (This table also contains the results of the model simulations discussed in Section IV.) Only in the case of ethane did any significant ozone formation occur; however that run had 14-20 times more initial ppmC of organic reactant than did the n-pentadecane or the printing oil runs. Indeed, if the reactivity of the test organic in these runs is measured by sum of the amount of ozone formed and the amount of NO oxidized per hour, divided by the amount of test compound added, i.e., by $[\Delta([O_3]-[NO])/\Delta t]/\Delta RHC$, then on a per carbon basis n-pentadecane and Magie-47 are more reactive than ethane by a factor of ~3, and Magie-470 is more reactive than ethane by a factor of 4.7, under the conditions of these experiments. As discussed elsewhere (Carter and Atkinson 1987a, 1987b), $\Delta([O_3]-[NO])$ is a more useful measure of reactivity than $\Delta[O_3]$ alone under conditions where ozone formation is limited because of incomplete consumption of the initially present NO.

It can also be seen from Table 2 that in all cases the addition of the test substance suppressed radical levels, but the suppression of radical levels was significantly greater for n-pentadecane and the printing oils than for ethane. While the addition of ~45 ppmC of ethane suppressed OH radical levels by a factor of ~2, relative to control runs where no test compound is added, the addition of only 2.4 ppmC of n-pentadecane or 3 ppmC Magie-47 suppressed OH radical levels by over a factor of 5. Magie-470 also suppressed OH radical levels to a significant extent, though somewhat less so than did Magie-47 or pure n-pentadecane.

Table 2. Summary of Results of the Single Component-NO_x-Air Runs Carried Out in the Printing Oil Reactivity Study[a]

ITC Run No.	Test Compound	----- Initial -----				Final O_3 (ppb)	Average Change ($[O_3]-[NO]$) (ppb hr^{-1})	Average 1-2 hr. [OH] (ppt)
		RHC (ppmC)	NO (ppb)	NO_2 (ppb)				
999a		0.0	62	22	Expt:	6	6	0.13
					Calc:	7	7	0.16
999b	Ethane	35.6	50	35	Expt:	234	64	0.06[b]
					Calc:	180	56	0.049
1001	n-Pentadecane	2.4	68	26	Expt:	31	11	0.024
					Calc B:	45	16	0.028
					Calc A:	22	10	0.020
1002	Magie-47	3.0	69	40	Expt:	46	12	0.023
					Calc B:	45	16	0.022
					Calc A:	23	10	0.015
1003	Magie-470	3.3	86	26	Expt:	77	22	0.034
					Calc B:	37	17	0.022
					Calc A:	17	10	0.015
1004		0.0	78	24	Expt:	8	8	0.10
					Calc:	6	6	0.14

[a] Results are for 2 hours of irradiation for ITC-999a and 1004, for 4 hours of irradiation for ITC-999, and for 6 hours for the other runs. Average OH radical concentrations are for the second hour of irradiation in each case. The changes in ($[O_3]-[NO]$) are divided by the number of hours of irradiation for easier comparison between different runs.

[b] Value estimated to be uncertain by ±50% because of need for large correction for consumption of propene by reaction with ozone.

Thus, normalizing to the amount of compound added, n-pentadecane, Magie-47 and Magie-470 suppressed radical concentrations by factors of ~50, ~40 and ~25 more than ethane, respectively. Thus, it is clear that radical inhibition by n-pentadecane and the two printing oils was significant.

It should be noted that because of the strong radical inhibition characteristics of n-pentadecane and the printing oils, carrying out runs with greater amounts of test compound added, such as, for example, ~50 ppmC for comparability for the ethane run, would not have resulted in significantly more ozone formation than was observed in these experiments. Indeed, beyond a certain point, increasing the levels of test compounds which are radical inhibiting would just cause a corresponding decrease in radical levels (down to levels which are too low to measure with any degree of precision), and very little net change in the amounts of ozone formed and NO oxidized. Preliminary model calculations indicated that with our assumed mechanisms for n-pentadecane (see Section IV), the most useful results for model testing were obtained when relatively low levels of test compound were added, as employed in these experiments. (Indeed, if too much compound is added, the results become totally insensitive even to the amount of compound added.) On the other hand, for compounds such as ethane, which have only minor radical inhibition characteristics (as well as for compounds which are initiators), the most useful results are obtained if sufficient compound is added that a "true" ozone maximum is attained. This is the reason that the runs with n-pentadecane and the printing oils were carried out using significantly lower amounts of test compound than was the case for ethane.

C. Results of the Incremental Reactivity Experiments

A total of 16 irradiations were carried out for the purpose of determining the incremental reactivities of ethane, n-pentadecane and the two printing oils. These included eight runs where one of the test compounds was added to a standard "mini-surrogate"-NO_x mixture, and eight control runs where the standard surrogate-NO_x mixture was irradiated with no test compound added. The experimental protocol was the same as that employed in a previous study in which the incremental reactivities of a number of representative organics (Atkinson et al. 1983, Carter and Atkinson 1987a), was measured. The same standard "mini-surrogate"-NO_x mixture was used so that the reactivities obtained could be compared with the existing data base for other compounds. As discussed in detail elsewhere (Carter and Atkinson 1987a, 1987b), the "incremental reactivity" of a compound under the conditions of a standard surrogate-NO_x-air experiment was defined as the change in ozone yields and amounts of NO oxidized caused by adding the test compound or mixture, relative to the amount of test substance added. The utility of the "incremental reactivity" concept for control strategy purposes, and the factors which affect reactivity when measured in this way, are dealt with extensively in a separate report (Carter and Atkinson 1987b), and thus are not discussed in detailed here. To the extent that the conditions of the standard environmental chamber experiment represents those of the atmosphere, these incremental reactivities can provide an indication of the relative tendency of these substances to promote ozone formation when they are emitted into polluted urban airsheds. Although, as discussed in detail in a separate report (Carter and Atkinson 1987b), incremental reactivities under atmospheric conditions may not necessarily be the same as those observed in environmental chamber experiments, such chamber data are useful both in indicating qualitative reactivity trends for the test substances, as well as providing necessary data for testing the model's ability to accurately simulate their atmospheric reactivities under more realistic conditions.

The initial reactant concentrations employed in the standard surrogate-NO_x-air experiments and in the incremental reactivity experiments carried out in this study are summarized in Table 3. The runs with the test compound added were carried out under the same conditions, with the same initial reactant concentrations, except for the presence of the test compound. All of these runs were 6-hour irradiations. The four-component "mini-surrogate" was designed as a simplified representative of a more complex surrogate developed at SAPRC to represent organic emissions into the California South Coast Air Basin, with trans-2-butene representing the aldehydes present, because of its rapid reaction to form acetaldehyde under atmospheric conditions (Carter and Atkinson 1987a). This surrogate is also the same as the simpler of the two surrogates employed in our theoretical study of incremental reactivities, described in a separate report (Carter and Atkinson 1987b). The total ROG and NO_x levels employed in the standard surrogate runs were such that most of the ozone formation occurred in the first three to four hours of irradiation, with the ozone concentrations increasing only slowly, or leveling off, after that. The concentration-time profiles for selected species in two representative standard surrogate runs are shown in Figure 2.

The 1-, 2-, 3-, and 6-hour ozone yields observed in the incremental reactivity experiments are summarized in Table 4. The results of the experiments with added test compound are analyzed to obtain the

Table 3. Summary of the Average Initial Reactant Concentrations Measured in the Standard "Mini-Surrogate"-NO_x-Air Experiments Used for the Incremental Reactivity Determinations

Compound	(ppm)
NO	0.090
NO_2	0.023
n-Butane	0.457
Propene	0.130
m-Xylene	0.0626
trans-2-Butene	0.0149
Total ROG	2.78 ppmC
ROG/NO_x ratio	24.6

differences in these ozone yields in the runs with the test compound added, relative to the averages of the corresponding yields in the standard runs, divided by the ppmC of test compound added. The effects of the addition of the test compound were determined as a function of time because different mechanistic factors affect the ozone yields at different stages of the experiments. In particular, aspects of the mechanism which influence rates of ozone formation (generally effects relating to radical initiation or termination) have the greatest effect on ozone yields during the initial stages of the experiments. On the other hand, aspects of the mechanism which affect maximum ozone yields (such as NO_x removal characteristics) have the greatest effect on the ozone yields during the later stages of the experiments. In addition, the reactivities observed during the initial stages of the runs are more representative of reactivities under high NO_x conditions, while the final reactivities are more representative of reactivities under conditions where NO_x is more limited (Carter and Atkinson 1987b). This is because NO_x is consumed more rapidly in organic-NO_x-air irradiations than are the organics. Thus reporting reactivities for various irradiation times gives more comprehensive information concerning the reactivity of the test compound under different conditions than just reporting reactivities in terms of effects on maximum ozone yields.

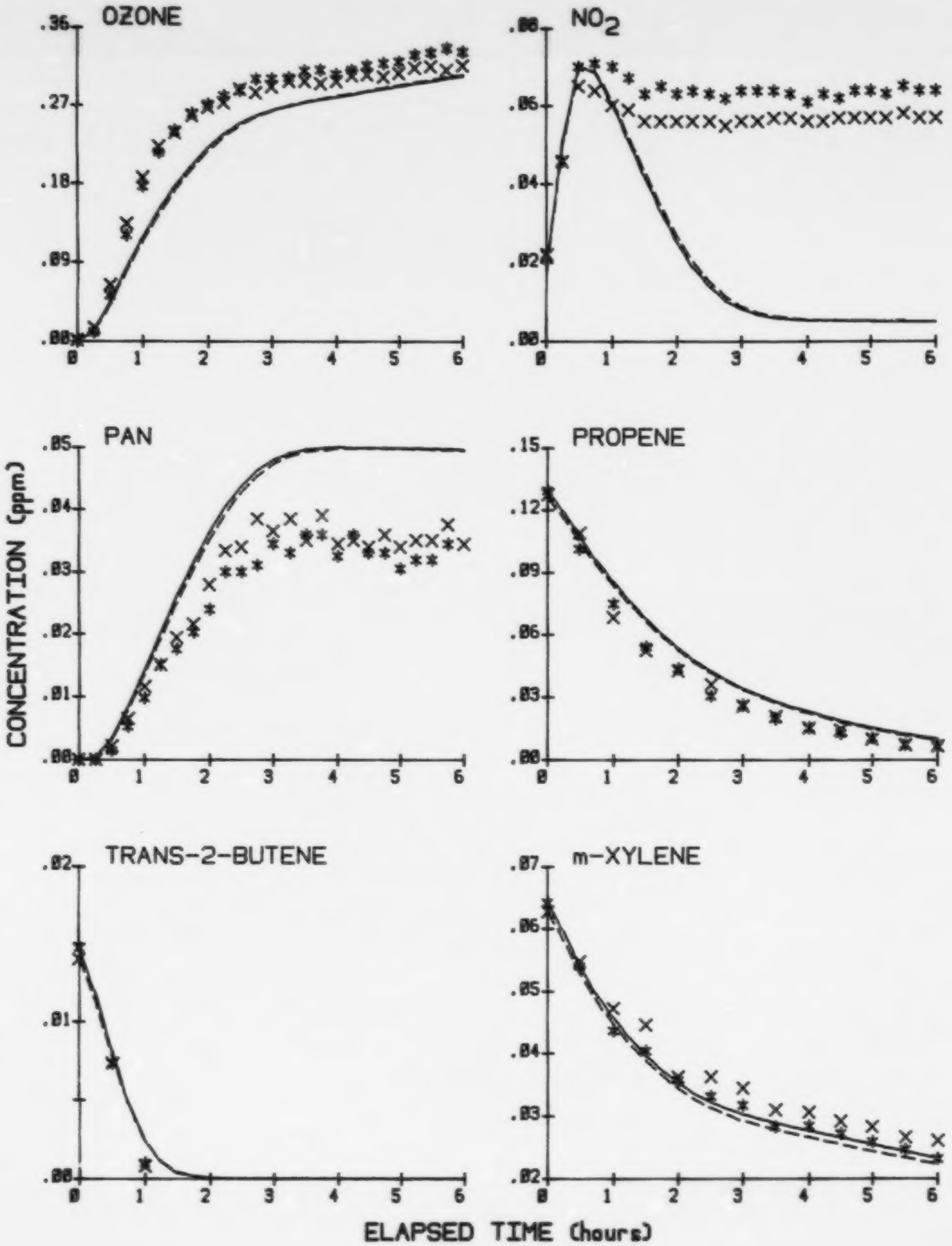

Figure 2. Experimental and calculated concentration-time profiles for ozone, NO and NO$_2$ observed in a representative standard "mini-surrogate"-NO$_x$-air irradiation used in the incremental Reactivity Determinations.

* = Experimental data, ITC-985
X = Experimental data, ITC-997
——— = Model calculation, ITC-985
- - - = Model calculation, ITC-997

Table 4. Summary of Ozone Yields Observed in the Incremental Reactivity Runs

ITC Run No.	Compound Added	Ozone Yield (ppb)			
		1 hr	2 hr	3 hr	6 hr
	Standard Runs				
977		183	279	302	322
978		183	268	290	310
980		(145	264	313	361)[a]
982		180	275	302	328
985		178	272	300	332
991		(227	317	344	379)[a]
994		189	279	285	318
997		188	268	292	316
	Average	184±8	274±10	295±14	321±16[b]
	Ethane				
979	14.9 ppmC	219	322	362	404
992	25.7 ppmC	242	324	354	376
	n-Pentadecane				
981	3.2 ppmC	78	250	306	324
993	4.5 ppmC	118	224	259	276
	Magie-47				
983	1.5 ppmC	41	221	306	345
984	1.6 ppmC	64	235	308	335
995	6.0 ppmC	60	211	257	274
	Magie-470				
996	6.1 ppmC	103	225	251	250

[a] Ozone data for these two runs appeared to be anomolous, for reasons which could not be determined. Because the ozone data for the other six, standard runs had reasonably good reproducibility, the results for the apparently anomolous runs were rejected and not used for calculating the average.

[b] Error shown is two standard deviations of the average.

In our previous studies of incremental reactivity (Atkinson et al. 1983, Carter and Atkinson 1987a, 1987b), reactivities were defined in terms of effects on $\Delta([O3] - [NO])$, but because of problems with the experimental NO measurements (discussed in Section II-C), in this study reactivity is defined in terms of effects on ozone yields alone. Defining reactivity in terms of $\Delta([O3] - [NO])$ has the advantages that this quantity has a direct relationship with the elementary processes responsible for ozone formation, that it is by nature less sensitive to the amount of NO initially present, and that it can be used to measure reactivity even under conditions where ozone formation is negligible due to the presence of excess NO. However, since ozone was formed within the first hour of all the experiments in this study, the ozone yield alone should provide an adequate indication of reactivity.

It should also be noted that in our previous studies (Atkinson et al. 1983, Carter and Atkinson 1987a, 1987b), reactivities were expressed in terms of effects of test compound added on a per mole basis, while in this study they are defined in terms of effects on a per mole carbon basis. Defining reactivity on a per-mole basis is useful in studies of mechanistic effects which influence reactivity, since that has a more direct relationship with such effects. However, when carrying out an assessment of reactivities for regulatory purposes, which is the ultimate objective of this study, reactivities on a per-mass basis is much more relevant. This is because emissions are measured and regulated in terms of mass emitted, (e.g., tons per day) and not on a molar basis. Since the carbon atoms represent most of the mass in hydrocarbons such as ethane, n-pentadecane, and the major constituents of the printing oils, we consider defining reactivity on a per-carbon basis to be appropriate in this study.

The experimental incremental reactivities defined as discussed above are given in Table 5. The incremental reactivities are plotted against amount of ethane added in Figure 3, and against the amount of n-pentadecane or printing oil added in Figure 4. Table 5 and Figures 3 and 4 also indicate estimated (two standard deviation) uncertainties for the incremental reactivities. These were derived based on the variability in the ozone yields observed in the replicate standard surrogate-NO_x-air irradiations.

Table 5. Experimental Incremental Reactivities Derived From the t = 1-, 2-, 3- and 6-Hour Ozone Yields Observed in the Mini-Surrogate-NO_x-Air Irradiations With and Without Added Test Compounds

ITC Run No.	Compound Added	Reactivity (ppb O_3/ppmC HC)[a]			
		1 hr	2 hr	3 hr	6 hr
	Ethane[b]				
979	14.9 ppmC	2.4 ± 1.0	3.2 ± 1.3	4.5 ± 1.9	5.6 ± 2.3
992	25.7 ppmC	2.3 ± 0.8	2.0 ± 0.8	2.3 ± 1.0	2.1 ± 1.2
	n-Pentadecane				
981	3.2 ppmC	-33 ± 4	-8 ± 5	3 ± 7	1 ± 9
993	4.5 ppmC	-15 ± 3	-11 ± 3	-8 ± 5	-10 ± 6
	Magie-47				
983	1.5 ppmC	-95 ± 9	-35 ± 10	7 ± 15	16 ± 18
984	1.6 ppmC	-75 ± 8	-24 ± 10	8 ± 14	9 ± 17
995	6.0 ppmC	-21 ± 2	-11 ± 3	-6 ± 4	-8 ± 5
	Magie-470				
996	6.1 ppmC	-13 ± 2	-8 ± 3	-7 ± 4	-12 ± 4

---

[a] Uncertainty values shown reflect uncertainties due to variabilities in ozone yields. The uncertainties for the ozone yields in the standard runs were based on the standard deviation of the average. The uncertainties used for the ozone yields in the runs with added test compound were estimated to be one half of the maximum range of observed ozone in the standard runs, excluding the apparently anomalous runs ITC-980 and ITC-991. Uncertainties shown are two standard deviations.

[b] Uncertainties shown for the ethane experiments also reflect the estimated ~25% uncertainty in the estimated initial ethane concentrations. (See Section II.C.1.)

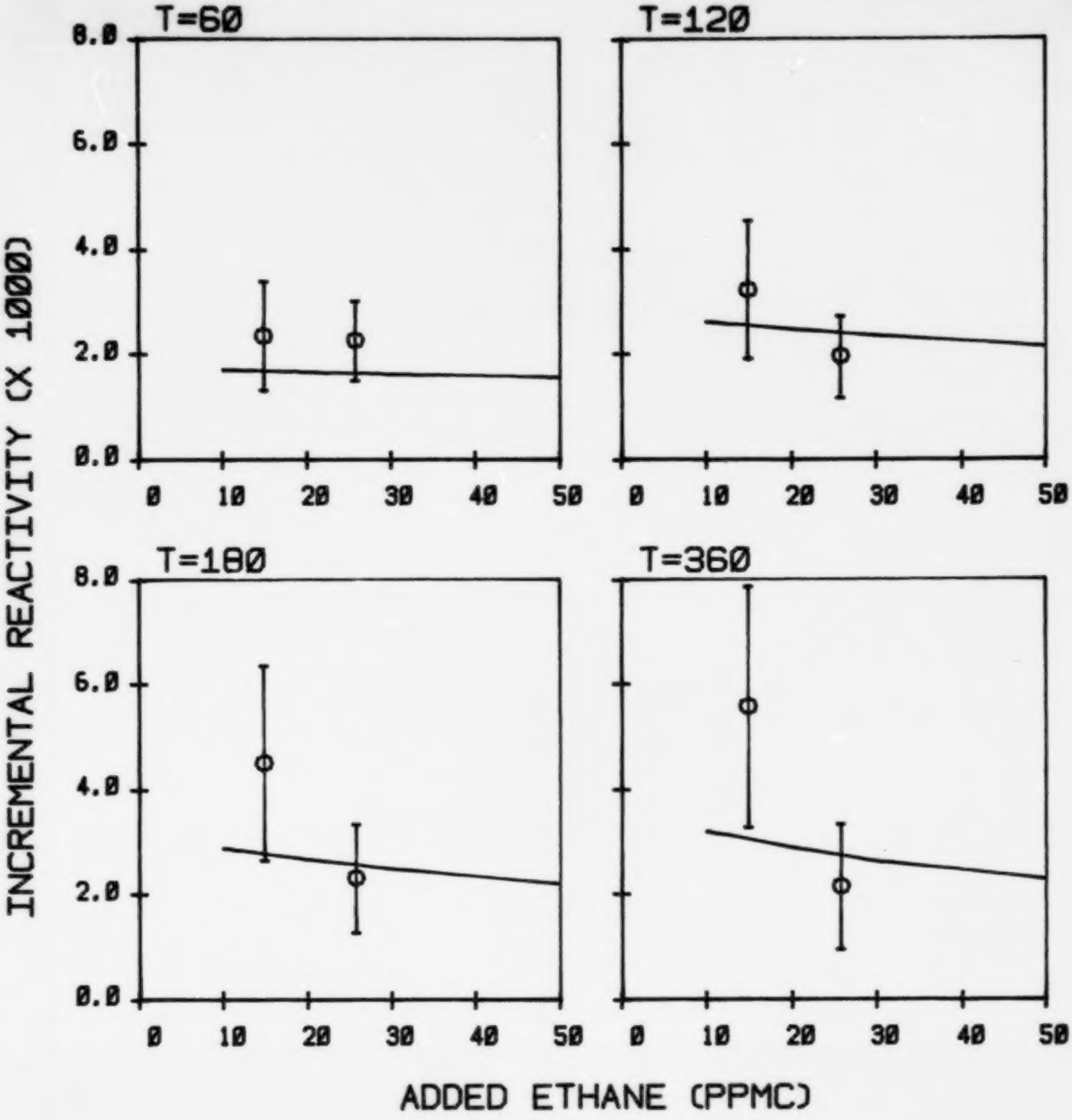

Figure 3. Plots of experimental and calculated incremental reactivities of ethane against amounts of ethane added in the ITC "mini-surrogate"-NO_x-air experiments.

O = Experimental.

______ = Model calculations of incremental reactivities for the times shown.

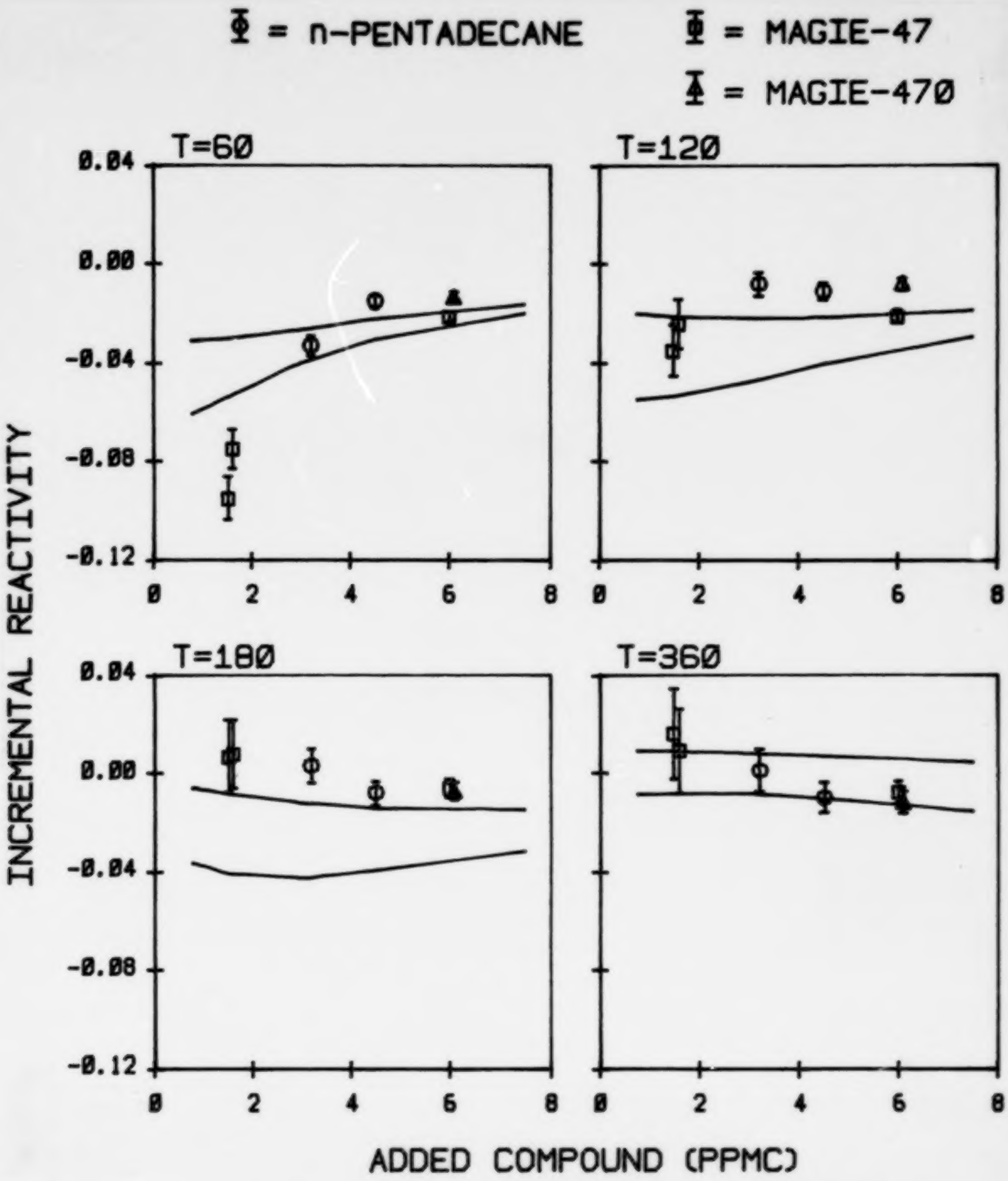

Figure 4. Plots of experimental and calculated incremental reactivities of n-pentadecane and the printing oils Magie-47 and Magie-470 against amounts of test substance added in the ITC "mini-surrogate"-NO_x-air experiments.

0 = Experimental. (See above for symbols for different types of runs.)

—— = Model calculations of incremental reactivities for the times shown. The lower lines were calculated using n-pentadecane Model A and the upper lines were calculated using Model B. (See Section IV.A.2 below for a discussion of the two n-pentadecane models used in the model simulations.)

It can be seen that under the conditions of these experiments, the incremental reactivities of ethane were in the range of 0.002 to 0.005 ppm O_3 per ppmC added ethane, and were only slightly affected by reaction time and amount of ethane added. However, the reactivities of n-pentadecane and the printing oils were significantly affected both by the reaction time and (at least for Magie-47) by the amount of test substance added. For these compounds, the reactivities derived from the t = 60-minute ozone approached or attained positive values as the irradiation time increased. The results of these incremental reactivity experiments did not indicate any significant differences in the reactivities of n-pentadecane and the two printing oils studied, particularly if the variation of the reactivities with amount of compound added was taken into account (as shown in Figure 4). The runs with Magie-47, which were carried out with the widest range of amounts of test substance added, were the most useful in indicating the dependence of the reactivities on the amount of test compound added. From Table 5, it can be seen that the reactivity early in the run becomes more negative as the amount of added printing oil is increasesd. On the other hand, the reactivity at the end of the run increases as the amount of added oil decreases. Extrapolating the Magie-47 reactivities to zero added test compound [the "limiting incremental reactivities" (Carter and Atkinson, 1987a, 1987b)] yield limiting incremental reactivities for this substance of approximately -0.12, -0.04, +0.012 and +0.020 ppm O_3/ppmC oil for t = 1, 2, 3 and 6 hours, respectively. Thus, under the conditions of these experiments, at the limit of zero added test compound the reactivity of Magie-47 in terms of the final ozone yields is approximately 5-10 times greater than that for ethane, and these data suggest that the reactivities of Magie-470 and n-pentadecane are probably similar. However, for for shorter reaction times, n-pentadecane and the printing oils are ozone inhibitors, and thus must be considered to be unreactive with respect to ozone formation under these conditions.

As discussed by Carter and Atkinson (1987a, 1987b), if a compound has significant radical sinks (or sources) in its mechanism, it will affect primarily its incremental reactivities measured during the initial stages of these irradiations, while NO_x sinks in its mechanism affect primarily its reactivity defined in terms of the final ozone yields. The fact that n-pentadecane and the printing oils have highly negative reactivities in the initial stages of the experiments can thus be attributed to radical sinks in their mechanism is consistent with the results of the single component-NO_x-air runs discussed above. Although these compounds are also expected to have NO_x sinks in their mechanisms, they do not appear to be strong enough to result in negative reactivities in terms of final ozone yields; though without such sinks the t = 6-hour reactivities would undoubtedly be significantly higher. It should be noted, however, that our theoretical calculations of incremental reactivities (Carter and Atkinson 1987b) indicate that the incremental reactivities observed under the conditions of these chamber experiments are less affected by the presence of NO_x sinks than are incremental reactivities calculated under the conditions representative of polluted airshed scenarios. The reactivities calculated for these compounds for conditions representative of polluted airsheds are discussed in the following section.

IV. MODEL CALCULATIONS

Computer model simulations were carried out as an integral portion of this study to determine whether our current understanding of the atmospheric reactions of n-pentadecane, and ethane is consistent with our experimental results, and to estimate the relative reactivities of these compounds under conditions of idealized ambient pollution scenarios. The model and input data used, the results obtained, the uncertainties in reaction mechanism used to simulate the reactivities of n-pentadecane and the printing oils, and the uncertainties in the model predictions of reactivities under atmospheric conditions are discussed in this section.

A. Chemical Mechanism Employed

1. Ethane and Base Case Surrogate Mechanism

The chemical reaction mechanism used to simulate the NO_x-air reactions of ethane and the organics present in the base case ROG surrogate mixtures in both the chamber and the airshed simulations has been described previously (Carter et al. 1986b), and is thus not discussed in detail here. The reaction mechanism was that employed in our theoretical study of incremental reactivities of organics (Carter et al. 1987b). This mechanism has been tested against results of over 400 environmental chamber experiments carried out at the University of North Carolina and in our laboratories (Carter et al. 1986b). The mechanism includes explicit reactions for ethane, n-butane, n-pentane, iso-octane, ethene, propene, trans-2-butene, toluene, m-xylene, and their major photooxidation products. A complete listing of this reaction mechanism is given in Appendix C.

Although this mechanism represents the current state-of-the-art of current homogeneous gas-phase reaction mechanisms for photochemical smog and is the most extensively tested of any single reaction mechanism currently in use, it should be recognized that it is not without a number of significant areas of uncertainty. These uncertainties are discussed in detail by Carter et al. 1986b). The largest uncertainty concerns the photooxidation mechanisms of the aromatics, which form a variety of highly reactive products whose specific identities, yields, and detailed photooxidation reactions have not been established, and whose reactions are represented in the model in a parameterized manner adjusted to fit the chamber data. There also remains significant uncertainties concerning the details of the ozone-alkene reactions, particularly with regard to the radical yields from such processes. In addition, because of chamber effects the mechanisms for the reactions of the higher alkanes have not been well tested.

There are several cases where models using this mechanism do not accurately simulate the results of environmental chamber experiments, and it is not clear to what extent this is due to uncertainties in chamber effects or uncertainties in the homogeneous mechanism (though in most cases the discrepancies are of a random nature, and are thus probably due to uncharacterized chamber effects (Carter et al. 1986b)]. However, despite these problems, this chemical mechanism can simulate ozone yields in environmental chamber experiments to within ~ ±30% (Carter et al. 1986b), and it is unlikely that any other mechanism currently in use can perform significantly better. Nevertheless, these uncertainties need to be recognized when assessing the performance of the model in simulating the experiments carried out in this study, and in interpreting the results of the airshed reactivity predictions.

2. n-Pentadecane Reaction Mechanisms

Prior to this experimental study, no data have been obtained concerning the overall atmospheric photooxidation of n-pentadecane, nor are there any data available concerning the details of its atmospheric reaction mechanism. However, the major features of its atmospheric reactions can be estimated by extrapolation of our general knowledge concerning the atmospheric reactions of alkanes (Carter and Atkinson 1985). As for the other alkanes, we assume that the only significant removal route for n-pentadecane in the atmosphere is reaction with OH radicals, with the subsequent reactions being assumed to proceed as shown below (Carter and Atkinson 1985).

$$\text{n-}C_{15}H_{32} + OH \xrightarrow{O_2} C_{15}H_{31}O_2\cdot \text{ (e.g., } CH_3CH(O_2\cdot)C_{13}H_{27}) \qquad (1)$$

$$C_{15}H_{31}O_2\cdot + NO \rightarrow a\ RONO_2 + (1-a)\ C_{15}H_{31}O + (1-a)NO_2\cdot \qquad (2)$$

$$C_{15}H_{31}O\cdot \xrightarrow{O_2} HOC_{15}H_{31}O_2\cdot \text{ (e.g., } CH_3CH(OH)CH_2CH_2CH_2(O_2\cdot)C_{10}H_{21}) \qquad (3)$$

$$HOC_{15}H_{31}O_2 + NO \rightarrow a'\ RONO_2 + (1-a')\ HOC_{15}H_{31}O + (1-a')NO_2\cdot \qquad (4)$$

$$HOC_{15}H_{31}O\cdot \xrightarrow{O_2} \text{bifunctional products} + HO_2 \qquad (5)$$

In this scheme, "$RONO_2$" represents the C_{15} organic nitrates expected to be formed when the C_{15} peroxy radicals react with NO; reaction (3) represents the isomerization of this alkoxy radical, followed by the rapid reaction of the carbon-centered radical with O_2; and reaction (5) incorporates the rapid subsequent isomerization of the bifunctional alkoxy radical expected to be formed, followed by the reaction of the α-hydroxy radical formed from the isomerization with O_2 to form HO_2 and bifunctional products. [See Carter and Atkinson (1985) for a more complete discussion of these reactions].

The major distinguishing features of the reaction mechanism of this and of other higher alkanes are the formation of bifunctional products following isomerization of the long chain alkoxy radicals expected to be formed, together with the formation of alkyl nitrates from the reactions of the larger peroxy radicals with NO. This latter reaction is particularly important in affecting reactivity, since alkyl nitrate formation represents both a radical termination and a NO_x removal process, both of which are expected to cause decreased reactivity with respect to ozone formation. The extent to which alkyl nitrate formation is important is determined by the parameters a and a', which refer respectively to the alkyl nitrate yields from the reactions of the unsubstituted and the substituted peroxy radicals with NO. Based on extrapolating the alkyl nitrate yields observed in the NO_x-air photooxidations of a number of C_4-C_8 alkanes (Carter and Atkinson 1985), we estimate that $a = 0.43$ for the C_{15} alkyl peroxy radicals formed subsequent to the reactions of OH radicals with n-pentadecane. While this extrapolation from C_8 to C_{15} is subject to uncertainties, the effect of any uncertainty in our estimate of a is overshadowed by the effect of the much greater uncertainty in the value of a', the alkyl nitrate yield in the reaction of C_{15} hydroxy-subsitituted peroxy radicals formed following the isomerization of the C_{15} alkoxy radicals. While the value assumed for a' is of comparable importance to the value assumed for a in affecting the results of model simulations, no data exist concerning nitrate yields in the reactions of NO with any hydroxy-substituted peroxy radicals.

Previous models and evaluations of the atmospheric reactions of the alkanes (e.g., Carter et al. 1979, Atkinson et al. 1982, Atkinson and Lloyd 1984) assume, for lack of data to the contrary, that hydroxy substitution has no effect on the nitrate yield in the reaction of NO with long-chain peroxy radicals, i.e., that a' = a. However, we have recently observed that with this assumption model simulations consistently over-predict the rates of ozone formation and NO oxidation in environmental chamber runs employing C_6-C_9 n-alkanes, and that in most cases better fits to the chamber data are obtained if it is assumed that a' = 0 (Carter et al. 1986b). Therefore, in the alkane photochemical reaction mechanisms of Carter et al. (1986b), which were used in our theoretical reactivity study (Carter et al. 1987b) as well as in this study as the mechanism for the base case ROG surrogate components, it is assumed that the reaction of NO with hydroxy substituted peroxy radicals do not give rise to alkyl nitrate formation, i.e., that a' = 0.

However, it should be recognized that the model evaluation of Carter et al. (1986b), in which it was concluded that a' = 0, should not be regarded as definitive. In particular, model simulations of alkane-NO_x-air runs are extremely sensitive to assumptions concerning the magnitude of the chamber radical source, which generally varies from run to run. This variability of the chamber radical source, combined with the extreme sensitivity of model simulations of alkane-NO_x-air irradiations to the assumed radical source, means that there is a corresponding large variability in the performance of the model in simulating the results of such runs. In other words, chamber simulation of low reactivity compounds are doubtful due to the large contribution from chamber wall effects such as alkanes. Indeed, of all the types of irradiations used in the model evaluation study of Carter et al. (1986b), including runs with complex mixtures and auto exhaust, it was the alkane runs which exhibited the widest range of discrepancies in fits of the model simulations to the experimental results. Although the model simulations of alkane runs do not show gross systematic discrepancies, this variability, combined with the relatively limited number of C_6+ alkane-NO_x -air runs available for model testing, means that it is difficult to evaluate the alkane photooxidation mechanisms with any precision.

Therefore, to show the impact on model simulations of the uncertainties in the overall nitrate yields in the photooxidation mechanisms of n-pentadecane and other similar high molecular weight, alkanes present in the printing oils, model simulations were carried out using two versions of the n-pentadecane mechanism, with varying assumptions in this regard. One version, designated "Model A" (to be consistent with the nomenclature used in our preliminary modeling study given in Appendix A), is based on the assumption that a = a'. This version of the mechanism is considered to correspond to an upper limit of the amount of total C_{15} nitrate formation from n-pentadecane (Carter et al. 1986b). The other version, designated "Model B", is based on the assumption that a' = 0, and is the reaction mechanism consistent with our standard reaction mechanism for the photooxidation of other alkanes. Although there are obviously other uncertainties other than the overall nitrate yields in the photooxidation mechanisms of these high molecular weight alkanes, uncertainties regarding nitrate yields are of major importance in affecting predictions of reactivity, and thus this was the only parameter in the n-pentadecane model which was varied in these calculations.

The rate constant assumed for the reaction of OH radicals with n-pentadecane was 2.6×10^4 ppm^{-1} min^{-1}, estimated from the OH radical rate constants for n-alkanes (Atkinson 1985). The subsequent reactions of the alkyl nitrate products were represented in the chemical mechanism by the reactions of 4-heptyl nitrate (which represented the higher organic nitrates), and the subsequent reactions of the bifunctional products were represented by reactions of methyl ethyl ketone and 3-pentanol, which represented general reactions of lumped higher ketones and organics with OH substituent groups, respectively. This representation is consistent with the general alkane representation used in the alkane model of Carter et al. (1986b). Listings of the n-pentadecane reaction mechanisms A and B are given, together with the listing of the overall mechanism, in Appendix C of this report.

B. Simulations of the Chamber Experiments

1. Chamber Effects Model and Simulations of Characterization Runs

Model simulations of environmental chamber irradiations must include provisions for representing chamber-dependent parameters such as the intensity and spectral characteristics of the light source, ozone wall loss, other heterogeneous processes, chamber dependent radical sources, and dilution. A detailed discussion of the methods we used to represent chamber-dependent parameters in simulations of experiments carried out in the SAPRC ITC is discussed elsewhere (Carter et al. 1986b), and the methods used in this study were consistent with those methods. The chamber-dependent input data used in the model simulations of the experiments carried out in this study are summarized on Table 6, together with an indication of the the sources of the individual parameter values employed.

This chamber effects model was tested in simulations of the acetaldehyde-air, pure air and selected NO_x-air irradiations. As indicated above, the ozone and PAN yields in the acetaldehyde-air run are sensitive to the rate of NO_x offgassing in the chamber, and the model simulations of acetaldehyde-air run ITC-1009 predicted final ozone and PAN yields of 69 ppb and 8 ppb, respectively, in reasonable agreement with the experimental yields of 78 ppb and 8 ppb, respectively. The model simulation of the pure air irradiation run ITC-1008, which is sensitive to the assumed background OH to HO_2 conversion rate (attributed to trace levels of reactive organic contaminants), predicted a final ozone yield of 78 ppb, in good agreement with the experimental value of 88 ppb. The tracer-NO_x-air irradiations are primarily sensitive to the magnitude of the chamber radical source, and the results of the simulations of two such runs (ITC-999a and ITC-1004) are given in Table 2. It can be seen that for ITC-999a the average t = 1- to 2-hr OH radical concentration predicted by the model agrees with the experimental value to within 10%, while for the simulations of run ITC-1004 the predicted average OH radical values was ~40% higher than observed. This variability is consistent with the run-to-run

Table 6. Summary of Chamber-Dependent Input Parameters Used in the Model Simulations of the ITC Chamber Runs Carried Out in This Study

Parameter(s)	Value and Derivation
NO_2 Photolysis Rate	0.310 min^{-1}. Based on Results of NO_2 actinometry experiments.
Other Photolysis Rates	Calculated from the NO_2 photolysis rate rate, the absorption coefficients and quantum yields of the photolysis reactions, and the ITC blacklight distribution given by Carter et al. (1986b)
Water Concentration	Based on measured temperature and humidity during the final pure air flush of the chamber. Typically 2.0×10^4 ppm.
Temperature	303 K. This is the typical average temperature in ITC chamber runs.
Dilution	No dilution, due to flexible nature of chamber walls.
Rates or Rate Constants of Chamber-Dependent Reactions:	
$O_3 \xrightarrow{\text{wall}}$ loss of O_3	1.3×10^{-4} min^{-1} (Carter et al. 1986b)
$h\nu \xrightarrow{\text{wall}} OH$	0.062 ppb min^{-1} Based on results of tracer-NO_x-air irradiations
wall -> NO_2	0.047 ppb min^{-1} (Carter et al. 1986b)
$N_2O_5 \xrightarrow{\text{wall, } H_2O}$ Loss of N_2O_5	$(2.5 \times 10^{-3} + 5.0 \times 10^{-8} [H_2O])$ min^{-1} (Carter et al. 1986b)
$NO_2 \xrightarrow{\text{wall}}$ 0.2 HONO + 0.8 loss of NO_2	1.4×10^{-4} min^{-1} (Carter et al. 1986b)

variability of the chamber radical source (Carter et al. 1982). The chaber effects model used in these calculations, summarized on Table 6, is thus consistent with the results of the characterization runs carried out in this study.

2. Results of Simulations of the Single Component Organic-NO_x-Air Irradiations

The results of the model simulations of the single component-tracer-NO_x-air irradiations employing ethane, n-pentadecane and the two printing oils are summarized, together with the experimental data, in Table 2. These calculations were carried out with no adjustment of chamber-dependent or mechanistic parameters to optimize the fits of the simulations to the experimental data. It can be seen that the model accurately predicts the ozone yield and average NO oxidation and ozone formation rate observed in the ethane run, and simulates the average OH radical concentration to within its experimental uncertainty. Since the photooxidation mechanism for ethane is considered to be well established, this good fit in the ethane run primarily reflects the appropriateness of our representation of chamber effects and other run-specific conditions in the model, particularly the magnitude of the chamber radical source, to which, as indicated above, the results of model simulations of alkane-NO_x-air irradiations are particularly sensitive.

The simulations of the n-pentadecane and the printing oil experiments were carried out using both versions of the n-pentadecane photooxidation mechanism discussed above in Section IV.A.2. It can be seen that, as expected, version "A", the version with the higher assumed total organic nitrate yield, predicts lower final ozone yields, average NO oxidation and ozone formation rates, and average OH radical levels than does version "B", which predicts lower overall radical termination due to nitrate formation. However, both models are successful in simulating the overall qualitative results that n-pentadecane and the printing oils significantly inhibit radical levels in NO_x-air irradiations, resulting in relatively little ozone formation and NO oxidation occurring. It can be seen that the experimental results of the n-pentadecane run lie somewhat between the predictions of the two models, while the results of the Magie-47 run are well simulated by the more reactive model "B", and both models underpredict the reactivity observed in the run with Magie-470.

In interpreting the implications of these results, the fact that simulations of alkane-NO_x-air runs are extremely sensitive to the assumed magnitude of the chamber radical source, which tends to vary from run to run, must be taken into account. This variability of the radical source would result in a corresponding variability in the observed average OH radical levels and the resulting amount of ozone formed and NO oxidized in these experiments. The fact that the model simulations using the assumed radical source listed in Table 6 gives good simulations of the results of the ethane run, but overpredicts the OH radical levels in the tracer-NO_x-air runs carried out before and after these runs by 25% and 40%, respectively, suggests an ~33% variability in the magnitude of the radical source for the conditions of these runs. Since this model predicts that the chamber radical source is also the major source of radicals in the n-pentadecane (and printing oil) simulations, this corresponds to a ~ ±33% variability in the predicted OH radical levels for these runs. If this variability is taken into account, then it can be concluded that the experimental data for the n-pentadecane irradiation are not inconsistent with either version of the n-pentadecane model, and that the results of the run with Magie-47 are not inconsistent with the predictions of model "B", but that model "A" will probably underpredict the reactivity of Magie-47, and that both models will probably overpredict the reactivity of Magie-470. This level of variability also indicates that these experiments do not necessarily imply any significant difference in reactivity between Magie-47 and pure n-pentadecane. However, the data suggest that Magie-470 is probably more reactive than either pure n-pentadecane or Magie-47, at least under the conditions of these experiments.

It should also be noted that while the results of these experiments are extremely sensitive to the radical inhibition characteristics of the test compounds employed, and thus are useful for testing this aspect of their reaction mechanisms, these experiments are not at all sensitive to NO_x removal characteristics of the reaction mechanisms. This was confirmed in test calculations, and arises from the fact that the overall reactivities in these runs were too low for the NO_x to be consumed, which means that ozone formation was not limited by NO_x availability. However, as shown in our theoretical incremental reactivity study (Carter and

Atkinson 1987b), the NO_x removal characteristics of the mechanism can be extremely important in influencing reactivity in airshed conditions. In this respect, the simulations of the incremental reactivity experiments, discussed below, are more useful in testing the accuracy of the model predictions.

3. Results of Simulations of Ozone Yields Observed in the Mini-Surrogate Runs

Before discussing the model performance in simulations of incremental reactivities observed in the mini-surrogate-NO_x runs, it is necessary to show its performance in simulating the overall results of these runs. This is shown in Figure 2 (in Section III.C) which gives plots of computed concentration-time profiles for selected species together with plots of the experimental data for two representative standard mini-surrogate runs. The results for most of the other standard mini-surrogate runs carried out in this study are similar. It can be seen that the model is reasonably accurate in its simulations of the maximum ozone yields observed in these experiments, but it tends to underpredict the rate of ozone formation in the $t = 0.5$ to $t = 1.5-2$ hour period, and tends to overpredict the PAN yields. [The apparent discrepancies between the model and experimental NO_2 data are due to the fact that the measured "NO_2" data include a positive interference by PAN and other organic nitrates (Winer et al. 1974).] The performance of the model in simulating the results of these runs is of comparable quality to its performance in simulating the results of other types of surrogate-NO_x-air runs carried out in this and other environmental chambers (Carter et al. 1986b), and as such represents the current state-of-the-art in the ability of up-to-date photochemical models in simulating the experimental data.

[It is interesting to note that when the same model is used to simulate the results of the mini-surrogate runs carried out in our previous experimental study of incremental reactivities (Carter and Atkinson 1987a), the model also accurately predicted the maximum ozone yields, but showed an opposite discrepancy in the predictions of the initial ozone formation rates, i.e., these rates were overpredicted. The fact that the same model overpredicts the initial rates of ozone formation in one series of similar experiments, and underpredicts them in another suggests that the discrepancies are more likely due to problems with characterizing the conditions of the runs, rather than with the chemical mechanism employed. However, this variability in the ability to simulate the initial ozone formation rate is unlikely to be due to variabilities in the magnitude of the chamber radical source, since surrogate runs show little sensitivity to this chamber effect and model simulations in which the magnitude of the chamber radical source was varied within by ~33% showed no significant change in the quality of the fits. The exact causes of this variability of the performance of the model in simulations of similar runs carried out at different time periods in the same chamber is unknown, though similar effects have been observed in simulations of other types of runs carried out in different chambers (Carter et al. 1986b).]

4. Results of Simulations of the Experimental Incremental Reactivities

Model simulations of incremental reactivities were carried out for ethane and the two alternative n-pentadecane mechanisms as a function of the amounts of ethane or n-pentadecane added to the standard mini-surrogate experiments. The calculated incremental reactivities, defined in terms of ozone yields at t = 60, 120, 180, and 360 minutes of irradiation are shown as the solid lines in Figures 3 and 4, where they can be compared with the experimental results.

In the case of the incremental reactivities of ethane shown on Figure 3, it can be seen that the model underpredicts the reactivity of ethane in the initial stages of the experiments, though the fit is usually to within the estimated experimental uncertainty ranges. Some of this discrepancy in the initial stages of the irradiation can be attributed to the fact that the model tends to underpredict the initial rate of NO oxidation and ozone formation in the surrogate-NO_x-air irradiations, rather than necessarily being a problem with the ethane mechanism itself. Test calculations using approximate methods to correct for this discrepancy in the model predictions of the standard surrogate runs suggest that this may be the case. However, even without such corrections, the model correctly predicts both the general magnitudes of the incremental reactivity values for ethane, and also the fact that they tend to increase slightly with reaction time.

Figure 4 shows that the two versions of the n-pentadecane reaction mechanism yield significant differences in the calculated incremental reactivities of this compound under the conditions of these experiments, though both are qualitatively similar in that they predict negative reactivities in terms of initial ozone yields, but with the magnitude of the negative reactivities decreasing with reaction time. As expected, model "A", with the higher assumed overall organic nitrate yield, yields consistently lower calculated incremental reactivities, and it calculates n-pentadecane reactivities which are always negative under conditions of these runs. Although the more reactive model "B" predicts negative reactivities during the initial stages of the irradiations, it predicts that n-pentadecane is slightly positively reactive in terms of the final ozone yields, with a final limiting incremental reactivity approximately three times that calculated for ethane.

In general, the experimental incremental reactivities for n-pentadecane and the printing oils appear to be most consistent with the predictions of the less reactive model "B", which is gratifying since this is the version more consistent with the mechanisms used for the reactions of the C_6-C_9 n-alkanes (Carter and Atkinson 1985, Carter et al. 1986b). However, in some cases the agreement between model predictions and the experimental data is not as good as for ethane. In particular, the initial incremental reactivities for the two runs with the lowest levels of Magie-47 are significantly more negative than predicted by model "B" (agreeing somewhat better with the predictions of model "A"), and the observed final reactivities in the experiments with the highest amount of added test compound also agree better with the lower (and negative) values predicted by model "A". It is unclear to what extent these discrepancies can be attributed to uncertainties in our assumed atmospheric reaction mechanism for n-pentadecane, to uncertainties in our assumed reaction mechanisms for the "mini-surrogate" components, to the fact that the printing oils contain contain compounds other than n-pentadecane, or to the the greater experimental difficulties and uncertainties expected when working with these compounds. However, considering the uncertainties involved, the n-pentadecane model "B" appears to perform reasonably well in simulating the experimentally determined incremental reactivities for both n-pentadecane itself and the printing oils Magie-47 and Magie-470.

The reactivities derived from the data of the two Magie-47 runs with the lowest amounts of added oil show the worst agreement with the model predictions and with the reactivities observed in the other experiments. The experimental data indicate a greater dependence of the reactivities on the amount of added test compound than predicted by the model. The fact that the t = 60 min reactivities derived from the data from these runs are much more negative than the model predictions suggests that much stronger radical sinks are involved in the photooxidation of the components of Magie-47 than predicted by our n-pentadecane model "B". However, this finding is not consistent with the results of our simulations of the Magie-47-tracer-NO_x-air with the same mechanism, where the model prediction is in good agreement with the observed radical inhibition caused by Magie-47. Clearly, the extent to which the predictions of model "B" are consistent with these data is somewhat uncertain, and more incremental reactivity experiments for these substances would have been useful verifying the consistency of the data obtained. However, this was not possible given the resources available for carrying out this study.

C. Simulations of Incremental Reactivities for Idealized Airshed Scenarios

In order to provide an indication of the model predictions of the relative reactivities of ethane and the printing oils (as represented by the two n-pentadecane mechanisms) for conditions more representative of polluted urban atmospheres than can be attained with environmental chamber experiments, model simulations of incremental reactivities were carried out using several idealized airshed model scenarios. The airshed scenarios were based on three different model formulations of emissions schedules, transport, dilution and background conditions, and employed two different surrogates to represent base case ROG emissions. For each scenario, reactivities were calculated over a range of ROG/NO_x ratios. The principles and scenarios employed, and the results obtained, are discussed in this section.

1. Principles and Model Scenarios Employed

The model simulations of reactivities under airshed conditions, and the specific idealized airshed scenarios employed, were essentially identical to those employed in our theoretical study of incremental reactivities, described in a separate report (Carter and Atkinson 1987b), and thus these are only briefly summarized here. The reactivities calculated are the "limiting incremental reactivities", which is defined as the difference in the maximum values of $\Delta([O_3]-[NO])$ in the simulations with and without the added test compound, divided by the amount of test organic added, at the limit as the amount of test compound approaches zero. For scenarios with dynamic emissions, the "amount of test organic added" is defined as the concentration of the organic at the end of the simulation (i.e., at the maximum inversion height) which would have been present if the compound did not react chemically. This means that the calculated "reactivities" refer to the numbers of moles of ozone formed and NO oxidized per mole (or mole carbon) of organic emitted. Although in our report on the theoretical reactivity calculations the reactivities were calculated on a molar basis, in this discussion we will present the reactivities calculated on a mole carbon (i.e., mass) basis, since, as discussed in Section III.C above, this is more appropriate for control strategy purposes.

The airshed scenarios for which incremental reactivities were calculated were based on three different model formulations of emissions schedules, transport, dilution and background conditions, and on two different organic surrogate mixtures used to represent base case ROG emissions. All three model formulations employed the simple "box model" formulation which, though highly approximate and simplified in its representation of transport and mixing of pollutants, has the significant advantage over more complex representations in that the relatively modest requirements of computational resources allows the chemical aspects which affect reactivity to be represented in more detail than would otherwise be the case. Although none of these scenarios should be taken as being representative of any particular airshed or episode, they should be sufficiently representative to give us at least a qualitative indication of how the reactivities predicted by our ethane and n-pentadecane models differ under airshed conditions than those observed in the chamber experiments, and how their relative reactivities may be affected by the conditions of the airsheds into which they are emitted.

The input data used to represent the three different model formulations used in the airshed scenarios are summarized in Table 7. Two of these formulations, designated EKMA-I and EKMA-III, were based on the standard city-specific EKMA inputs recommended by Gipson and Freas (1983)

Table 7. Summary of Conditions and Input Data Employed in the Airshed Scenarios Used for Reactivity Assessments

Scenario	EKMA-1		EKMA-3		MD	
Latitude	34.1		34.1		34.1	
Date	June 21		June 21		June 21	
Temperature (K)	300		300		300	
Relative Humidity (%)	50		50		50	
Calc. Sunrise (LDT)[a]	0552		0552		0552	
Sunset (LDT)	2008		2008		2008	
Rates of Photolysis reactions	Calculated for the dates and latitudes given above using the clear-sky actinic fluxes tabulated by Peterson (1976) using his "best estimate" surface albitos. See also Carter et al. (1986b).					
Heterogeneous reactions	Heterogeneous reactions assumed negligible.					
Inversion Height Schedule, ground[b]	(LDT)	(m)	(LDT)	(m)	(LDT)	(m)
	0552	250	0552	250	0552	100
	0651	250	0651	250	0800	100
	1247	492	1247	2492	1500	540
	1613	600	1613	3500	2100	540
	2100	600	2100	3500	0800[c]	100
					Day 1	Day 2
Simulation Start Time (LDT)	0800		0800		0600	0800
Simulation End Time (LDT)	2100		2100		0800[c]	2100
Initial + Emitted ROG (millimoles C m^{-2} day^{-1})	12.0		12.0		12.0[d]	
Initial + Emitted NO_x	Varied from 0.3 to 4.0 millimoles m^{-2} day^{-1} Initial and Emitted $[NO_2]/[NO] = 3.0$					
Initial Pollutants:					Day 1	Day 2
ROG	67.1% of total ROG input				0	Calc'd.
NO_x	56.5% of total NO_x input				0	Calc'd.
ROG and NO_x Emissions Schedule[f]	(LDT)	(fac)	(LDT)	(fac)	(LDT)	(fac)
	0800	1	0800	1	0600	0
	1430	1	1430	1	0800	1
	1530	0	1530	0	1830	1
	2100	0	2100	0	1930	0
Pollutants Aloft					Day 1	Day 2
Ozone (ppb)	70		70		0	Calc'd.[e]
Total ROG (ppbC)	20		20		0	Calc'd.

(continued)

Table 7 (continued) - 2

Scenario		EKMA-1	EKMA-3	MD	
Aloft ROG Composition				0	Calc'd.
Propene	(ppm/ppmC)	0.010	0.010		
n-Butane	(ppm/ppmC)	0.138	0.138		
m-Xylene	(ppm/ppmC)	0.019	0.019		
Formaldehyde	(ppm/ppmC)	0.075	0.075		
Acetaldehyde	(ppm/ppmC)	0.075	0.075		
Δ[organic] /added organic				Day 1	Day 2
(ppb/millimolesC m^{-2} day^{-1})[g]		41.03	7.03	45.59	71.87

---

[a] No correction made for latitude; i.e., differences between local sun time and standard clock time neglected.

[b] Values used for intermediate times obtained by interpolating between tabulated values.

[c] Time on following day.

[d] Does not count pollutants left over from the previous day, when applicable.

[e] The pollutants aloft on day 2 were calculated in separate simulations The aloft level simulations begin at 2100 LDT on day 1, using as initial conditions the pollutant concentrations at the ground level at that time, and they continue until the inversion height increase is assumed to end. No emissions are assumed to occur into this aloft air mass, and the aloft air mass is assumed to be diluted with clean air by a factor of 2 between 0800 and 1500 LDT.

[f] Emissions schedules are given in terms of relative emission rates (factors) at various times, with factors for intermediate times obtained by interpolating between tabulated values. Absolute emission rates are such that the total daily "initial + emitted" ROG and NO_x are as tabulated above.

[g] Factors relating Δ[organic], the final concentration of the test organic which would be present if it did not react, to the number of millimoles C m^{-2} day^{-1} of test organic added in the reactivity assessment calculations.

for use in Regulatory Impact Analyses for the national ozone standard to be applied in various regions of the United States, and differ only in the total amount of dilution assumed. The EKMA-I formulation employed the input data recommended for the low dilution region (designated Region I), and the EKMA-III scenario employed the mixing height schedule recommended for Region III, the highest dilution region. These are designated "EKMA" scenarios because they were designed to represent input data used for various site-specific EKMA models used in State Implementation Plans (Gipson and Freas 1983). Since the two "EKMA" scenarios employed in this study both incorporated the same representations of emissions schedules and levels of pollutants present initially and aloft, calculations were also carried out using a third, slightly more complex scenario which represented these factors somewhat differently, and which was also more suitable for multi-day simulations than the one-day "EKMA" scenarios. This scenario consisted of a two-day simulation, and was therefore designated the "multi-day" (MD) scenario. Carter and Atkinson (1987b) should be consulted for more details concerning the formulation of these scenarios, and the source of the input data used.

Because the reactivities of organic compounds depend significantly on the ROG/NO_x ratios, for all scenarios the calculations were carried out using eight different ROG/NO_x ratios, ranging from 4 to 40 ppmC ROG/ppm NO_x. The same ratios were employed for all scenarios.

Two separate surrogate mixtures were used to simulate the base-case ROG emissions in these calculations. The mixture designated "Surg-4" was essentially the same as the "mini-surrogate" mixture employed in the incremental reactivity experiments carried out in this study, and also in our previous experimental incremental reactivity study (Carter and Atkinson 1987a). This mixture was used with the "EKMA-I" formulation only. The other base-case ROG surrogate mixture employed, which was used with all three model formulations, was the more complex "Surg-8" mixture designed to represent the default surrogate composition recommended by the EPA for use in EKMA calculations in cases where no composition data are available (EPA, 1984). The derivation of the compositions of these two mixtures, summarized in Table 8, are discussed in more detail by Carter and Atkinson (1987b).

In order to provide a comparison of the airshed reactivity calculations with reactivities which might be observed in environmental chamber experiments carried out at the same base case ROG and NO_x levels, calculations using the "ITC" scenario, representing the conditions of the environmental chamber used in this and our previous experimental reactivity study (Carter and Atkinson 1987a), were also carried out. These calculations employed the "Surg-4" (i.e., the "mini-surrogate") mixture

Table 8. Compositions of the Surrogate Mixtures Used to Represent Base-Case ROG Emissions

Compound	ppm Compound per ppmC Surrogate	
	SURG-4	SURG-8
Ethene	0.0	0.025
Propene	0.0417	0.0167
trans-2-Butene	0.0064	0.0
n-Butane	0.177	0.0375
n-Pentane	0.0	0.0400
iso-Octane	0.0	0.0188
Toluene	0.0	0.0179
m-Xylene	0.0177	0.0156
Formaldehyde	0.0	0.0375
Inert	0.0	0.113

which was used in the experiments. The input data used in the ITC, Surg-4 simulations were the same as employed in our theoretical incremental reactivity study (Carter and Atkinson 1987b), and are summarized in Table 9. Since the calculations of Carter and Atkinson (1987b) were carried out prior to the experiments discussed in this report, the representation of chamber conditions was slightly different than used in the present simulations of these experiments (shown in Table 6), but these differences are expected to be minor in terms of predictions of calculated incremental reactivities. The main difference between the "ITC" reactivity calculations discussed in this section and the simulations of our experimental reactivity determinations is that the present simulations were carried out at a variety of ROG/NO_x ratios, and the reactivities derived from the final maximum ozone yields and amounts of NO oxidized, rather than the reactivities being derived as a function of time for the conditions of a single high ROG/NO_x experiment, as was the case out in the experimental study.

2. Results of the Airshed Reactivity Simulations

The maximum ozone yields observed in the base-case simulations for all six representative airshed and ITC scenarios and the eight ROG/NO_x ratios are shown in Table 10, and the incremental reactivities calculated

Table 9. Summary of Conditions, Input Data and Values of Chamber-Dependent Parameters Employed in the Model Simulations of the ITC, Surg-4 Scenario

Parameter(s)	Value or Derivation
Initial ROG	4.0 ppmC
Initial NO_x	varied; $NO/NO_2 = 3.0$
Reaction Conditions	Static. No reactant injections after the irradiation begins. No dilution.
NO_2 Photolysis Rate	$0.325\ min^{-1}$
Other Photolysis Rates	Calculated from the NO_2 photolysis rate, the absorption coefficients and quantum yields of the photolysis reactions, and the ITC blacklight distribution given by Carter et al. (1986b)
Water Concentration	2.0×10^4 ppm
Temperature	300 K
Rates or Rate Constants of Chamber-Dependent Reactions:	
$O_3 \xrightarrow{\text{wall}} \text{loss of } O_3$	$1.3 \times 10^{-4}\ min^{-1}$
$hv \xrightarrow{\text{wall}} OH$	$0.049\ ppb\ min^{-1}$
$\text{wall} \rightarrow NO_2$	$0.049\ ppb\ min^{-1}$
$N_2O_5 \xrightarrow{\text{wall, } H_2O} \text{Loss of } N_2O_5$	$3.5 \times 10^{-3}\ min^{-1}$
$NO_2 \xrightarrow{\text{wall}} 0.2\ HONO + 0.8 \text{ loss of } NO_2$	$1.4 \times 10^{-4}\ min^{-1}$

Table 10. Calculated Daily Maximum Ozone Yields for the Base-Case Simulations for the Airshed and ITC Scenarios

	Daily Maximum Ozone (ppm)					
ROG/	ITC	EKMA-1		EKMA-3	MD, Surg-8	
NO_x	Surg-4	Surg-4	Surg-8	Surg-8	Day 1	Day 2
4	0.017	0.058	0.085	0.093	0.031	0.060
6	0.061	0.136	0.175	0.099	0.075	0.242
8	0.152	0.195	0.209	0.096	0.130	0.257
10	0.239	0.201	0.203	0.093	0.159	0.247
12	0.309	0.193	0.193	0.090	0.159	0.233
16	0.404	0.176	0.175	0.085	0.146	0.207
20	0.428	0.162	0.161	0.081	0.134	0.188
40	0.306	0.122	0.121	0.070	0.096	0.132

(on a per carbon basis) for ethane and the two n-pentadecane models for the conditions of those simulations are given in Table 11. The ratios of the reactivities calculated for the two n-pentadecane models to those calculated for ethane are given in Table 12. The general features of the base-case simulations for these scenarios, and of calculated incremental reactivities for the conditions of these scenarios and the kinetic, mechanistic, and environmental factors which affect them, are discussed in detail elsewhere (Carter and Atkinson 1987b), and in the following discussion only on those results relevant to the specific purpose of this study are dealt with.

The calculated reactivities of ethane are seen to be always positive, and depend primarily on the amount of dilution occurring in the scenario, being highest in the highest dilution "EKMA-3" scenario, and the lowest in the "ITC" scenario, where no dilution is assumed to occur. The reactivity of ethane also depends on the ROG/NO_x ratio, being the highest for ratios slightly less than those most favorable for ozone formation, and lowest at the highest ROG/NO_x ratio examined in this study. The maximum reactivity of ethane also appears to be somewhat higher when the Surg-8 mixture rather than the Surg-4 mixture is used for the base case ROG surrogate, and is also somewhat higher on day 2 of the Multi-Day simulation than on day 1.

Table 11. Calculated Incremental Reactivities for Ethane and n-Pentadecane for the Airshed and ITC Scenarios

ROG/	Calculated Incremental Reactivity (per carbon basis)					
	ITC	EKMA-1		EKMA-3	MD, Surg-8	
NO_x	Surg-4	Surg-4	Surg-8	Surg-8	Day 1	Day 2
Ethane						
4	0.003	0.012	0.023	0.072	0.012	0.022
6	0.003	0.023	0.042	0.054	0.024	0.060
8	0.004	0.026	0.027	0.043	0.036	0.023
10	0.004	0.016	0.019	0.036	0.026	0.020
12	0.005	0.013	0.015	0.030	0.017	0.016
16	0.005	0.010	0.011	0.023	0.012	0.011
20	0.004	0.008	0.009	0.019	0.009	0.009
40	0.003	0.005	0.005	0.010	0.005	0.005
n-Pentadecane, Model "B"						
4	-0.016	-0.018	0.038	0.155	0.018	0.051
6	-0.015	-0.014	0.061	0.126	0.040	0.112
8	-0.012	-0.003	0.057	0.094	0.048	0.050
10	-0.009	0.019	0.040	0.068	0.042	0.041
12	-0.006	0.012	0.026	0.047	0.033	0.031
16	-0.001	-0.001	0.008	0.017	0.019	0.017
20	0.009	-0.008	-0.002	-0.002	0.008	0.008
40	0.007	-0.024	-0.025	-0.039	-0.017	-0.014
n-Pentadecane, Model "A"						
4	-0.042	-0.078	-0.017	0.058	-0.011	0.011
6	-0.040	-0.109	-0.031	0.081	-0.013	0.026
8	-0.039	-0.103	0.012	0.053	-0.027	0.028
10	-0.040	-0.034	0.004	0.025	-0.005	0.019
12	-0.041	-0.034	-0.008	0.000	0.005	0.013
16	-0.037	-0.044	-0.027	-0.037	-0.008	-0.002
20	-0.016	-0.051	-0.040	-0.062	-0.019	-0.012
40	-0.007	-0.067	-0.069	-0.105	-0.052	-0.042

Table 12. Ratios of Calculated Incremental Reactivities for n-Pentadecane to Those for Ethane for the Airshed and ITC Scenarios

	n-Pentadecane Reactivity/Ethane Reactivity					
ROG/	ITC	EKMA-1		EKMA-3	MD, Surg-8	
NO_x	Surg-4	Surg-4	Surg-8	Surg-8	Day 1	Day 2
n-Pentadecane Model "B"						
4	-4.9	-1.5	1.7	2.1	1.6	2.3
6	-4.7	-0.6	1.4	2.3	1.6	1.9
8	-3.3	-0.1	2.2	2.2	1.3	2.2
10	-2.1	1.2	2.1	1.9	1.7	2.0
12	-1.3	0.9	1.7	1.6	1.9	2.0
16	-0.2	-0.1	0.8	0.8	1.6	1.6
20	2.2	-1.1	-0.3	-0.1	0.9	0.9
40	2.6	-5.2	-4.8	-3.8	-3.8	-3.2
n-Pentadecane Model "A"						
4	-12.6	-6.4	-0.7	0.8	-1.0	0.5
6	-12.7	-4.7	-0.7	1.5	-0.5	0.4
8	-10.8	-4.0	0.5	1.2	-0.8	1.2
10	-9.3	-2.0	0.2	0.7	-0.2	1.0
12	-8.3	-2.7	-0.5	0.0	0.3	0.9
16	-7.3	-4.5	-2.5	-1.6	-0.7	-0.2
20	-4.1	-6.6	-4.7	-3.3	-2.1	-1.4
40	-2.8	-14.1	-13.3	-10.4	-11.4	-9.3

The calculated reactivities for n-pentadecane depend significantly on which mechanism is assumed, with the reactivities calculated assuming the higher overall nitrate formation of mechanism "A" in all cases being less than calculated when using mechanism "B". However, regardless of which mechanism was employed, the calculated reactivities depended significantly on the conditions of the scenario, and in general the nature of the dependences for both mechanisms were similar. Unlike ethane, but consistent with the results of our chamber experiments, the reactivities of n-pentadecane can be negative under some conditions and positive under others. For the airshed scenarios, the general tendency is for the incremental reactivities to be the lowest or the most negative at the extreme high or low ROG/NO_x ratios, and the highest or least negative at the mid

ROG/NO_x ratios which are the most favorable to ozone formation. On the other hand, the n-pentadecane reactivity calculated for the ITC scenario tends to increase monotonically as the ROG/NO_x ratio is increased. For both n-pentadecane mechanisms, the reactivity at low and middle ROG/NO_x ratios are significantly affected by the base case ROG surrogate employed, with significantly higher reactivities being calculated for the more complex (and representative) Surg-8 mixture than for the Surg-4 mixture used in the experiments carried out in this study. In addition, the reactivities of both n-pentadecane mechanisms a low and mid-ROG/NO_x ratios tend to increase with the number of days in the multi-day scenario, going from generally negative on day 1 to positive on day 2 in the case of the less reactive model "A". The negative reactivities at the highest ROG/NO_x ratios appear to be much less sensitive to the conditions of the scenarios, at least for the scenarios representing airshed conditions, though they are highly sensitive to which of the two alternative n-pentadecane mechanisms is assumed.

The dependencies of the calculated reactivities on scenario conditions are, as expected, based on the nature of the n-pentadecane reaction mechanisms employed, and are consistent with the general trends and dependences for calculated reactivities for other compounds and reaction mechanisms (Carter and Atkinson 1987b). The low or negative reactivities at the low ROG/NO_x ratios is attributed to the radical inhibition characteristics of the n-pentadecane mechanism, the low or negative reactivities at the high ratios are attributed to the presence of NO_x sinks, and the positive or higher reactivities at the mid ROG/NO_x range is due to the NO to NO_2 conversions involved in the n-pentadecane photooxidation reactions. In the case of the higher alkanes, both the radical and NO_x sinks result from the formation of organic nitrates, and the mechanism which assumes higher nitrate yields consistently causes lower reactivities throughout the entire ROG/NO_x range, regardless of the scenario. The much less dramatic dependences of the ethane reactivities on ROG/NO_x ratio are due to the fact that the ethane photooxidation mechanism does not have significant radical or NO_x sinks (or sources), with the major mechanistic factor influencing its reactivity being its tendency to convert NO to NO_2, leading to positive reactivities under all conditions.

Table 12 shows that the question of whether n-pentadecane is more reactive than ethane under atmospheric conditions depends significantly not only on which mechanism is assumed to be correct, but also on the conditions of the scenario and the nature of the base-case ROG surrogate. If the more complex Surg-8 mixture is assumed to be a more appropriate representative of of organic emissions into real airsheds, and if the more reactive n-pentadecane model "B" is assumed, then these calculations indicate that under conditions most favorable for ozone formation, n-pentadecane is approximately twice as reactive as ethane. Based on these assumptions, n-pentadecane is predicted to inhibit ozone only under very low NO_x concentration conditions; these conditions being those which many compounds which are otherwise considered to be highly reactive, such as aromatics and internal alkenes, are also inhibitors (Carter and Atkinson 1987b). However, if the less reactive model "A" is assumed, then the reactivity of n-pentadecane is calculated to approach or exceed that of ethane only in the highest dilution scenario or on day 2 of the multi-day scenario, and only then under the conditions most favorable to ozone formation.

Although the effects of the nature of the base-case ROG surrogate on calculated reactivities has not been comprehensively examined, the results of these calculations indicate that this can be highly important in affecting the reactivities calculated for species like n-pentadecane. This is indicated by the significantly lower reactivities calculated for either n-pentadecane mechanism when the Surg-4 mixture was used rather than Surg-8 to represent base case emissions in the EKMA-1 scenario. This is despite the fact that both these surrogate mixtures are themselves very similar in their overall reactivities, both in terms of overall ozone formation when they are used to represent the base case ROG mixtures, and in terms of their incremental reactivities in these model scenarios (Carter and Atkinson 1987b). It can be argued that the Surg-8 mixture, being more complex, is probably more representative of emissions into real airsheds than is the Surg-4 mixture. However, the possibility that the use of other complex, and perhaps even more representative, mixtures to represent base case ROG emissions in these scenarios may also result in predictions of significantly different reactivities of n-pentadecane relative to those of ethane cannot be ruled out. Thus the effects of base case ROG emissions on incremental reactivities is clearly an important area of uncertainty in the predictions of relative atmospheric reactivities of these species, and this has not been adequately investigated.

The implications of the results of these calculations with regard to the question of the reactivities of the printing oils under atmospheric conditions is discussed in the following section.

V. CONCLUSIONS

The experiments carried out in this study have provided useful data for the purpose of assesing the reactivities of two representative heatset printing oils with respect to ozone formation in the atmosphere. However, major uncertainties still remain as to whether they should be judged to be more reactive than ethane under realistic atmospheric conditions. The results of the experiments carried out in this study were consistent with the earlier Battelle results in that they indicated that these printing oils can inhibit ozone formation under some conditions and promote it under others, and thus the experiments do not, in themselves, clearly indicate whether the printing oils are more likely to inhibit or promote ozone formation when emitted into the atmosphere. For compounds such as these, whose effects on ozone formation are highly dependent on conditions under which they react, model simulations of conditions more representative of real airsheds than can be attained in environmental chamber experiments are required to assess their atmospheric reactivities. Thus, the primary utility of the experiments carried out in this study was to provide the data needed to test the reliability of the model predictions.

The predictions of the model were reasonably consistent with the results of the experiments employing ethane, the compound which is used as the standard to define the reactivity cutoff. The experiments with n-pentadecane and the printing oils Magie-47 and Magie-470 indicate that these substances are approximately similar in overall reactivity, though Magie-470 may be slightly more reactive than the other when irradiated in NOx-air mixtures in the absence of other organic pollutants. This suggests that a mechanism based on the chemistry of n-pentadecane should be appropriate in estimating the approximate atmospheric reactivities of Magie-47, and the approximate lower limit of the reactivity of Magie-470.

However, the atmospheric reaction mechanisms of high molecular weight alkanes such as n-pentadecane are highly uncertain, and have to be estimated based on existing mechanisms for much lower molecular weight (i.e., $\leq C_9$) alkanes, whose mechanism are themselves uncertain. Two alternative n-pentadecane mechanisms, based on differing assumptions concerning overall organic nitrate yields, were examined in the model calculations carried out in this study. Overall organic nitrate yields are probably the most important single factor affecting predictions of overall reactivities of alkanes. The n-pentadecane mechanism with the lower nitrate yield, which also is the mechanism which is more consistent with the mechanism used in our model for the lower molecular weight (C_6-C_9) alkanes, was found to give better fits to the data. This model was able to predict the approximate magnitudes of the reactivities of n-pentadecane and the printing oils, and the dependences of these reactivities on reaction time in the incremental reactivity experiments.

However, there were areas of discrepancy in the model simulations of the experiments with n-pentadecane and the printing oils, particularly in predictions of incremental reactivities in experiments with the lowest amounts of added printing oil. Without carrying out additional experiments, it is not clear whether these discrepancies are due to problems with the mechanism, or to problems in our characterization of the conditions of the incremental reactivity experiments. In addition, experiments where n-pentadecane or the printing oils are irradiated by themselves in NOx-air mixtures do not provide a very precise test for the mechanism because of their sensitivities to the variabilities in the chamber radical source. However, those experiments did confirm the prediction of the model that these substances tend to inhibit radical levels. Thus, although the model predictions based on our best estimate of the n-pentadecane reaction mechanism was able to at least approximately simulate our experimental results, this mechanism has significant areas of uncertainty, and the available data base is insufficient for this mechanism to be considered to be completely validated for use in predicting atmospheric reactivities of n-pentadecane and the printing oils.

However, given our current limited knowledge of the details of atmospheric photooxidation reactions of the higher alkanes and the products formed, the performance of the model in simulating the results of the experiments with n-pentadecane and the printing oils is probably as good as can reasonably be expected at the present time. For this reason, and in order to obtain at least a qualitative indication of how the reactivities of the printing oils and ethane under atmospheric conditions might differ from thos observed in environmental chamber experiments, simulations of incremental reactivities under atmospheric conditions were also carried out.

These atmospheric simulations indicate that if our n-pentadecane mechanism is at least approximately appropriate for estimating the reactivities of the printing oils, then the reactivities of these oils will depend significantly on the conditions under which they are emitted. This is true regardless of whether the reactivities are considered in an absolute sense (in terms of moles additional ozone formed per mole carbon n-pentadecane or printing oil emitted) or in terms of reactivities relative to those of ethane. The reactivities predicting using our n-pentadecane mechanism are highly dependent not only on ROG/NO_x ratio, but also on the mixture used as a surrogate to represent base case ROG emissions. This mechanism predicts that under atmospheric conditions, the printing oils are negatively reactive with respect to ozone formation at high ROG/NO_x ratios under most conditions, and also at low ROG/NO_x ratios under some conditions, but that they are positively reactive under the ROG/NO_x conditions which tend to be the most favorable for ozone formation. In particular, if the eight-component ROG surrogate mixture, which is based on EPA recommended defaults for use in EKMA calcuations where no ROG composition data are available (EPA 1984), is used in the airshed model simulations, then the standard n-pentadecane mechanism predicts that the printing oils would be approximately twice as reactive as ethane (on a per carbon basis) under ROG/NO_x conditions which are the most favorable to ozone formation. However, the sensitivity of the predicted relative reactivities to the conditions under which they are emitted, particularly the ROG/NOx ratio and the nature of the base case ROG surrogate, combined with uncertainties in the n-pentadecane mechanism, means that our estimates of the atmospheric reactivities of the printing oils are subject to a considerable degree of uncertainty.

Thus to conclude, the currently available experimental data and theoretical estimates and calculations suggest that, with respect to atmospheric ozone formation, it is more probable than not that under some conditions the printing oils may be more reactive than ethane. However, for the reasons indicated above, the possibility that the printing oils may be significantly more or less reactive than predicted by this model cannot at present be ruled out. Until more is known about the details of the atmospheric photooxidation reactions of the higher alkanes and other components of the printing oils and how their reactivities will depend on the conditions of the airshed into which they are emitted, it will not be possible to make definitive conclusions as to whether the printing oils should be judged to be reactive for regulatory purposes.

Finally, it should be recognized that this study addressed only the effects of emissions of the printing oils on ozone formation. The emissions of these oils could have other impacts on air quality, such as aerosol formation, formation of toxic products, etc., which should also be taken into account in making any decisions on whether to regulate the emissions of these oils. A discussion of these aspects is beyond the scope of this study, but obviously they should not be ignored.

VI. REFERENCES

Atkinson, R., A. C. Lloyd, and L. Winges (1982), Atmos. Environ., 16, 1341.

Atkinson, R., W. P. L. Carter, and A. M. Winer (1983), "Evaluation of Hydrocarbon Reactivities for Use in Control Strategies," Final Report to California ARB Contract No. A0-105-32, May.

Atkinson, R. and A. C. Lloyd (1984), J. Phys. Chem. Ref. Data, 13, 315.

Atkinson, R. (1986), "Kinetics and Mechanisms of the Gas-Phase Reactions of the Hydroxyl Radical with Organic Compounds Under Atmospheric Conditions", Chemical Reviews, 86, 69.

Battelle, Columbus Laboratories (1982), "Investigation of the Volatility of Heat Set Printing Oils", Summary Report on Task 1 to the Graphics Arts Technical Foundation, September.

Battelle, Columbus Laboratories (1983), "Investigation of the Photochemical Reactivity of Heat Set Printing Oils", Summary Report on Task 2 to Graphic Arts Technical Foundation, April.

Battelle, Columbus Laboratories (1984), "Further Investigation of the Photochemical Reactivity of Heatset Printing Oils", Summary Report on Tasks A and B to The Environmental Conservation Board of the Graphics Communications Industries c/o Graphics Arts Technical Foundation, August.

Bufalini, J. J., T. A. Walter, and M. M. Bufalini (1977), Environ. Sci. Technol., 11, 1181.

Carter, W. P. L., A. C. Lloyd, J. L. Sprung, and J. N. Pitts, Jr. (1979), Int. J. Chem. Kinet, 11, 45.

Carter, W. P. L., R. Atkinson, A. M. Winer and J. N. Pitts, Jr. (1982), Int. J. Chem. Kinet., 14, 1071.

Carter, W. P. L., A. M. Winer, R. Atkinson, M. C. Dodd, W. D. Long, and S. M. Aschmann (1984), "Atmospheric Photochemical Modeling of Turbine Engine Fuels. Phase I. Experimental Studies," Final Report to the U. S. Air Force, ESL-TR-84-32, September.

Carter, W. P. L. and R. Atkinson (1985), J. Atmos. Chem., 3, 377.

Carter, W. P. L., M. C. Dodd, W. D. Long, and R. Atkinson (1985), "Outdoor Chamber Study to Test Multi-Day Effects", EPA-600/3-84-115, March.

Carter, W. P. L., W. D. Long, L. N. Parker, and M. C. Dodd (1986a), "Effects of Methanol Fuel Substitution on Multi-Day Air Pollution Episodes," Final Report on California Air Resources Board Contract No. A3-125-32, April.

Carter, W. P. L., F. W. Lurmann, R. Atkinson, and A. C. Lloyd (1986b), "Development and Testing of a Surrogate Species Chemical Reaction Mechanism," EPA-600/3-86-031, August.

Carter, W. P. L. and R. Atkinson (1987a), "An Experimental Study of Incremental Hydrocarbon Reactivity," Environ. Sci. Technol., 21, 670.

Carter, W. P. L., and R. Atkinson (1987b), "A Computer Modeling Study of Incremental Hydrocarbon Reactivity," Report on U. S. EPA Cooperative Agreement No. CR810214-01.

Darnall, K. R., R. Atkinson, A. M. Winer, and J. N. Pitts, Jr. (1981), J. Air Pollut. Contr. Assoc., 31, 262.

Doyle, G. J., P. J. Bekowies, A. M. Winer, and J. N. Pitts, Jr. (1977), Environ. Sci. Technol. 11, 45.

EPA (1984) "Guideline for Using the Carbon Bond Mechanism in City Specific EKMA", EPA-450/4-84-005, February.

Gipson, G. L. and W. P. Freas (1983), "Use of City-Specific EKMA in the Ozone RIA", U. S. Environmental Protection Agency, July.

Peterson, J. T. (1976) "Calculated Actinic Fluxes (290 - 700 nm) for Air Pollution Photochemistry Applications", EPA-600/4-76-025, June.

Pitts, J. N., Jr., K. Darnall, W. P. L. Carter, A. M. Winer, and R. Atkinson (1979), "Mechanisms of Photochemical Reactions in Urban Air," EPA-600/3-79-110, November.

Stephens, E. R., F. R. Burleson, and E. A. Cardiff (1965), J. Air Pollut. Contr. Assoc., 15, 87.

Stephens, E. R. and M. A. Price (1973), J. Chem. Educ., 50, 351.

Winer, A. M., J. M. Peters, J. P. Smith, and J. N. Pitts, Jr. (1974), Environ. Sci. Technol., 8, 1118.

Zafonte, L., P. L. Rieger, and J. R. Holmes (1977), Environ. Sci. Technol. 11, 483.

APPENDIX A

PRELIMINARY REPORT ON COMPUTER MODELING OF THE BATTELLE CHAMBER DATA

In this Appendix, the full text of the report submitted to the EPA describing our preliminary computer modeling study of the Battelle chamber studies of heatset printing oils is attached. The report was submitted on April 7, 1986, and is reproduced without modification. It is entitled "A Computer Modeling Study of the Photochemical Reactivity of Heatset Printing Oils", and the authors are William P. L. Carter and Roger Atkinson.

SUMMARY

A preliminary set of computer model simulations of the environmental chamber experiments conducted at Battelle, Columbus Laboratories, aimed at determining the relative ozone atmospheric formation potentials of ethane and heatset printing oils, both by themselves and in the presence of a mixture of other organics representative of emissions into urban atmospheres, have been carried out. The purpose of these model simulations was to determine if our current understanding of the atmospheric chemistry of the larger alkanes, the predominant components of the printing oils, is consistent with the results of the Battelle experiments.

The results of the chemical computer model simulations were generally in qualitative agreement with the Battelle chamber experimental data. However, the chemical mechanisms for the atmospheric reactions of the major constituents of the printing oils are highly uncertain, and the model did not fit the experimental maximum ozone yields and times unless it was assumed that other classes of highly reactive constituents were present in the printing oils. In addition, the model did not correctly simulate the ozone yields observed in the ethane-NO_x-air irradiations, suggesting that chamber effects were not correctly characterized in the model. Thus, it is concluded that the chemical mechanism employed in these calculations is not sufficiently well validated for use in airshed calculations of the type needed for control strategy calculations.

It is clear that further studies are necessary before any decision can be made concerning the contribution that emissions of these printing oils make to ozone formation in the atmosphere, or even as to whether they are more reactive than ethane under conditions representative of the atmosphere. At a minimum, further environmental chamber studies are required so the model can be tested under a wider variety of conditions and with fewer uncertainties regarding chamber characterization.

A. INTRODUCTION

Web-offset printing operations can result in the emission of printing oils into the atmosphere, and these vaporized oils may undergo photochemical reaction and hence contribute to the formation of atmospheric ozone. Since ozone is a major air quality problem in many urban areas, the precursors to ozone formation are subject to regulatory control under State Implementation Plans. To determine whether controls of printing oil emissions need to be included in such plans, it is necessary to establish whether the presence of these oils in the atmosphere can contribute significantly to ozone formation, i.e., to establish whether these oils can be considered to be "reactive" with respect to ozone formation.

To be considered to be "reactive", an organic compound or mixture must (1) be sufficiently volatile so that it can react in the gas phase, (2) react in the atmosphere sufficiently rapidly that its reactions can be of significance, and (3) react in such a manner that it contributes to ozone formation. In many cases it is obvious whether or not a compound or mixture can be considered to be reactive or unreactive. If a compound has a negligible volatility or is essentially inert in the atmosphere, it can be considered to be unreactive. If however, relatively low concentrations of a compound cause significant ozone formation when irradiated in the presence of NO_x in environmental chambers, then it is clearly reactive. In cases when a compound or mixture is either marginally volatile, reacts in the atmosphere but does so relatively slowly, or reacts in such a way that it is not clear whether or not its reactions enhance or suppress ozone formation, then it is not immediately obvious whether to classify this compound or mixture as reactive or unreactive. In these cases, the current regulatory policy is to use the reactivity of ethane, with respect to reaction with the OH radical, to define the borderline between reactive and unreactive organic compounds.

In order to obtain the data necessary to assess whether heatset printing oils must be considered to be reactive the Environmental Conservation Board of the Graphic Arts Technical Foundation contracted Battelle, Columbus, Laboratories to determine the volatility of representative printing oils and to study their photochemical reactivity in environmental chamber irradiations. The results of these Battelle studies are reported elsewhere (Battelle, 1982, 1983, 1984). In summary, they determined that these oils are sufficiently volatile that "virtually all of the oil constituents are available to participate in gas phase photochemical reactions" (Battelle, 1983), and thus they cannot be considered to be unreactive on the basis of volatility. The results of the environmental chamber experiments are more ambiguous since some experiments indicate that, with respect to ozone formation, the printing oils studied are somewhat more reactive than ethane, while others indicated that they were less reactive. Thus these printing oils appear to be on the borderline of being defined as reactive, and despite the Battelle study it is still uncertain as to whether regulation of these oils as ozone precursors is appropriate, if ethane is to be used as the cutoff in defining reactivity.

A significant amount of this uncertainty arises from the problems of interpreting environmental chamber data when used to study relatively unreactive compounds. This is because the conditions under which environmental chamber experiments are carried out are never exactly the same as those in the ambient atmosphere, and these differences become highly significant when comparing relatively unreactive substances such as ethane and printing oils. In particular, chamber effects (Carter et al., 1982) have a significant influence on the result of environmental chamber irradiations of less reactive mixtures (Bufalini et al., 1977), and this must be taken into account in interpreting the results of such experiments. In addition, it is rarely practical to use environmental chamber experiments to attempt to simulate the full range of reaction conditions which occur in the atmosphere, and which affect the relative reactivity of the substances being compared.

In principle, computer model simulations, in which the chemical mechanism used is tested by comparing its predictions against the available environmental chamber data, can be employed to predict reactivities under atmospheric conditions. Thus, the computer model can be used to correct for chamber effects and to make extrapolations from the conditions of the environmental chamber experiments to bc those in urban airsheds. However, in order for this procedure to be scientifically credible, and hence appropriate as a basis for control decisions, it is necessary that the model employed be consistent with our current understanding of atmospheric chemistry in general, and with our knowledge of the atmospheric reactions of the major constituents of the printing oils in particular. Heatset printing oils consist primarily of saturated hydrocarbons with an average molecular weight of approximately 205. This corresponds to that of n-pentadecane (n-$C_{15}H_{32}$). Such high molecular weight alkanes are expected to be reactive in the sense that they have relatively high rate constants for reaction with OH radicals (the primary mode of reaction of saturated compounds in the atmosphere), but react in a manner which removes radicals and NO_x from the system (Carter and Atkinson, 1985). This latter tendency reduces their reactivity, and may even make them ozone inhibitors under certain conditions. However, without the benefit of computer chemical model calculations it is not obvious whether or not the expected atmospheric chemistry of these larger alkanes is consistent with the results of the Battelle experiments.

Therefore, in order to help elucidate the interpretation of the results of the Battelle experiments the EPA requested the Statewide Air Pollution Research Center (SAPRC) of the University of California in Riverside, as part of our ongoing Cooperative Agreement to study mechanistic aspects of reactivity, to carry out a chemistry modeling study of the printing oils used in the Battelle experiments.

The results of the initial computer model simulations of the Battelle chamber experiments are discussed in this Preliminary Report.

B. MODEL SIMULATIONS OF CHAMBER EXPERIMENTS

1. Chamber Experiments Modeled

Three types of environmental chamber experiments were carried out in Battelle's study of the photochemical reactivity of printing oils: (1) single component-NO_x-air irradiations in which either MagieSol 47 oil, Magie 470 oil, or ethane were irradiated in the presence of NO_x without other added reactants, (2) incremental reactivity experiments in which one of the oils or ethane was added to an "urban surrogate" - NO_x mixture and irradiated, and (3) a control experiment in which the "urban surrogate" was irradiated in the presence of NO_x without any added ethane or printing oil. All of the experiments were carried out with the initial NO and NO_2 being approximately 0.2 ppm each, and thus the only parameters varied were the amount and nature of organics present. Most of the experiments were of the incremental reactivity type, and these were carried out at several hydrocarbon/NO_x ratios and with varying amounts of oil or ethane added.

The composition of the "urban surrogate" employed in the incremental reactivity experiments is given in Table 1. While most of the experiments with added oils employed the Magie 47 or Magie 470 oils, one experiment was carried out utilizing Magie 500 oil. A summary of the conditions and major results of the experiments examined in this study is given in Tables 2 and 3 (taken from Battelle, 1983, 1984).

The results of these experiments have been discussed previously (Battelle, 1983, 1984). Briefly, the following relevant observations are noted:

(1) In terms of the time required to reach the ozone maximum in the single component irradiations, the Magie 47 oil and the Magie 470 oil were found to be more reactive than ethane, with the Magie 47 oil being the more reactive of the two. However, slightly less ozone was formed in the single component irradiations of the oils than in the comparable experiment with ethane, but the difference is probably not experimentally significant.

(2) A series of experiments was carried out in which 33% (on a molar carbon basis) of the "urban surrogate" was replaced by ethane, Magie 47 oil or Magie 470 oil. In all cases, the substitution caused the time to reach the ozone maximum to increase, with the amount of increase being only slightly greater for ethane than for the two oils. There was no significant change in the maximum ozone yield caused by the substitutions. Thus, contrary to the results of the single-component runs, these runs suggest the oils are similar in reactivity to ethane.

(2) Several other experiments were carried out where ethane or the oils were added to the "urban surrogate" at different hydrocarbon/NO_x ratios, but in these experiments no corresponding runs without the added ethane or oil were carried out, and the amounts of ethane added in these runs was much less, on a mole carbon basis, than the amount of added oils. The data from these runs are consistent with the single component runs in that they indicate that the 470 oil is more reactive than the 47 oil. However, some of these runs also suggest that under some conditions the oils can be less reactive than ethane, contrary to the results indicated above. In particular, the 4 ppmC surrogate runs with relatively large amounts of added oil had somewhat longer times to ozone maximum, and formed less ozone, than did the run with the same amount of added surrogate, and a lesser amount of added ethane.

Table 1. Representation of Battelle 17-Hydrocarbon "Urban Mixture" by Species in the Model Employed in This Study

Battelle Urban Mixture		Representation in Model		Comments
Compound	ppm in 1 ppmC tot	Compound	ppm in 1 ppmC tot	
acetylene	0.0337			Acetylene reacts slowly, so its reactions can be ignored.
ethane	0.0248	ethane	0.0248	
propane	0.0099	ethane n-butane	0.0050 0.0050	
n-butane	0.0245	n-butane	0.0245	
n-pentane	0.0092	n-pentane	0.0092	
2-methylpropane 2-methylbutane 2-methylpentane	0.0057 0.0173 0.0109	isooctane	0.0339	This amount of isooctane has the same total OH reactivity[a] and total ppm as the three branched alkanes it represents.
ethene	0.0401	ethene	0.0401	
propene	0.0087	propene	0.0087	
trans-2-butene	0.0106	acetaldehyde	0.0213	Rapid reaction of internal alkenes to form the expected carbonyl fragments assumed. Acetone reacts slowly, so is ignored.
2-methyl-2-butene	0.0032	acetaldehyde	0.0032	
benzene toluene m-xylene p-ethyltoluene 1,2,4-trimethyl benzene	0.0072 0.0151 0.0171 0.0062 0.0032	toluene m-xylene	0.0248 0.0240	This representation gives the same OH reactivity[a] and total ppm of aromatics.

---

[a] "OH reactivity" is the sum of the product of the concentrations of the reactants and their OH radical rate constants.

Table 2. Observed and Calculated Ozone Maxima for the Single Component Environmental Chamber Experiments Carried Out in the Battelle Study of the Photochemical Reactivity of Heatset Printing Oils[a]

Run ID[b]	Compound	Init. HC ppmC	Experimental Ozone Max. (ppm)	(hours)	Calculated Ozone Maximum Model A (ppm)	(hrs)	Model B (ppm)	(hrs)	Parameter Varied in Calc.
									k_{RS} (ppb)
					0.03	>24			0.3
2-16	ethane	4	0.22	22.0	0.13	22.5			0.6
					0.16	16.0			1.0
					0.13	>24			0.3
2-7	ethane	12	0.37	21.0	0.24	20.0			0.6
					0.28	14.5			1.0
									% m-Xylene
					0.17	21.5	0.28	20.0	0
2-5	47 oil	12	0.34	15.0	0.22	18.5	0.33	16.5	2
2-6	470 oil	12	0.31	12.0	0.28	14.5	0.41	13.0	5
					0.36	10.0	0.48	8.5	10
					0.20	21.0	0.36	19.0	0
2-18	47 oil	30	0.31	10.5	0.26	17.5	0.44	15.0	2
2-17	470 oil	30	0.35	7.6	0.36	13.0	0.52	10.5	5
					0.41	8.5	0.57	6.5	10

[a] Initial NO and NO_2 = 0.2 ppm each.
[b] From Battelle (1983).

Table 3. Observed and Calculated Ozone Maxima for selected "Urban Surrogate" Environmental Chamber Experiments Carried Out in the Battelle Study of the Photochemical Reactivity of Heatset Printing Oils[a]

Run ID[b]	Urban Surg.	Added Compound		Experimental Ozone Max.		Calc. Ozone Maximum Model A		Model B		Xylene in Oil
	(ppmC)	(name)	(ppmC)	(ppm)	(hrs)	(ppm)	(hrs)	(ppm)	(hrs)	(%)
2-2	6	-	0	0.47	4.8	0.50	4.5			-
A-2	4	ethane	0.25	0.51	5.0	0.46	6.5			-
2-4,2-12	4	ethane	2	0.49	7.2	0.47	6.5			-
2-8,A-10	4	47 oil	2	0.44	6.8	0.47	7.0	0.49	7.0	0
2-9	4	470 oil	2	0.46	6.8					
2-11,2-13	4	47 oil	15	0.47	7.0	0.47	10.5	0.57	9.0	0
2-10,2-14	4	470 oil	15	0.43	5.4					
A-3	1.2	ethane	0.6	0.26	12[c]	0.20	12[c]			-
A-14	1.2	500 oil	4.5	0.21	12[c]	0.24	12[c]	0.32	12[c]	0
A-9	1.2	47 oil	4.5	0.27	12[c]					
A-8	1.2	470 oil	4.5	0.31	12[c]					

[a] Initial NO and NO_2 = 0.2 ppm each.

[b] Runs designated 2-n from Battelle (1983) and runs designated A-n from Battelle (1984). If two run ID's are given, then two duplicate runs were carried out, and experimental data are averages of the results from those runs.

[c] Ozone maximum not reached in this run before 12 hours of irradiation. 12-hour value is given.

(3) The one experiment carried out with Magie 500 oil indicated that it is less reactive than either the Magie 47 or the Magie 470 oils, at least under the conditions where relatively high levels of oil are added. The conditions of this experiment were those where the other oils appeared to be less reactive than ethane; the data are inadequate to determine whether the Magie 500 oil would also appear to be less reactive than ethane under the conditions where the other two oils appeared to be more reactive than ethane.

In order to determine whether the general trends and relative reactivities observed experimentally can be at least qualitatively reproduced in model simulations, all of the experiments summarized in Tables 2 and 3 were simulated in model calculations. The results of these calculations are also summarized on those tables and are discussed below. The purpose of these model simulations was not to try to fit the measured data exactly, but to see if our current understanding of the atmospheric chemistry of ethane, the components of the urban surrogate, and the types of compounds expected to be present in the printing inks studies is consistent with the general trends observed in the experiments. Exact simulations of all aspects of these data are not required for this purpose, and is not practical in any case, because the experiments were not carried out for the specific purpose of model testing. Thus, for example, many of the characterization and control experiments required for this model testing were not carried out. However, sufficient chamber characterization information is available for these experiments to allow qualitative simulations to be carried out. The parameters, assumptions, and chemical mechanism employed in the model calculations carried out are summarized in the following section.

2. Calculation Parameters and Mechanism

Chamber Dependent Parameters. Chemical computer model simulations of environmental chamber experiments must include provision for a number of chamber dependent parameters, such as light intensity and spectral distribution, dilution rates, ozone wall decay and other heterogeneous processes, and chamber dependent radical sources. Some of these parameters are given by Battelle (1984), but appropriate values of others had to be assumed or, in the case of the chamber radical source, adjusted to fit some of the data. These are discussed in this section.

A description of Battelle's smog chamber is given by Battelle (1984). Briefly, the 17,300-liter chamber is lined with 5-mil FEP Teflon film and is irradiated with blacklights and sunlamps. The chamber dilution rate for these experiments is given as 6×10^{-4} min^{-1}, the temperature as 31 ± 2 C, the humidity as 10%, and the stated light intensity corresponds to an NO_2 photolysis rate of 0.27 min^{-1}. These parameters were used in all of the computers model simulations of the chamber data discussed here.

The rate constants for the photolysis reactions, other than that of NO_2, were calculated using the stated value for the NO_2 photolysis rate, the assumed spectral distribution of the photolyzing light in the chamber, and the absorption coefficients and quantum yields for NO_2 and the other photolyzing species. (The absorption coefficients and quantum yields are considered part of the chemical mechanism, as discussed below.) The spectral distribution of the lights in the Battelle chamber is not given, and thus needs to be estimated. Since the purpose of combining sunlamps and blacklamps is to approximate the solar spectrum, we assumed for these calculations that the spectrum of the light source for this chamber is the same as the solar spectrum for a directly overhead sun (zenith angle of 0 degrees). This yielded somewhat better predictions of the times required to reach the maximum ozone yield in the urban surrogate experiments than when using a spectral distribution appropriate for blacklights alone. No individual photolysis rate constants were treated as adjustable parameters in this study.

Computer model simulations of environmental chamber experiments must also contain provision for a chamber-dependent input of radicals in order to be consistent with the experimental data (Carter et al., 1982). An extensive study of this topic in the SAPRC 5800-liter evacuable chamber and in SAPRC Teflon film chambers, ranging in volume from approx. 100 liters to approx. 50,000 liters, has been carried out by us previously (Carter et al., 1982, Pitts et al., 1983). More recently we have also attempted to quantify the chamber radical source in the 150,000-liter University of North Carolina (UNC) outdoor chamber (Carter et al., 1986). As far as we are aware, no comparable study of the Battelle chamber has been carried out. However, since its walls are constructed of the same material as the SAPRC Teflon film chambers and the UNC outdoor chamber (namely FEP Teflon film), it should be reasonable to expect the magnitude of the chamber radical source in the Battelle chamber to be similar to that observed in the other three chambers. For the larger SAPRC Teflon chambers and for the UNC chamber, the chamber dependent radical input is represented in the model by the "reaction"

$$hv \rightarrow OH \qquad\qquad k = k_1 \times k_{RS}$$

where k_1 is the NO_2 photolysis rate and k_{RS} is a chamber-dependent proportionality factor. For the larger SAPRC Teflon chambers and the UNC chamber, the value of k_{RS} which best fit the data tended to vary from run to run, but was generally within a factor of 2 of 0.3 ppb for all these chambers (Carter et al., 1986). Thus it is reasonable to expect the magnitude of the radical input rate for the Battelle chamber to be within this range.

In order to determine the appropriate magnitude of k_{RS} to be used in modeling the Battelle chamber data, computer model simulations of the ethane-NO_x-air experiments were carried out in which this chamber radical source was varied. These runs were used because the homogeneous gas-phase reactions occurring in these experiments are well understood (and thus the major uncertain parameters concern only chamber effects). Furthermore, alkane-NO_x-air experiments are among the most sensitive to the chamber radical source, since the alkanes have relatively few radical sources in their gas-phase chemistry, and the chemical transformations observed in such experiments are initially almost entirely due to the chamber radical source. Surrogate-NO_x-air runs are much less sensitive to this chamber radical source parameter since the photooxidations of many of the surrogate components involve significant homogeneous radical sources, which make initiation by the chamber radical source relatively less important. Irradiations employing the printing oils are obviously not suitable for this purpose, since the appropriate homogeneous reaction mechanism to be used in simulating these experiments is uncertain.

The results of the model simulations of the ethane-NO_x-air irradiations, using assumed values of k_{RS} of 0.3, 0.6, and 1.0 ppb, are summarized in Table 2. Calculations without any assumed chamber radical source were also carried out; as expected, these significantly underpredicted the observed reactivity. In order to obtain a value of k_{RS} appropriate for the Battelle chamber, the magnitude of the chamber radical source was varied to match the times to the ozone maxima in the ethane runs. The radical source was adjusted to fit the time to the maximum and not the maximum ozone yield since the primary effect of the chamber radical source on model calculations affects mainly the rate of ozone production; the amount of ozone formed is much less sensitive to variations in this parameter (provided sufficient time is allowed for the ozone maximum to be reached.) The best fit is obtained when a k_{RS} of approximately 0.6 ppb is assumed, approximately twice the "typical" value assumed for the larger SAPRC Teflon chambers and the UNC outdoor chamber but within their range of variability. This is thus considered to be reasonable. All subsequent model simulations of the Battelle chamber experiments were carried out assuming $k_{RS} = 0.6$ ppb. This is the only parameter whose value was adjusted to fit the data of these experiments, other than the aromatic content assumed for the printing oils, as discussed below.

There are several other chamber-dependent parameters which need to be specified in model calculations, for which direct information concerning the appropriate value for the Battelle chamber is not available. These concern wall offgassing of NO_x, the heterogeneous hydrolysis rate of N_2O_5 to HNO_3, the heterogeneous hydrolysis of NO_2 to HONO and HNO_3, the wall loss of HNO_3, and the presence of initial HONO. For these parameters, we used the geometric mean of the values which were derived or assumed to be appropriate when modeling experiments carried out in the SAPRC 6400-liter indoor Teflon chamber (ITC) and the SAPRC 50,000-liter outdoor Teflon chamber (OTC), since the volume of the Battelle chamber is approximately the geometric mean of the volume of those two chambers and it has the same FEP Teflon surfaces as the SAPRC chambers. The values used and the derivation of these parameters used for modeling the SAPRC ITC and OTC are given elsewhere (Carter et al., 1986). The assumptions concerning these reactions do not have a major effect on the results of these calculations, and thus these were not modified for the purpose of computer modeling these experiments.

Chemical Mechanism. A detailed mechanism for the NO_x-air reactions of ethene, propene, ethane, n-butane, n-pentane, isooctane, toluene, m-xylene, and their oxygenated reaction products was employed to represent the reactions of ethane and the the components of the urban surrogate. The specific reaction mechanism employed for these compounds is based on that given by Atkinson et al. (1982), updated based on more recent evaluations of available data (Atkinson and Lloyd, 1984, Carter et al., 1986) and is not discussed in detail here.

Since, as seen from Table 1, the mechanism we employed in this study does not include explicitly the reactions of all of the components of Battelle's urban surrogate, an approximate representation for the components of that mixture was used in these calculations. The representation used is indicated on Table 1, together with brief comments indicating how that representation was derived.

As indicated above, the printing oils employed in this study are believed to consist primarily of higher alkanes, with an average molecular weight similar to that of n-pentadecane. (Magie 500 oil has a somewhat higher molecular weight (Battelle, 1984), but only one experiment employing that oil was carried out.) For the purpose of this study, the NO_x-air reactions of these alkanes were represented in the model by those expected to be applicable for n-pentadecane itself. Although there have been no direct studies concerning the atmospheric reactions of n-pentadecane and similar very large alkanes, the most probable set of reactions for this compound (Carter and Atkinson 1985) are indicated below:

$$\text{n-}C_{15}H_{32} + OH \xrightarrow{O_2} C_{15}H_{31}O_2\cdot \text{ (e.g., } CH_3CH(O_2\cdot)C_{13}H_{27}) \qquad (1)$$

$$C_{15}H_{31}O_2\cdot + NO \rightarrow a\ RONO_2 + (1-a)\ C_{15}H_{31}O\cdot + (1-a)\ NO_2\cdot \qquad (2)$$

$$C_{15}H_{31}O\cdot \xrightarrow{O_2} HOC_{15}H_{31}O_2\cdot \text{ (e.g., } CH_3CH(OH)CH_2CH_2CH_2(O_2\cdot)C_{10}H_{21}) \qquad (3)$$

$$HOC_{15}H_{31}O_2\cdot + NO \rightarrow a'\ RONO_2 + (1-a')\ HOC_{15}H_{31}O\cdot + (1-a')\ NO_2\cdot \qquad (4)$$

$$HOC_{15}H_{31}O\cdot \xrightarrow{O_2} \text{bifunctional products} + HO_2 \qquad (5)$$

where "$RONO_2$" represents the alkyl nitrates expected to be formed when the C_{15} peroxy radicals react with NO, reaction (3) represents the isomerization of this alkoxy radical, followed by the rapid reaction of the carbon-centered radical with O_2, and reaction (5) incorporates the rapid subsequent isomerization of the bifunctional alkoxy radical expected to be formed, followed by the reaction of the α-hydroxy radical formed from the isomerization with O_2 to form HO_2 and bifunctional products.

The major distinguishing features of the reaction mechanism of this and of other higher alkanes is the formation of bifunctional products following isomerization of the long chain alkoxy radicals which expected to be formed, together with the formation of alkyl nitrates in the reactions of the larger peroxy radicals with NO. The latter reaction is particularly important in affecting reactivity, since alkyl nitrate formation represents both a radical termination and a NO_x removal process, both of which are expected to cause decreased reactivity with respect to ozone formation. The extent to which alkyl nitrate formation is important is determined by the parameters a and a', which refer to the alkyl nitrate yields from the reactions of the unsubstituted and the substituted peroxy radicals with NO, respectively. Extrapolating the alkyl nitrate yields observed in the NO_x-air photooxidations of a number of C_4-C_8 alkanes (Carter and Atkinson, 1985), we estimate that a = 0.43 at room temperature and atmospheric pressure. However, the appropriate value of a', the alkyl nitrate yield in the reaction of hydroxy-substituted peroxy radicals, is much more uncertain, and two sets of calculations were carried out based on differing assumptions concerning this parameter.

In the set of calculations, designated "Model A", it was assumed that a' = a, i.e., that hydroxy substitution 3 carbons away from the radical center does not affect the branching ratio for the reaction of the peroxy radical with NO. Although there are no data to support this assumption, it is clearly chemically reasonable, and has been incorporated into a number of previously published models and evaluations (e.g., Carter et al., 1979, Atkinson et al., 1982, Atkinson and Lloyd, 1984). However, we recently found in carrying out model simulations of several C_5 through C_9 n-alkane-NO_x-air environmental chamber experiments carried out at SAPRC and the University of North Carolina, that much better fits to the data are obtained assuming that a' = 0 (Carter and Atkinson, 1985, Carter et al., 1986). Thus a second set of model calculations, designated "Model B", were carried out assuming that a' = 0. This results in significantly lower nitrate yields, and thus a more reactive system, than is predicted using Model A. In all other respects, the two chemical mechanisms were the same.

The rate constant used for the reaction of OH radicals with n-pentadecane was 2.6×10^4 ppm^{-1} min^{-1}, estimated from the OH radical rate constants for other n-alkanes (Atkinson, 1986). Since the rate constant for the reaction of OH radicals with ethane is 4.1×10^2 ppm^{-1} min^{-1}, the OH radical rate constant for the compound assumed to represent the major components of the printing oils is about 8 times as high, on a per carbon basis, than that for ethane. Thus if the OH radical rate constant were the only factor affecting reactivity, n-pentadecane (and by implication the printing oils) would be much more reactive than ethane. However, other aspects of the reaction mechanism can have significant effects on the ozone forming potential of the organic compounds, as indicated below.

The subsequent reactions of the alkyl nitrate products were represented in the model by the reactions of 4-heptyl nitrate (which represented the other higher organic nitrates formed in the surrogate model), and the subsequent reactions of the bifunctional products were represented by reactions of methyl ethyl ketone and 3-pentanol, which represented general reactions of lumped higher ketones and organics with OH substituent groups, respectively, in the overall model.

At the time that the computer calculations were carried out, a further uncertainty concerned the amounts, if any, of aromatic hydrocarbons and alkenes present in these predominantly alkane printing oils. While Magie 47 oil was believed to consist essentially entirely of alkanes, it was expected that both of the Magie 470 and 500 oils could contain small amounts of aromatic hydrocarbons and alkenes. Subsequent analyses of the Magie 47 and 470 oils carried out at the request of the EPA (at the EPA and other laboratories) showed that Magie 470 oil has at most 1% of aromatics (mostly alkyl-naphthalenes) and that Magie 47 oil has no detectable amounts of aromatics.

While it is now clear that these printing oils contain no significant ($\lesssim$1%) amounts of aromatics, computer calculations were also carried out in which the oils were assumed to have up to 10% aromatic content, with these aromatics being represented by m-xylene (while m-xylene clearly not a good representation of the expected alkyl-naphthalenes, even approximately chemically valid mechanisms for the higher aromatic hydrocarbons are not available).

3. Results of Chamber Simulations

Single Component Runs. The results of the model simulations of ozone levels and times to maximum ozone yields in the ethane-NO_x-air runs and the oil-NO_x-air runs are summarized in Table 2. This table also indicates the values of the parameters which were varied in the calculations.

As indicated above, the magnitude of the chamber radical source was varied to find the value which best fit the time to the ozone maximum in the ethane runs. It can be seen that the calculations consistently underpredict the maximum ozone yields, even when a high radical input parameter (which significantly underpredicts the time to the ozone maximum) is used. This underprediction of the ozone yields from the ethane-NO_x-air irradiation may be due to the model not including provisions for other chamber effects, particularly the effects of reactive contaminants, and this clearly limits the usefulness of this chemical modeling study. However, contamination effects are probably much less important in irradiations of more rapidly reacting organics, such as the constituents of the urban surrogate.

As noted above, calculations simulating the single component printing oil experiments were carried out with an assumed aromatic (represented by m-xylene) content varied from 0 to 10%. Based on the results of the simulations of the ethane experiment, all these calculations used k_{RS} = 0.6 ppb for the radical input parameter.

As seen from Table 2, the computer calculations with no aromatic included consistently overpredict the time required to obtain the ozone maximum in the single component oil experiments, regardless of whether Model A or Model B were used, although for Model B (for which a' = 0) the predicted maximum O_3 yields are in reasonable agreement with the experimental data. Assuming an aromatic to be present in the oil resulted in an increased predicted reactivity for both models. Clearly, since these oils have $\leq 1\%$ aromatic content, these comparisons indicate that neither of the n-pentadecane reaction models used are appropriate representations for the atmospheric reactions of the constituents of the printing oils studied. Consistent with our previous conclusion based upon computer modeling nC_6 through nC_9 n-alkane-NO_x-air irradiations (Carter and Atkinson 1985, Carter et al., 1986), the chemical mechanism with a' = 0 (Model B) gives the best fits to the maximum O_3 yields for a zero aromatic content of these oils.

Urban Surrogate Experiments. The results of model simulations of the urban surrogate-NO_x experiment, and the urban surrogate experiments with added ethane or printing oil, are summarized in Table 3, where they can be compared with the experimental results. In these computer calculations it was assumed, in agreement with the EPA chemical analyses, that no aromatics were present in these printing oils. A comparison of the experimental maximum ozone yields and the times to the ozone maxima with the calculated values from the Models A or B show general agreement, with no obvious choice between Model A or B (indeed, Model A tends to fit the experimental data somewhat better for these irradiations, in contrast to the single component irradiations compared in Table 2).

For the 4 ppmC urban surrogate + 2 ppmC printing oil-NO_x-air irradiations, both Model A and Model B gave reasonable fits to both the maximum ozone yields and time of this maximum. However, for the 4 ppmC urban surrogate + 15 ppmC printing oil-NO_x-air irradiations, both models were slower than the experimental data in attaining the ozone maximum (more so for Model A), but Model B significantly overpredicted the maximum ozone yield. Since ozone maxima were not attached for the 1.2 ppmC urban surrogate + 4.5 ppmC printing oil-NO_x-air irradiations, these experiments do not provide clear-cut evidence for the relative suitabilities of Model A or Model B.

C. CONCLUSION

This comparison of the chemical computer calculations with the experimental data obtained by Battelle shows that the chemical model used to represent the printing oils, and possibly also the urban surrogate mix, is not sufficiently well validated to be used for control strategy decisions. In fact, taking into account the discrepancies between the calculations and experimental data for the ethane-NO_x-air irradiations and the significant uncertainties in the chemical mechanism used to represent the printing oils, it is clear that further studies are necessary before any decision can be made as to the reactivity of the printing oils (with respect to ozone formation) relative to that of ethane. Future experimental studies of the ozone forming reactivity of these printing oils must use a well-characterized environmental chamber, with chamber characterization and control runs being frequently interdispersed with the ethane, printing oil and surrogate-NO_x-air irradiations.

The alternative approach, to develop and adequately test a chemical mechanism for the printing oils for use in chemical computer calculations, would appear to be a relatively long-term and potentially experimentally difficult project. The development of such a chemical mechanism will necessitate obtaining a significant amount of basic laboratory and environmental chamber data concerning the reaction mechanisms and products formed during the atmospheric photooxidations of the C_{15} alkanes present in the printing oils. In addition, a set of well-characterized environmental chamber data, such as that described above, will be necessary to test the chemical mechanisms developed for these printing oils.

E. REFERENCES

Atkinson, R., A. C. Lloyd, and L. Winges (1982), Atmos. Environ., 16, 1341.

Atkinson, R. and A. C. Lloyd (1984), J. Phys. Chem. Ref. Data, 13, 315.

Atkinson, R. (1986), Chem. Rev., in press.

Battelle, Columbus Laboratories (1982), "Investigation of the Volatility of Heat Set Printing Oils", Summary Report on Task 1 to the Graphics Arts Technical Foundation, September.

Battelle, Columbus Laboratories (1983), "Investigation of the Photochemical Reactivity of Heat Set Printing Oils", Summary Report on Task 2 to Graphic Arts Technical Foundation, April.

Battelle, Columbus Laboratories (1984), "Further Investigation of the Photochemical Reactivity of Heatset Printing Oils", Summary Report on Tasks A and B to The Environmental Conservation Board of the Graphics Communications Industries c/o Graphics Arts Technical Foundation, August.

Bufalini, J. J., T. A. Walter, and M. M. Bufalini (1977), Environ. Sci. Technol., 11, 1181.

Carter, W. P. L., A. C. Lloyd, J. L. Sprung, and J. N. Pitts, Jr. (1979), Int. J. Chem. Kinet., 11, 45.

Carter, W. P. L., R. Atkinson, A. M. Winer and J. N. Pitts, Jr. (1982), Int. J. Chem. Kinet., 14, 1071.

Carter, W. P. L. and R. Atkinson (1985), J. Atmos. Chem., 3, 377.

Carter, W. P. L., R. Atkinson, F. W. Lurmann, and A. C. Lloyd (1986), "Evaluation of a Surrogate Species Chemical Mechanism for use in Atmospheric Simulation Models", Draft Final Report to the U. S. Environmental Protection Agency, Contract No 68-02-4104.

Pitts, J. N., Jr., R. Atkinson, W. P. L. Carter, A. M. Winer and E. C. Tuazon (1983), "Chemical Consequences of Air Quality Standards and of Control Implementation Programs" Final Report to California Air Resources Board, Contract No. A1-030-32, April.

APPENDIX B

COMPUTER TAPE CONTAINING RESULTS OF THE CHAMBER EXPERIMENTS

The results of all the environmental chamber experiments carried out in this study are available on magnetic tape in computer-readable format. The format of the data on this tape, and descriptions of the data sets on the tape are given in this Appendix. This tape was submitted to the United States Environmental Protection Agency along with this report, and copies of this tape are available from SAPRC for handling and distribution costs. Requests for copies of this tape should be addressed to:

Dr. William P. L. Carter
Statewide Air Pollution Research Center
University of California
Riverside, CA 92521

The computer tape has a data density of 1600 BPI, uses ASCII character format, and has a maximum blocksize of 5280 bytes. The tape contains a total 61 files, of three different types. File 1, which has a logical record length of 80 bytes, is the same as Table B-1 in this Appendix, which contains the complete list of run numbers, run types, and file numbers for the chamber runs carried out in this program. Files 2-31, which have logical record lengths of 132 bytes, consists of "printout images" of the tabulated data formatted in a manner most suitable for obtaining hard-copy printouts for manual inspection. A description of the data contained in these "printout" files is given in Section 1, below. Files 32-61, which have logical record lengths of 80 bytes, contain the data in a compressed format which is more suitable for being read by computer programs for purposes of, for example, data manipulation or plotting. The format of these these compressed data sets is described in Section 2. The data set numbers for the printout and the compressed data sets for each of the runs included on the tape are given in Table B-1.

Table B-1. Run Numbers, Run Types, and File Numbers for All Chamber Runs on the Data Tape

ITC Run No.	Run Type	File Numbers[a] Printout Format	File Numbers[a] Compressed Format
975	Propene-NOx	2	32
976	Tracer-NOx	3	33
977	Mini-Surrogate	4	34
978	Mini-Surrogate	5	35
979	Mini-Surrogate + Ethane	6	36
980	Mini-Surrogate	7	37
981	Mini-Surrogate + n-C15	8	38
982	Mini-Surrogate	9	39
983	Mini-Surrogate + Magie-47	10	40
984	Mini-Surrogate + Magie-470	11	41
985	Mini-Surrogate	12	42
990	Propene-NOx	13	43
991	Mini-Surrogate	14	44
992	Mini-Surrogate + Ethane	15	45
993	Mini-Surrogate + n-C15	16	46
994	Mini-Surrogate	17	47
995	Mini-Surrogate + Magie-47	18	48
996	Mini-Surrogate + Magie-470	19	49
997	Mini-Surrogate	20	50
999	Tracer-NOx + Ethane	21	51
1000	Tracer-NOx + Acetylene	22	52
1001	n-C15-NOx	23	53
1002	Magie-47-NOx	24	54
1003	Magie-470-NOx	25	55
1004	Tracer-NOx	26	56
1005	Propene-NOx	27	57
1006	Acetylene-NOx	28	58
1007	Acetylene-NOx	29	59
1008	Pure Air Irrad.	30	60
1009	Acetaldehyde-Air	31	61

[a] File no. 1 consists of this table.

1. Data Sets in "Printout" Format

These data sets contain tabulations of the results of the chamber experiments in a format suitable for manual inspection. If hard copies of these data sets are required, these can be printed out on any printer which can print 132 columns, has a page length of 60 lines or more, and which recognizes the "form feed" (ASCII code 12) character. Each of these "printouts" contains the following information (where applicable).

- The indoor Teflon chamber (ITC) run number.
- A brief run description.
- The date the run was carried out (given below the run description).
- The date the printout files was created (given in right hand corner on each page).
- Comments for the run, including experimental operations and operator's comments taken from the log book, problems encountered (if any), etc.
- The initial concentrations of injected reactants which were monitored.
- Lists of all instruments used in these runs. For each instrument, this list indicates the ID number (used internally at SAPRC), the label identifying the instrument on the data tabulation, and a brief description giving information identifying the instrument and/or technique.
- The data tabulations. The tabulations indicate the compound or parameter measured, the units in which the measurements are reported, and the instrument. Because of space and format limitations, the compound names frequently had to be abbreviated on the tabulations. The meanings of representative abbreviations which may not be obvious are listed in Table B-2. For each data point, the clock time and (in most cases) the elapsed time (in minutes) since the irradiation began (or since the first measurement for dark runs) are indicated.
- If any of the data are flagged (indicated by an "A", or "B", etc., immediately to the right of the value), footnotes giving the reason it is flagged appear at the end of the tabulation for the run.

Table B-2. Representative Abbreviations Used in the Data Tabulations

Abbreviation	Meaning
NO2-UNC	NO_2 readings, uncorrected for interferences by organic nitrates and HNO_3
N-C4	n-Butane
I-C4	Isobutane
ISO-C8	Iso-Octane (2,2,4-trimethylpentane)
I-C4=	Isobutene
M-XYL	m-Xylene
C5-K-3	3-Pentanone (diethyl ketone)
C5-N-2	2-Pentyl nitrate
ACETALD	Acetaldehyde[a]
MEK	Methyl ethyl ketone[a]
PROX	Propene oxide[a]
BUTYRAL	Butyraldehyde[a]
LN C4/C3=	ln([n-butane]/[propene]), whose rate of change is used to derive OH radical concentrations[b]
DEW PT	Dew point (units of degrees C)
K1	k_1, the NO_2 photolysis rate (units of min^{-1})
UV RAD	UV radiometer readings (units of $mW\ cm^{-2}$)

[a] Or some other compound with the same retention time on the gas chromatographic system employed.

[b] Concentration units are arbitrary; only the slope of the log is of interest.

2. Data Sets in Compressed Format

If it is desired to use the data from these experiments as input to computer programs, for purposes such as data analysis, plotting, etc, then the data sets in the "compressed" format would be more useful. These data sets consists of records in card image format, and are organized as described in Table B-3. The following points should be noted regarding these data sets:

- Because this data format is used for a number of different types of experiments at SAPRC, the records contain provisions for data values which are not used in these particular runs. These should be ignored; usually (but not always) they are zero.
- The types of data on the data sets can be categorized by (a) general information data, such as run title, date, number of instruments, comments, chambers, etc., (b) comments, (c) instrument descriptions, (d) channel parameters and (e) channel data. By "channel" we mean the set of experimental measurements which depend on time, such as ozone concentrations, temperature readings, etc.
- Channels which have data have associated with them a "time set," which is an array of the times at which the measurements for that channel were made. The time sets are stored separately from the channel data because in general more than one channel may have the same time set.
- T = 0 refers to the clock time at which the irradiation began; or, for dark runs, the time the first measurement was made.
- Some data points are "flagged" with a non-blank character (as indicated by the values in the "LFLGS" and "FLGS arrays in group 3 of Table C-3), which associates it with a comment which has the same character as its associated flag ("FLGCOM" in group 5 of Table C-3). These comments indicate problems, etc., with the "flagged" data point, or set of data points starting with the one which is flagged. If a comment has FLGCOM = "N," the comment line is a continuation of the previous flagged comment, and the character "N" does not appear on the "printout" format data sets.

Table B-3. Organization of the Compressed Data Files for Chamber Runs

Re- cord	Col- umn	Format[a]	Name	Description
Group 1. Four Records. General Information				
1	1-7	(1X,I6)	IRUNID	Run number + 10000 x chamber number (chamber numbers: 2 = ITC, 4 = OTC)
	8-13	(I6)	FORM	File format; always 1.
	14-29	(A16)	UPDRUN	Date of last update (internal SAPRC use)
	30-69	(A40)	TITLE	Run title
	70-77	(A8)	DATE(1)	First half of run date
2	1-9	(1X,A8)	DATE(2)	Second half of run date
	10-25	(I6)	TZERO	Clock time at T = 0
	16-21	(I6)	PSTPDT	1 for PST, 2 for PDT
	22-39	(3I6)	-	(Ignore)
	40-45	(I6)	BAGNO	ITC or OTC reaction bag number (If zero, bag number is not specified)
	46-78	(3G11.4)	-	(Ignore)
3	1-57	(1X,6E11.4)	-	(Ignore)
	50-64	(I7)	-	(Ignore - should be zero)
	65-70	(I6)	NSIDES	Number of sides if chamber is divided applicable to outdoor chamber runs only (Note: "Side 3" always refers to ambient air outside chamber.)
4	1-7	(1X,I6)	NTS	Number of time sets
	8-13	(I6)	NCHN	Number of channels
	14-19	(I6)	-	(Ignore - should be zero)
	20-25	(I6)	NINS	Number or instruments
	26-31	(I6)	NCOMS	Number of comments
	32-37	(I6)	-	(Ignore)
	38-48	(E11.4)	-	(Ignore)
	49-54	(I6)	-	(Ignore)
Group 2. One Set of One or More Records for Each of the NTS Time Sets				
1	1-7	(1X,I6)	NPTS	Number of points in this time set
	8-73	(11I6)	TIMES	Clock times + 10000 x day number. (Day number: 0 = first day, 1 = second day, etc. E.G., 10930 = 9:30 AM on day 2 of the run.)

(continued)

Table B-3 (continued) - 2

Re-cord	Col-umn	Format[a]	Name	Description
2+	1-73	(1X,12I6)	TIMES	Rest of clock times. (No records of this type if NPTS ≤ 11.)
Group 3. One Set of Three or More Records for Each of the NCHN Data Channels				
1	1-7	(1X,I6)	ID1	Data type identification number (internal SAPRC use).
	8-13	(I6)	INST	Instrument number - i.e., record number in group 4 that describes the instrument used for this channel. (0 = instrument undefined)
	14-19	(I6)	SIDE	Side number (3 = outside). Ignore if NSIDES = 0 or 1.
	20-25	(I6)	TIMSET	Time set number. (If TIMSET = 0, there are no data for this channel.)
	26-31	(I6)	NP	Number of data points (ignore if TIMSET = 0)
	32-37	(I6)	NF	Number of flagged data points (Ignore if TIMSET = 0)
	38-67	(5I6)	-	(Ignore)
	68-73	(I6)	PRTORD	If >0, determines order channel appears on printouts - lower number printed first. If PRTORD = -1, channel is not printed. If PRTORD is -2, the data for this channel are printed out separately at the end.
	74-79	(I6)	DIG	(DIG-2) = number of digits to the right of the decimal point that appears on printouts. If DIG = ≥ 0 or ≤ 7, data prints out in exponential notation.
2	1-7	(1X,I6)	UNTS	Code number for units of data: 1 = ppm, 2 = degree C, 7 = mw-cm^{-2}, 8 = blank (no units), 9 = ppmC, 10 = ppb, 11 = degree F, 14 = "raw data," 17 = min^{-1}.
	8-19	(2I6)	-	(Ignore)

(continued)

Table B-3 (continued) - 3

Record	Column	Format[a]	Name	Description
	20-41	(2E11.4)	FAC,ZERO	Factor and zero corrections. Data values = factor x (raw data - zero) (Note however that data values stored on the data sets are already calculated, so these quantities can be ignored.)
	42-52	(E11.4)	-	(Ignore)
	53-63	(E11.4)	CONC0	Initial concentration (if SDEV, below, <0) or average (if SDEV ≥0) to appear at the start of the printouts. If CONC0 = -9.9999E+9, initial concentration or average is not used. If CONC0 = -9.9999E+9, it needs to be calculated from the data.
	64-74	(E11.4)	SDEV	If SDEV <0, CONC0 is an initial concentration. If SDEV = -1, the initial concentration was assigned; if SDEV = -9.9999E+9, the data value at T = 0 is used as the initial concentration. If SDEV ≥0, CONC0 is the average of the data, and SDEV is the (1σ) standard deviation. If SDEV = 9.999E+9, the standard deviation is unknown.
3	1-9	(1X,A8)	NAME	Channel name
4+	1-78	(1X,7E11.4)	DATA	The data values. As many records as needed for the NP values. A data value of 9.9999E+9 means no data is available for that time point. No records if TIMSET = 0.
5+	1-73	(1X,9(I6,A2))	LFLCS, FLGS	For each of the NF flagged data points, LFLGS is the index number for the point, and the first byte of FLGS is the flag character. As many records as needed for the NF values; no record if NF = 0.

(continued)

Table B-3 (continued) - 4

Re-cord	Col-umn	Format[a]	Name	Description
Group 4. One Record for Each of the NINS Instruments				
1	1-7	(1X,I6)	INSCOD	Instrument code number
	7-19	(6A2)	-	(Ignore)
	20-27	(A8)	INSLBL	Instrument label
	28-67	(A40)	INSDSC	Instrument description
	68-78	(E11.4)	-	(Ignore)
Group 5. One Record for Each of the NCOMS Comments				
1	1-3	(2X,A1)	FLGCOM	If blank, the comment appears on the first page of the printouts. If not blank, the comment is a footnote which is printed along with the first byte of FLGCOM at the end of the printout.
	4-80	(A77)	COMENT	The comment line

---

[a] FORTRAN format code.

APPENDIX C

CHEMICAL MECHANISM AND PARAMETERS USED IN MODEL SIMULATIONS

This Appendix gives the reactions and kinetic and mechanistic parameters used in the model simulations discussed in this report. The reactions and kinetic parameters used are given in Table C-1, and Table C-2 gives a list of the species used in the mechanism. Some of the mechanistic parameters are temperature dependent; the values given on Table C-1 are for 300 K, the temperature used in all of the simulations discussed in Section IV of this report. The temperature used in the simulations of the chamber experiments was 303 K, so the differences in the temperature-dependent coefficients in those simulations are negligible. Table C-1 gives the temperature dependence of all temperature dependent rate constants. The rate constants for photolysis reactions were obtained as indicated below.

Rate constants for photolysis reactions are calculated from the products of the absorption coefficients and quantum yields, given as a function of wavelength for each type of photolysis reaction in Table C-3, and the intensity and spectral distribution of the light source. For ITC simulations, intensity and spectral distribution of the light source was constant (see Carter et al. 1986 for a tabulation of the ITC spectral distribution) and the rate constants for each type of photolysis reaction used in the ITC simulations is given in Table C-4. For the simulations of the airshed scenarios, the photolysis rate constants were calculated as described in detail by Carter et al. (1986). Briefly, the photolysis rate constants were calculated theoretically as a function of zenith angle using their absorption coefficients x quantum yield products given in Table C-3, and the actinic irradiances given by Peterson (1976) for his "best estimate" surface albitos. The calculated solar photolysis rate constants for zenith angles of 0, 40, and 70 degrees are also given on Table C-4.

References

Carter, W. P. L., F. W. Lurmann, R. Atkinson and A. C. Lloyd (1986b), "Development and Testing of a Surrogate Species Chemical Reaction Mechanism," EPA-600/3-86-031, August.

Peterson, J. T. (1976), "Calculated Actinic Fluxes (290-700 nm) for Air Pollution Photochemistry Applications," EPA-600/4-76-025, June.

Table C-1. Reactions and Rate Constants Used in the Model Simulations of the Surrogate-NO_x-Air Irradiations

Reaction label[a]		Kinetic Parameters[b]			Reaction[c]
					Inorganic Reactions
1)		PHOT. = NO2			NO2 + HV = NO + O
2)		2.155E-05	0.00	-4.300	O + O2 + M = O3 + M
3A)		1.365E+04	0.00	-1.000	O + NO2 = NO + O2
3B)		3.232E-03	0.00	-4.000	O + NO2 + M = NO3 + M
4)		2.642E+03	2.72	-1.000	O3 + NO = NO2 + O2
5)		1.761E+02	4.87	-1.000	O3 + NO2 = O2 + NO3
6)		1.174E+04	-0.50	-1.000	NO + NO3 = #2 NO2
7)		1.185E-10	-1.05	-2.000	NO + NO + O2 = #2 NO2
8)		FALLOFF F= 0.600, N= 0.972			NO2 + NO3 = N2O5
	KO:	7.182E-02	0.00	-6.300	
	KI:	2.055E+03	0.00	-1.500	
9)		4.333E+13	22.55	0.000	N2O5 + #RCON8 = NO2 + NO3
10)		1.468E-06	0.00	-1.000	N2O5 + H2O = #2 HONO2
11)		3.670E+01	2.44	-1.000	NO2 + NO3 = NO + NO2 + O2
12A)		PHOT. = NO3NO			NO3 + HV = NO + O2
12B)		PHOT. = NO3NO2			NO3 + HV = NO2 + O
13A)		PHOT. = O3O3P			O3 + HV = O + O2
13BM)		PHOT. = O3T300			O3 + HV = O*1D2 + O2
14)		3.229E+05	0.00	-1.000	O*1D2 + H2O = #2 HO.
15)		4.257E+04	0.00	-1.000	O*1D2 + M = O + M
16)		FALLOFF F= 0.600, N= 1.000			HO. + NO = HONO
	KO:	2.406E-02	0.00	-5.300	
	KI:	4.404E+04	0.00	-2.000	
17)		PHOT. = HONO			HONO + HV = HO. + NO
18)		FALLOFF F= 0.600, N= 1.000			HO. + NO2 = HONO2
	KO:	9.337E-02	0.00	-5.200	
	KI:	3.523E+04	0.00	-2.300	
19)		1.380E+01	-1.55	-1.000	HO. + HONO2 = H2O + NO3
21)		3.200E+02	0.00	-1.000	HO. + CO = HO2. + CO2
22)		2.349E+03	1.87	-1.000	HO. + O3 = HO2. + O2
23)		5.431E+03	-0.48	-1.000	HO2. + NO = HO. + NO2
24)		FALLOFF F= 0.560, N= 1.000			HO2. + NO2 = HO2NO2
	KO:	8.260E-03	0.00	-6.600	
	KI:	6.165E+03	0.00	-0.800	
25)		1.754E+13	21.60	1.000	HO2NO2 + #RCON24 = HO2. + NO2
27)		5.872E+03	0.00	-1.000	HO2NO2 + HO. = H2O + NO2 + O2
28)		2.055E+01	1.15	-1.000	HO2. + O3 = HO. + #2 O2
29A)		3.229E+02	-1.23	-1.000	HO2. + HO2. = HO2H + O2
29B)		6.823E-05	-1.95	-2.000	HO2. + HO2. + M = HO2H + O2
29C)		1.113E-05	-5.60	-2.000	HO2. + HO2. + H2O = HO2H + O2 + H2O
29D)		2.370E-06	-6.32	-2.000	HO2. + HO2. + H2O = HO2H + O2 + H2O
30A)		SAME K AS 29A			NO3 + HO2. = HONO2 + O2

(continued)

Table C-1 (continued) - 2

Reaction label[a]	Kinetic Parameters[b]	Reaction[c]
30B)	SAME K AS 29B	NO3 + HO2. + M = HONO2 + O2
30C)	SAME K AS 29C	NO3 + HO2. + H2O = HONO2 + O2 + H2O
30A)	SAME K AS 29D	NO3 + HO2. + H2O = HONO2 + O2 + H2O
31)	PHOT. = H2O2	HO2H + HV = #2 HO.
32)	4.550E+03 0.37 -1.000	HO2H + HO. = HO2. + H2O
		General Peroxy Radical Reactions[d]
B1)	6.165E+03 -0.36 -1.000	RO2. + NO = NO
B2)	6.165E+03 -0.36 -1.000	RCO3. + NO = NO
B4)	4.110E+03 -0.36 -1.000	RCO3. + NO2 = NO2
B5)	4.404E+03 0.00 -1.000	RO2. + HO2. = HO2.
B6)	4.404E+03 0.00 -1.000	RCO3. + HO2. = HO2.
B7)	PHOT. = CO2H	-OOH + HV = HO2. + HO.
B8)	1.468E+00 0.00 -1.000	RO2. + RO2. =
B9)	4.404E+03 0.00 -1.000	RO2. + RCO3. =
B10)	3.670E+03 0.00 -1.000	RCO3. + RCO3. =
F7)	SAME K AS B1	R2O2. + NO = NO2
F8)	SAME K AS B5	R2O2. + HO2. =
F9)	SAME K AS B8	R2O2. + RO2. = RO2.
F10)	SAME K AS B9	R2O2. + RCO3. = RCO3.
		Reactions of Formaldehyde
C1)	PHOT. = HCHOR	HCHO + HV = #2 HO2. + CO
C2)	PHOT. = HCHOM	HCHO + HV = H2 + CO
C3)	1.321E+04 0.00 -1.000	HCHO + HO. = HO2. + CO + H2O
C4)	1.468E+01 0.00 -1.000	HCHO + HO2. = HOC-O2. + RO2.
C5)	SAME K AS B1	HOC-O2. + NO = NO2 + HO2. + -C
C6)	SAME K AS B5	HOC-O2. + HO2. = -OOH + -C
C7)	SAME K AS B8	HOC-O2. + RO2. = RO2. + #.5 HO2. + RO2. + -C
C8)	SAME K AS B9	HOC-O2. + RCO3. = RCO3. + #.5 HO2. + RCO3. + -C
C9)	8.807E+02 4.09 -1.000	HCHO + NO3 = HONO2 + HO2. + CO
		Reactions of Acetaldehyde and PAN
C10)	1.013E+04 -0.50 -1.000	CCHO + HO. = CCO-O2. + H2O + RCO3.
C11A)	PHOT. = CCHOR	CCHO + HV = CO + C-O2. + HO2. + RO2.
C12)	4.404E+02 2.84 -1.000	CCHO + NO3 = HONO2 + CCO-O2. + RCO3.
C13)	SAME K AS B2	CCO-O2. + NO = C-O2. + CO2 + NO2 + RO2.

(continued)

Table C-1 (continued) - 3

Reaction label[a]	Kinetic Parameters[b]	Reaction[c]
C14)	SAME K AS B4	CCO-O2. + NO2 = C-PAN
C15)	SAME K AS B6	CCO-O2. + HO2. = -OOH + CO2 + HCHO
C16)	SAME K AS B9	CCO-O2. + RO2. = RO2. + #.5 HO2. + CO2 + HCHO
C17)	SAME K AS B10	CCO-O2. + RCO3. = RCO3. + HO2. + CO2 + HCHO
C18)	1.200E+18 26.91 0.000	C-PAN = CCO-O2. + NO2 + RCO3.
C19)	SAME K AS B1	C-O2. + NO = C-O. + NO2
C20)	SAME K AS B5	C-O2. + HO2. = -OOH + HCHO
C21)	SAME K AS B8	C-O2. + RO2. = RO2. + #.5 HO2. + HCHO
C22)	SAME K AS B9	C-O2. + RCO3. = RCO3. + #.5 HO2. + HCHO
C23)	8.073E+01 1.99 -1.000	C-O. + O2 = HCHO + HO2.
C24)	2.202E+04 0.00 -1.000	C-O. + NO2 = CONO2
		Reactions of Propionaldehyde and the Higher Alaphatic Aldehydes
C25)	1.248E+04 -0.50 -1.000	RCHO + HO. = C2CO-O2. + RCO3.
C26)	PHOT. = RCHO	RCHO + HV + #.2 = C2-O2. + RO2. + CO + HO2.
C27)	4.404E+02 2.84 -1.000	NO3 + RCHO = C2CO-O2. + RCO3.
C28)	SAME K AS B2	C2CO-O2. + NO = C2-O2. + CO2 + NO2 + RO2.
C29)	SAME K AS B4	C2CO-O2. + NO2 = C2-PAN
C30)	SAME K AS B6	C2CO-O2. + HO2. = -OOH + CCHO + CO2
C31)	SAME K AS B9	C2CO-O2. + RO2. = RO2. + #.5 HO2. + CCHO + CO2
C32)	SAME K AS B10	C2CO-O2. + RCO3. = RCO3. + HO2. + CCHO + CO2
C33)	1.200E+18 26.91 0.000	C2-PAN = C2CO-O2. + NO2 + RCO3.
C34)	SAME K AS B1	C2-O2. + NO = NO2 + CCHO + HO2.
C35)	SAME K AS B5	C2-O2. + HO2. = -OOH + CCHO
C36)	SAME K AS B8	C2-O2. + RO2. = RO2. + #.5 HO2. + CCHO
C37)	SAME K AS B9	C2-O2. + RCO3. = RCO3. + #.5 HO2. + CCHO
		Reactions of Acetone
C38)	1.468E+04 2.23 -1.000	C-CO-C + HO. = C-CO-C-O2. + RO2.
C39)	PHOT. = KETONE	C-CO-C + HV + #.07 = CCO-O2. + C-O2. + RCO3. + RCO3. + RO2.
C40)	SAME K AS B1	C-CO-C-O2. + NO = NO2 + CCOCHO + HO2.

(continued)

Table C-1 (continued) - 4

Reaction label[a]	Kinetic Parameters[b]	Reaction[c]
C41)	SAME K AS B5	C-CO-C-O2. + HO2. = -OOH + CCOCHO
C42)	SAME K AS B8	C-CO-C-O2. + RO2. = RO2. + #.5 HO2. + CCOCHO
C43)	SAME K AS B9	C-CO-C-O2. + RCO3. = RCO3. + #.5 HO2. + CCOCHO
		Reactions of Methyl Ethyl Ketone and the Higher Ketones
C44)	1.761E+04 1.48 -1.000	MEK + HO. = H2O + MEK-O2. + RO2.
C45')	SAME K AS B1	MEK-O2. + NO = NO2 + #.5 "CCO-O2. + CCHO + MEK(2)-O2. + RCO3. + RO2."
C46')	SAME K AS B5	MEK-O2. + HO2. = -OOH + CO2 + HCHO + CCHO
C47')	SAME K AS B8	MEK-O2. + RO2. = RO2. + #.5 HO2. + CO2 + HCHO + CCHO
C48')	SAME K AS B9	MEK-O2. + RCO3. = RCO3. + #.5 HO2. + CO2 + HCHO + CCHO
C50)	SAME K AS B1	MEK(2)-O2. + NO = NO2 + HCHO + C2CO-O2.
C54)	SAME K AS B5	MEK(2)-O2. + HO2. = -OOH + CO2 + HCHO + CCHO
C55)	SAME K AS B8	MEK(2)-O2. + RO2. = RO2. + #.5 HO2. + CO2 + HCHO + CCHO
C56)	SAME K AS B9	MEK(2)-O2. + RCO3. = RCO3. + #.5 HO2. + CO2 + HCHO + CCHO
C57)	PHOT. = KETONE	MEK + HV + #.1 = CCO-O2. + C2-O2. + RCO3. + RO2.
		Reactions of the Lumped Higher Alcohol (used to represent the reactions at the -OH group for the isomerization products of the higher alkanes)
C111)	2.055E+04 0.00 -1.000	ROH + HO. = #.2 "ROH-O2. + RO2." + #.8 "MEK + HO2. + -C"
C112)	SAME K AS B1	ROH-O2. + NO = NO2 + #2 RCHO + HO2. + #-1 -C
C113)	SAME K AS B5	ROH-O2. + HO2. = -OOH + #2 RCHO + #-1 -C
C114)	SAME K AS B8	ROH-O2. + RO2. = RO2. + #.5 HO2. + #2 RCHO + #-1 -C
C115)	SAME K AS B9	ROH-O2. + RCO3. = RCO3. + #.5 HO2. + #2 RCHO + #-1 -C

(continued)

Table C-1 (continued) - 5

Reaction label[a]	Kinetic Parameters[b]			Reaction[c]
				Reactions of Glyoxal
C58)	PHOT. = GLYOXAL			HCOCHO + HV + #.029 = #.13 HCHO + #.87 H2 + #1.87 CO
C59)	1.688E+04	0.00	-1.000	HCOCHO + HO. = HCOCO.
C60)	8.807E+02	4.09	-1.000	HCOCHO + NO3 = HONO2 + HCOCO.
C61)	6.000E+01			HCOCO. = #.63 HO2. + #1.26 CO + #.37 "HCOCO-O2. + RCO3."
C62)	SAME K AS B2			HCOCO-O2. + NO = NO2 + CO2 + CO + HO2.
C63)	SAME K AS B4			HCOCO-O2. + NO2 = HCO-PAN
C64)	1.200E+18	26.91	0.000	HCO-PAN = HCOCO-O2. + NO2 + RCO3.
C65)	SAME K AS B6			HCOCO-O2. + HO2. = -OOH + CO2 + CO
C66)	SAME K AS B9			HCOCO-O2. + RO2. = RO2. + #.5 HO2. + CO2 + CO
C67)	SAME K AS B10			HCOCO-O2. + RCO3. = RCO3. + HO2. + CO2 + CO
				Reactions of Methylglyoxal
C68)	PHOT. = MEGLYOX			CCOCHO + HV + #.107 = HO2. + CO + CCO-O2. + RCO3.
C69)	2.495E+04	0.00	-1.000	CCOCHO + HO. = CO + CCO-O2. + RCO3.
C70)	4.404E+03	2.84	-1.000	CCOCHO + NO3 = HONO2 + CO + CCO-O2. + RCO3.
				Reactions of Glycolaldehyde
C72)	3.376E+04	0.00	-1.000	HOCCHO + HO. = HOCCO-O2. + H2O + RCO3.
C73)	SAME K AS B2			HOCCO-O2. + NO = NO2 + CO2 + HCHO + HO2.
C74)	SAME K AS B4			HOCCO-O2. + NO2 = HOC-PAN
C75)	1.200E+18	26.91	0.000	HOC-PAN = HOCCO-O2. + NO2 + RCO3.
C76)	SAME K AS B6			HOCCO-O2. + HO2. = -OOH + CO2 + HCHO
C77)	SAME K AS B9			HOCCO-O2. + RO2. = RO2. + #.5 HO2. + CO2 + HCHO
C78)	SAME K AS B10			HOCCO-O2. + RCO3. = RCO3. + HO2. + CO2 + HCHO
C79)	PHOT. = CCHOR			HOCCHO + HV = CO + HCHO + #2 HO2.
C80)	4.404E+02	2.84	-1.000	HOCCHO + NO3 = HONO2 + HOCCO-O2. + RCO3.

(continued)

Table C-1 (continued) - 6

Reaction label[a]	Kinetic Parameters[b]	Reaction[c]
		Reactions of the $\geq C_4$ Alkyl Nitrates
C81)	2.936E+04 2.02 -1.000	C4ONO2 + HO. = #.2 "NO2 + MEK" + #.8 "C4ONO2-O2. + RO2."
C82')	SAME K AS B1	C4ONO2-O2. + NO = #1.6 NO2 + #.6 "CCHO + C2-O2." + #.4 C4ONO2(2)-O2. + RO2.
C84)	SAME K AS B1	C4ONO2(2)-O2. + NO = #2 NO2 + HCHO + RCHO
C85')	SAME K AS B5	C4ONO2-O2. + HO2. = -OOH + NO2 + #1.2 CCHO + #.4 "HCHO + RCHO"
C87)	SAME K AS B5	C4ONO2(2)-O2. + HO2. = -OOH + NO2 + HCHO + RCHO
C88')	SAME K AS B8	C4ONO2-O2. + RO2. = RO2. + #.5 HO2. + NO2 + #1.2 CCHO + #.4 "HCHO + RCHO"
C90)	SAME K AS B8	C4ONO2(2)-O2. + RO2. = RO2. + #.5 HO2. + NO2 + HCHO + RCHO
C91')	SAME K AS B9	C4ONO2-O2. + RCO3. = RCO3. + #.5 HO2. + NO2 + #1.2 CCHO + #.4 "HCHO + RCHO"
C93)	SAME K AS B9	C4ONO2(2)-O2. + RCO3. = RCO3. + #.5 HO2. + NO2 + HCHO + RCHO
C94)	4.404E+04 1.29 -1.000	C7ONO2 + HO. = C7ONO2-O2. + RO2.
C95')	SAME K AS B1	C7ONO2-O2. + NO = #1.34 NO2 + #.11 MEK + #.66 C7ONO2(2)-O2. + #.46 RCHO + #.56 -C
C98)	SAME K AS B1	C7ONO2(2)-O2. + NO = #2 NO2 + #2 RCHO + -C
C99')	SAME K AS B5	C7ONO2-O2. + HO2. = -OOH + NO2 + #.11 MEK + #1.78 RCHO + #1.22 -C
C102)	SAME K AS B5	C7ONO2(2)-O2. + HO2. = -OOH + NO2 + #2 RCHO + -C
C103)	SAME K AS B8	C7ONO2-O2. + RO2. = RO2. + #.5 HO2. + NO2 + #.11 MEK + #1.78 RCHO + #1.22 -C
C106)	SAME K AS B8	C7ONO2(2)-O2. + RO2. = RO2. + #.5 HO2. + NO2 + #2 RCHO + -C
C107)	SAME K AS B9	C7ONO2-O2. + RCO3. = RCO3. + #.5 HO2. + NO2 + #.11 MEK + #1.78 RCHO + #1.22 -C
C110)	SAME K AS B9	C7ONO2(2)-O2. + RCO3. = RCO3. + #.5 HO2. + NO2 + #2 RCHO + -C

(continued)

Table C-1 (continued) - 7

Reaction label[a]	Kinetic Parameters[b]			Reaction[c]
				Reactions of Benzaldehyde
G30)	1.761E+04	0.00	-1.000	BZ-CHO + HO. = BZ-CO-O2. + RCO3.
G31)	PHOT. = BZCHO			BZ-CHO + HV + #QY.BZA = -C (Where QY.BZA = 0.05 for airshed simulations, and QY.BZA = 0.0 for ITC simulations.)
G32)	4.404E+02	2.97	-1.000	BZ-CHO + NO3 = HONO2 + BZ-CO-O2.
G33)	SAME K AS B2			BZ-CO-O2. + NO = BZ-O2. + CO2 + NO2 + RO2.
G34)	SAME K AS B4			BZ-CO-O2. + NO2 = BZ-PAN
G35)	9.600E+16	25.90	0.000	BZ-PAN = BZ-CO-O2. + NO2 + RCO3.
G36)	SAME K AS B6			BZ-CO-O2. + HO2. = -OOH + CO2 + PHENOL
G37)	SAME K AS B9			BZ-CO-O2. + RO2. = RO2. + #.5 HO2. + CO2 + PHENOL
G38)	SAME K AS B10			BZ-CO-O2. + RCO3. = RCO3. + HO2. + CO2 + PHENOL
G39)	SAME K AS B1			BZ-O2. + NO = BZ-O. + NO2
G40)	SAME K AS B5			BZ-O2. + HO2. = -OOH + PHENOL
G41)	SAME K AS B8			BZ-O2. + RO2. = RO2. + #.5 HO2. + PHENOL
G42)	SAME K AS B9			BZ-O2. + RCO3. = RCO3. + HO2. + PHENOL
G43)	2.202E+04	0.00	-1.000	BZ-O. + NO2 = NITROPHEN
G44)	4.404E+03	0.00	-1.000	BZ-O. + HO2. = PHENOL
G45)	6.000E-02	0.00	0.000	BZ-O. = PHENOL
				Reactions of Phenol
G46)	4.154E+04	0.00	-1.000	HO. + PHENOL = HO-PHEN-O2. + RO2.
G47)	SAME K AS B1			HO-PHEN-O2. + NO = #.15 NITROPHEN + #.2 HCOCHO + #.85 "NO2 + HO2." + #4.7 -C
G48)	SAME K AS B5			HO-PHEN-O2. + HO2. = -OOH + #.24 HCOCHO + #5.52 -C
G49)	SAME K AS B8			HO-PHEN-O2. + RO2. = RO2. + #.24 HCOCHO + #5.52 -C
G50)	SAME K AS B9			HO-PHEN-O2. + RCO3. = RCO3. + #.5 HO2. + #.24 HCOCHO + #5.52 -C
G51)	5.578E+03	0.00	-1.000	NO3 + PHENOL = HONO2 + BZ-O.

(continued)

Table C-1 (continued) - 8

Reaction label[a]	Kinetic Parameters[b]			Reaction[c]
				Reactions of Alkyl-Substituted Phenols
G52)	6.018E+04	0.00	-1.000	HO. + CRES = HO-CRES-O2. + RO2.
G53)	SAME K AS B1			HO-CRES-O2. + NO = #.15 NITROPHEN + #.2 CCOCHO + #.85 "NO2 + HO2." + #5.5 -C
G54)	SAME K AS B5			HO-CRES-O2. + HO2. = -OOH + #.24 CCOCHO + #6.28 -C
G55)	SAME K AS B8			HO-CRES-O2. + RO2. = RO2. + #.24 CCOCHO + #6.28 -C
G56)	SAME K AS B9			HO-CRES-O2. + RCO3. = RCO3. + #.5 HO2. + #.24 CCOCHO + #6.28 -C
G57)	3.229E+04	0.00	-1.000	NO3 + CRES = HONO2 + BZ-O. + -C
				Reactions of Nitrophenol
G58)	5.578E+03	0.00	-1.000	NITROPHEN + NO3 = HONO2 + BZ(NO2)-O.
G59)	2.202E+04	0.00	-1.000	BZ(NO2)-O. + NO2 = -N + #6 -C
G60)	4.404E+03	0.00	-1.000	BZ(NO2)-O. + HO2. = NITROPHEN
G61)	6.000E-02	0.00	0.000	BZ(NO2)-O. = NITROPHEN
				Reactions of Ethene
D1)	3.156E+03	-0.82	-1.000	C:C + HO. = HOC2-O2. + RO2.
D2)	SAME K AS B1			HOC2-O2. + NO = NO2 + #.22 HOCCHO + #1.56 HCHO + HO2.
D3)	SAME K AS B5			HOC2-O2. + HO2. = -OOH + #.22 HOCCHO + #1.56 HCHO
D4)	SAME K AS B8			HOC2-O2. + RO2. = RO2. + #.5 HO2. + #.22 HOCCHO + #1.56 HCHO
D5)	SAME K AS B9			HOC2-O2. + RCO3. = RCO3. + #.5 HO2. + #.22 HOCCHO + #1.56 HCHO
D6)	1.761E+01	5.23	-1.000	C:C + O3 = HCHO + (HCHO2)
D8)	1.527E+04	1.57	-1.000	C:C + O = C-O2. + HO2. + CO + RO2.
D9)	2.936E+03	5.81	-1.000	C:C + NO3 = C:C-N-O2. + RO2.
D10)	SAME K AS B1			C:C-N-O2. + NO = #2 NO2 + #2 HCHO
D11)	SAME K AS B5			C:C-N-O2. + HO2. = -OOH + NO2 + #2 HCHO
D12)	SAME K AS B8			C:C-N-O2. + RO2. = RO2. + #.5 HO2. + NO2 + #2 HCHO
D13)	SAME K AS B9			C:C-N-O2. + RCO3. = RCO3. + #.5 HO2. + NO2 + #2 HCHO

(continued)

Table C-1 (continued) - 9

Reaction label[a]	Kinetic Parameters[b]	Reaction[c]
D7)	(fast)	(HCHO2) = #.4 HCHO2 + #.18 CO2 + #.42 CO + #.12 H2 + #.42 H2O + #.12 HO2.
D65)	7.927E-03 0.00 -1.000	HCHO2 + H2O = -C
		Reactions of Propene
D14)	7.119E+03 -1.00 -1.000	C:CC + HO. = C:CC-O2. + RO2.
D15)	SAME K AS B1	C:CC-O2. + NO = NO2 + HCHO + CCHO + HO2.
D16)	SAME K AS B5	C:CC-O2. + HO2. = -OOH + HCHO + CCHO
D17)	SAME K AS B8	C:CC-O2. + RO2. = RO2. + #.5 HO2. + HCHO + CCHO
D18)	SAME K AS B9	C:CC-O2. + RCO3. = RCO3. + #.5 HO2. + HCHO + CCHO
D19)	1.938E+01 4.18 -1.000	C:CC + O3 = #.5 "CCHO + (HCHO2) + HCHO + (CCHO2)"
D21)	1.732E+04 0.64 -1.000	C:CC +O = #.6 C-CO-C + #.4 CO + #.4 C-O2. + #.2 C2-O2. + #.2 HO2. + #.6 RO2.
D22)	7.340E+03 3.84 -1.000	C:CC + NO3 = C:CC-N-O2. + RO2.
D23)	SAME K AS B1	C:CC-N-O2. + NO = #2 NO2 + CCHO + HCHO
D24)	SAME K AS B5	C:CC-N-O2. + HO2. = -OOH + NO2 + CCHO + HCHO
D25)	SAME K AS B8	C:CC-N-O2. + RO2. = RO2. + #.5 HO2. + NO2 + CCHO + HCHO
D26)	SAME K AS B9	C:CC-N-O2. + RCO3. = RCO3. + #.5 HO2. + NO2 + CCHO + HCHO
D20)	(fast)	(CCHO2) = #.2 CCHO2 + #.14 CH4 + #.29 CO2 + #.15 CO + #.03 HCHO + #.27 "C-O2. + RO2." + #.21 HO2. + #.12 HO. + #.72 -C
D66)	7.927E-03 0.00 -1.000	CCHO2 + H2O = #2 -C
		Reactions of trans-2-Butene
D40)	1.483E+04 -1.09 -1.000	CC:CC + HO. = CC:CC-O2. + RO2.
D41)	SAME K AS B1	CC:CC-O2. + NO = NO2 + HO2. + #2 CCHO
D42)	SAME K AS B5	CC:CC-O2. + HO2. = -OOH + #2 CCHO
D43)	SAME K AS B8	CC:CC-O2. + RO2. = RO2. + #.5 HO2. + #2 CCHO
D44)	SAME K AS B9	CC:CC-O2. + RCO3. = RCO3. + #.5 HO2. + #2 CCHO

(continued)

Table C-1 (continued) - 10

Reaction label[a]	Kinetic Parameters[b]	Reaction[c]
D45)	1.333E+01 2.26 -1.000	CC:CC + O3 = CCHO + (CCHO2)
D46)	3.317E+04 -0.02 -1.000	CC:CC + O = MEK + #.4 HO2.
D47)	1.468E+04 1.94 -1.000	CC:CC + NO3 = CC:CC-N-O2. + RO2.
D48)	SAME K AS B1	CC:CC-N-O2. + NO = #2 "NO2 + CCHO"
D49)	SAME K AS B5	CC:CC-N-O2. + HO2. = -OOH + NO2 + #2 CCHO
D50)	SAME K AS B8	CC:CC-N-O2. + RO2. = RO2. + #.5 HO2. + NO2 + #2 CCHO
D51)	SAME K AS B9	CC:CC-N-O2. + RCO3. = RCO3. + #.5 HO2. + NO2 + #2 CCHO
		Reactions of Ethane
E1)	1.806E+04 0.88 1.000	C2 + HO. = C2-O2. + RO2.
		Reactions of n-Butane
E11)	2.275E+04 1.07 -1.000	C4 + HO. = #.15 C4-O2. + #.85 C3(C)-O2. + RO2.
E12)	SAME K AS B1	C4-O2. + NO = #.03 C4ONO2 + #.97 NO2 + #.757 "HOC4-O2. + RO2." + #.213 "RCHO + -C + HO2."
E13)	SAME K AS B1	C3(C)-O2. + NO = #.08 C4ONO2 + #.92 NO2 + #.58 "MEK + HO2." + #.34 "CCHO + C2-O2. + RO2."
E14)	SAME K AS B1	HOC4-O2. + NO = NO2 + HO2. + RCHO + -C
E15)	SAME K AS B5	C4-O2. + HO2. = -OOH + RCHO + -C
E16)	SAME K AS B5	C3(C)-O2. + HO2. = -OOH + #.63 MEK + #.37 "CCHO + CCHO"
E17)	SAME K AS B5	HOC4-O2. + HO2. = -OOH + RCHO + -C
E18)	SAME K AS B8	C4-O2. + RO2. = RO2. + #.5 HO2. + RCHO + -C
E19)	SAME K AS B8	C3(C)-O2. + RO2. = RO2. + #.5 HO2. + #.63 MEK + #.37 "CCHO + CCHO"
E20)	SAME K AS B8	HOC4-O2. + RO2. = RO2. + #.5 HO2. + RCHO + -C
E12)	SAME K AS B9	C4-O2. + RCO3. = RCO3. + #.5 HO2. + RCHO + -C
E22)	SAME K AS B9	C3(C)-O2. + RCO3. = RCO3. + #.5 HO2. + #.63 MEK + #.37 "CCHO + CCHO"
E23)	SAME K AS B9	HOC4-O2. + RCO3. = RCO3. + #.5 HO2. + RCHO + -C

(continued)

Table C-1 (continued) - 11

Reaction label[a]	Kinetic Parameters[b]	Reaction[c]
		Reactions of n-Pentane
C5F1)	2.950E+04 0.97 -1.000	HO. + C5 = C5-RO2. + RO2.
C5F2)	SAME K AS B1	C5-RO2. + NO = #.0849 C4ONO2 + #.0423 C7ONO2 + #.873 "HO2. + NO2" + #.515 "R2O2. + RO2." + #.0065 HCHO + #.0735 CCHO + #.163 RCHO + #.584 MEK + #.277 ROH
C5F3)	SAME K AS B5	C5-RO2. + HO2. = -OOH + C5-PROD
C5F4)	SAME K AS B8	C5-RO2. + RO2. = RO2. + #.5 HO2. + C5-PROD
C5F5)	SAME K AS B9	C5-RO2. + RCO3. = RCO3. + #.5 HO2. + C5-PROD
C5F6)	(fast)	C5-PROD = #.0075 HCHO + #.0849 CCHO + #.181 RCHO + #.675 MEK + #.316 ROH
		Reactions of iso-Octane
I8F1)	1.596E+04 0.50 -1.000	HO. + ISO-C8 = I8-RO2. + RO2.
I8F2)	SAME K AS B1	I8-RO2. + NO = #.0054 C4ONO2 + #.171 C7ONO2 + #.0008 -N + #.823 "HO2. + NO2" + #.956 "R2O2. + RO2." + #.117 HCHO + #.26 C-CO-C + #.747 RCHO + #.0776 MEK + #.578 ROH + #.446 -C
I8F3)	SAME K AS B5	I8-RO2. + HO2. = -OOH + I8-PROD
I8F4)	SAME K AS B8	I8-RO2. + RO2. = RO2. + #.5 HO2. + I8-PROD
I8F5)	SAME K AS B9	I8-RO2. + RCO3. = RCO3. + #.5 HO2. + I8-PROD
I8F6)	(fast)	I8-PROD = #.175 HCHO + #.339 C-CO-C + #.883 RCHO + #.115 MEK + #.644 ROH + #.476 -C
		Reactions of n-Pentadecane: Model "A" ("High Nitrate" model)
KAOH)	2.649E+4 0.00 -1.000	C15 + HO. = C15-RO2.(A) + RO2.
AF2)	SAME K AS B1	C15-RO2.(A) + NO = #.6769 C7ONO2 + #.3231 "HO2. + NO2" + #.6221 "R2O2. + RO2." + #.0004 RCHO + #.3227 ALPA MEK + #.3440 ROH
AF3)	SAME K AS B5	C15-RO2.(A) + HO2. = -OOH + #.0008 RCHO + #.9992 MEK + #1.1053 ROH

(continued)

Table C-1 (continued) - 12

Reaction label[a]	Kinetic Parameters[b]	Reaction[c]
AF4)	SAME K AS B8	C15-RO2.(A) + RO2. = RO2. + #.5 HO2. + #.0008 RCHO + #.9992 MEK + #1.1053 ROH
AF5)	SAME K AS B9	C15-RO2.(A) + RCO3. = RCO3. + #.5 HO2. + #.0008 RCHO + #.9992 MEK + #1.1053 ROH
		Reactions of n-Pentadecane: Model "B" ("Standard" model)
KBOH)	2.649E+4 0.00 -1.000	C15 + HO. = C15-RO2.(B) + RO2.
BF2)	SAME K AS B1	C15-RO2.(B) + NO = #.4152 C7ONO2 + #.5848 "HO2. + NO2" + #.6514 "R2O2. + RO2." + #.0007 RCHO + #.5841 ALPA MEK + #.6514 ROH
BF3)	SAME K AS B5	C15-RO2.(B) + HO2. = -OOH + #.0008 RCHO + #.9992 MEK + #1.1053 ROH
BF4)	SAME K AS B8	C15-RO2.(B) + RO2. = RO2. + #.5 HO2. + #.0008 RCHO + #.9992 MEK + #1.1053 ROH
BF5)	SAME K AS B9	C15-RO2.(B) + RCO3. = RCO3. + #.5 HO2. + #.0008 RCHO + #.9992 MEK + #1.1053 ROH
		Reactions of Toluene (and its uncharacterized ring-opening products)
G6)	3.083E+03 -0.64 -1.000	HO. + TOLU = #.16 "CRES + HO2." + #.08 BZ-C-O2. + #.76 HO-TOLU-O2. + #.84 RO2.
G7)	SAME K AS B1	BZ-C-O2. + NO = NO2 + HO2. + BZ-CHO
G8)	SAME K AS B5	BZ-C-O2. + HO2. = -OOH + BZ-CHO
G9)	SAME K AS B8	BZ-C-O2. + RO2. = RO2. + #.5 HO2. + BZ-CHO
G10)	SAME K AS B9	BZ-C-O2. + RCO3. = RCO3. + #.5 HO2. + BZ-CHO
G11)	SAME K AS B1	HO-TOLU-O2. + NO = NO2 + HO2. + #.15 HCOCHO + #.19 CCOCHO + TOLU-UNKN
G12)	SAME K AS B5	HO-TOLU-O2. + HO2. = -OOH + #.15 HCOCHO + #.19 CCOCHO + TOLU-UNKN
G13)	SAME K AS B8	HO-TOLU-O2. + RO2. = RO2. + #.5 HO2. + #.15 HCOCHO + #.19 CCOCHO + TOLU-UNKN

(continued)

Table C-1 (continued) - 13

Reaction label[a]	Kinetic Parameters[b]	Reaction[c]
G14)	SAME K AS B9	HO-TOLU-O2. + RCO3. = RCO3. + #.5 HO2. + #.15 HCOCHO + #.19 CCOCHO + TOLU-UNKN
G622)	4.404E+04 0.00 -1.000	HO. + TOLU-UNKN = TOLU-RCO3. + RCO3.
G632)	SAME K AS B2	TOLU-RCO3. + NO = NO2 + CO2 + TOLU-R1O2. + RO2.
G642)	SAME K AS B4	TOLU-RCO3. + NO2 = TOLU-PAN
G652)	1.200E+18 26.91 0.000	TOLU-PAN = TOLU-RCO3. + RCO3. + NO2
G662)	SAME K AS B1	TOLU-R1O2. + NO = NO2 + TOLU-R2O2. + RO2.
G672)	SAME K AS B1	TOLU-R2O2. + NO = NO2 + #.73 "CO + HO2." + #1.12 HCOCHO + #.54 CCOCHO + #.27 "CCO-O2. + RCO3."
G682)	SAME K AS B6	TOLU-RCO3. + HO2. = -OOH + CO2 + #.73 CO + #1.12 HCOCHO + #.54 CCOCHO + #.27 "HCHO + CO2"
G692)	SAME K AS B9	TOLU-RCO3. + RO2. = RO2. + #.5 HO2. + CO2 + #.73 CO + #1.12 HCOCHO + #.54 CCOCHO + #.27 "HCHO + CO2"
G702)	SAME K AS B10	TOLU-RCO3. + RCO3. = RCO3. + HO2. + CO2 + #.73 CO + #1.12 HCOCHO + #.54 CCOCHO + #.27 "HCHO + CO2"
G712)	SAME K AS B5	TOLU-R1O2. + HO2. = -OOH + #.73 CO + #1.12 HCOCHO + #.54 CCOCHO + #.27 "HCHO + CO2"
G722)	SAME K AS B8	TOLU-R1O2. + RO2. = RO2. + #.5 HO2. + #.73 CO + #1.12 HCOCHO + #.54 CCOCHO + #.27 "HCHO + CO2"
G732)	SAME K AS B9	TOLU-R1O2. + RCO3. = RCO3. + #.5 HO2. + #.73 CO + #1.12 HCOCHO + #.54 CCOCHO + #.27 "HCHO + CO2"
G742)	SAME K AS B5	TOLU-R2O2. + HO2. = -OOH + #.73 CO + #1.12 HCOCHO + #.54 CCOCHO + #.27 "HCHO + CO2"
G752)	SAME K AS B8	TOLU-R2O2. + RO2. = RO2. + #.5 HO2. + #.73 CO + #1.12 HCOCHO + #.54 CCOCHO + #.27 "HCHO + CO2"
G762)	SAME K AS B9	TOLU-R2O2. + RCO3. = RCO3. + #.5 HO2. + #.73 CO + #1.12 HCOCHO + #.54 CCOCHO + #.27 "HCHO + CO2"
G772)	PHOT. = AROMUNKN	TOLU-UNKN + HV = #1.66 HCOCHO + #.81 "CCO-O2. + RCO3." + #1.19 "HO2. + CO"

(continued)

Table C-1 (continued) - 14

Reaction label[a]	Kinetic Parameters[b]	Reaction[c]
		Reactions of m-Xylene (and its uncharacterized ring-opening products)
G15)	2.437E+04 -0.23 -1.000	HO. + M-XYEN = #.04 BZ-C-O2. + #.17 "CRES + HO2." + #.79 HO-MXYL-O2. + #.83 RO2. + #.21 -C
G16)	SAME K AS B1	HO-MXYL-O2. + NO = NO2 + HO2. + #.12 HCOCHO + #.40 CCOCHO + MXYL-UNKN
G17)	SAME K AS B5	HO-MXYL-O2. + HO2. = -OOH + #.12 HCOCHO + #.40 CCOCHO + MXYL-UNKN
G18)	SAME K AS B8	HO-MXYL-O2. + RO2. = RO2. + #.5 HO2. + #.12 HCOCHO + #.40 CCOCHO + MXYL-UNKN
G19)	SAME K AS B9	HO-MXYL-O2. + RCO3. = RCO3. + #.5 HO2. + #.12 HCOCHO + #.40 CCOCHO + MXYL-UNKN
G623)	4.404E+04 0.00 -1.000	HO. + MXYL-UNKN = MXYL-RCO3. + RCO3.
G633)	SAME K AS B2	MXYL-RCO3. + NO = NO2 + CO2 + MXYL-R1O2. + RO2.
G643)	SAME K AS B4	MXYL-RCO3. + NO2 = MXYL-PAN
G653)	1.200E+18 26.91 0.000	MXYL-PAN = MXYL-RCO3. + RCO3. + NO2
G663)	SAME K AS B1	MXYL-R1O2. + NO = NO2 + MXYL-R2O2. + RO2.
G673)	SAME K AS B1	MXYL-R2O2. + NO = NO2 + #.47 "CO + HO2." + #.41 HCOCHO + #1.07 CCOCHO + #.53 "CCO-O2. + RCO3."
G683)	SAME K AS B6	MXYL-RCO3. + HO2. = -OOH + CO2 + #.47 CO + #.41 HCOCHO + #1.07 CCOCHO + #.53 "HCHO + CO2"
G693)	SAME K AS B9	MXYL-RCO3. + RO2. = RO2. + #.5 HO2. + CO2 + #.47 CO + #.41 HCOCHO + #1.07 CCOCHO + #.53 "HCHO + CO2"
G703)	SAME K AS B10	MXYL-RCO3. + RCO3. = RCO3. + HO2. + CO2 + #.47 CO + #.41 HCOCHO + #1.07 CCOCHO + #.53 "HCHO + CO2"
G713)	SAME K AS B5	MXYL-R1O2. + HO2. = -OOH + #.47 CO + #.41 HCOCHO + #1.07 CCOCHO + #.53 "HCHO + CO2"
G723)	SAME K AS B8	MXYL-R1O2. + RO2. = RO2. + #.5 HO2. + #.47 CO + #.41 HCOCHO + #1.07 CCOCHO + #.53 "HCHO + CO2"

(continued)

Table C-1 (continued) - 15

Reaction label[a]	Kinetic Parameters[b]			Reaction[c]
G733)	SAME K AS B9			MXYL-R1O2. + RCO3. = RCO3. + #.5 HO2. + #.47 CO + #.41 HCOCHO + #1.07 CCOCHO + #.53 "HCHO + CO2"
G743)	SAME K AS B5			MXYL-R2O2. + HO2. = -OOH + #.47 CO + #.41 HCOCHO + #1.07 CCOCHO + #.53 "HCHO + CO2"
G753)	SAME K AS B8			MXYL-R2O2. + RO2. = RO2. + #.5 HO2. + #.47 CO + #.41 HCOCHO + #1.07 CCOCHO + #.53 "HCHO + CO2"
G763)	SAME K AS B9			MXYL-R2O2. + RCO3. = RCO3. + #.5 HO2. + #.47 CO + #.41 HCOCHO + #1.07 CCOCHO + #.53 "HCHO + CO2"
G773)	PHOT. = AROMUNKN			MXYL-UNKN + HV + #2 = #1.48 HCOCHO + #1.68 "CCO-O2. + RCO3." + #.32 "HO2. + CO"
				Chamber-Dependent Reactions (used in ITC simulations only)
O3W)	1.300E-04	0.00	0.000	O3 =
N25I)	2.500E-03	0.00	0.000	N2O5 = #2 NOX-WALL
N25S)	5.000E-08	0.00	-1.000	N2O5 + H2O = #2 NOX-WALL
NO2W)	1.400E-04	0.00	0.000	NO2 = #.2 HONO + #.8 NOX-WALL
RSI)	PHOT. = NO2			HV + #RS-I = HO. (Where RS-I = 2.0E-04 for simulations of experiments in this study [Section IV.B], and RS-I = 1.5E-04 for ITC model scenario simulations [Section IV.C].)
ONO2)	PHOT. = NO2			#1.5E-4 = NO2 + #-1 NOX-WALL

Notes:

[a] Reaction label notation of Carter et al. (1986).

[b] The kinetic parameters in this mechanism, which are used by the computer modeling software to define the rate constants as a function of temperature, light intensity and spectral distribution, or rate constants for other reactions, are specified in one of four ways:

1. Simple Thermal Reactions:

   If the kinetic parameters are given as three numbers without any additional notation, then the numbers given are (in order) A, Ea, and B, and the rate constant, k, is calculated by the modified Arrhenius expression.

$$k = A \times (T/300)^{B} \times \exp\ [-Ea\ /\ (0.0019872 \times T]\ )$$

(continued)

where T is the temperature in K, Ea is given in kcal mole^{-1}, and the units of k and A are min^{-1} for first order reactions, ppm^{-1} min^{-1} for second order reactions, or min^{-1} for third order reactions. (The order of the reaction is determined by the number of non-coefficient reactants; see note b, below)

(If a reaction has the symbol "#RCONxxxx as one of the "reactants", [where "xxxx" is the reaction label of some previously input reaction which should be the reverse of this reaction] then the "k" calculated as given above is actually an equilibrium constant, since the rate constant for this reaction is given by "k" times the rate constant for reaction "xx". See Footnote c for a discussion of coefficients as reactants.)

2. "Falloff" Thermal Reactions:

If the kinetic parameters are given as seven nunbers in the following format,

	FALLOFF F= f,		N= n
k_0:	A_0,	Ea_0,	B_0
k_I:	A_I,	Ea_I,	B_I

then the rate constant, k is calculated by

$$k = [(k_0 \text{ x } M)/(1 + [k_0 \text{ x } M / k_I])] * f^{1/[1 + (\log10 [k_0 \text{ x } M / k_I]/n)^2]}$$

where

$$k_0 = A_0 \text{ x } (T/300)^{B_0} * \exp (-Ea_0 / [0.0019872 \text{ x } T]),$$
$$k_I = A_I \text{ x } (T/300)^{B_I} * \exp (-Ea_I / [0.0019872 \text{ x } T]),$$

T is the temperature in K. and M is the concentration of the constant species "M", which is the the total pressure in ppm. In these calculations, M is always 10^6 ppm.

Reactions of this type are always second order, so the units of k, k_I and A_I are ppm^{-1} min^{-1}, and the units of k_0 and A_0 are ppm^{-2} min^{-2}. The units of Ea_0 and Ea_I are kcal/mole,

3. Reactions with Same Rate Constants as Other Reactions:

The notation "SAME K AS xxxx", where "xxxx" is the reaction label for some other reaction, means that the reaction always has the same rate constant as reaction "xxxx".

4 Photolysis Reactions:

Photolysis reactions are indicated by the notation "PHOT. = filename", where "filename" refers to a "photolysis file", which gives the

(continued)

absorption coefficients and quantum yields, as a function of wavelength, which are used to calculate the photolysis rate constants given the spectral distribution of the light source. The contents of the photolysis files used in this mechanism are given in Table C-3.

[c] The following examples indicate the notation used to define the reactants, products, and (where applicable) coefficients involved in the reactions in the mechanism:

```
reactant1 + reactant2 + ... = product1 + product2 + ...
reactant1 + ... = #coefficient2 product1 + ...
reactant1 + ... = #coefficient3 "product1 + product2 + ..." + ...
reactant1 + #coefficient1 + ... = product1 + ...
```

The first example is a simple reaction without any coefficients. The second and third have product coefficients which give the yield of the products. The notation in the third reaction is used to indicate that both "product1" and "product2" have the same coefficient, and thus that reaction is equivalent to

```
reactant1 + ... = #coefficient3 product1 + #coefficient3 product2 + ....
```

When a coefficient is shown as a "reactant", as in the fourth example, the coefficient is multiplied by the rate constant calculated from the kinetic parameters (as described in footnote b, above), to give the rate constant of the reaction. For example, the one of the reactions used to represent the chamber radical source is

```
RSI)            PHOT. = NO2              HV + #RS-I = HO.
```

and for this reaction, the rate constant, defining the rate of OH generation, is given by the photolysis rate of NO2 mulltiplied by the value of the coefficient specified, which in this case is the value assigned to the parameter RS-I. A special kind of reactant coefficient is that of the form "#RCONxxxx", whose value is the rate constant for the reaction labeled "xxxx".

Regardless of how the coefficients are used, they can be either constant as indicated by numbers, or variable coefficients, which have non-numeric names. In some cases the coefficients can depend on other coefficients or on temperature. The values of the variable coefficients are given in the table with the listing of the reactions which use them.

If the list of reactants, products, and coefficients do not fit on one line, then it continues on the following line.

(continued)

[d] The pseudo-species "RO2" and "RCO3" are used to keep track of the total concentrations of of all peroxy and acyl peroxy radicals, respectively, which are used to calculate the rates of peroxy + peroxy radical reactions. These are calculated by including "RO2" as a "product" for each reaction which forms peroxy radicals, with the same yield as the total peroxy radical yield in that reaction, (and likewise for "RCO3" and acyl peroxy radicals), and reactions B1 through B10 to represent their consumption processes. Note that reactions B1 - B10 are the only reactions which represent a net sink for these pseudo species; in the reactions used to represent the reaction of a given peroxy radical with all others (e.g., reactions C7, C8, C16, and C17, etc.), these are given as products as well as reactants. See the discussion of representation of peroxy radical reactions in Carter et al (1986).

The pseudo-species R2O2 is used to represent the additional oxidation of NO to NO2 caused by reactions of subsequently formed peroxy radicals in the alkane photooxidation mechanisms.

Table C-2. List of Species used in the Model Simulations of the Surrogate-NO_x-Air Irradiations

Species Name	Compound or Use
1. Species Integrated Explicitly	
O3	Ozone
NO	Nitric Oxide
NO2	Nitrogen Dioxide
NO3	Nitrate Radical
N2O5	N_2O_5
HONO2	Nitric Acid
HONO	Nitrous Acid
HO2.	HO_2 Radicals
HO2NO2	Peroxy Nitric Acid
HO2H	Hydrogen Peroxide
CO	Carbon Monoxide
RO2.	Lumped Alkyl Peroxy Radicals (sum of all alkyl peroxy radicals.)
RCO3.	Lumped Acyl Peroxy Radicals (sum off all acyl peroxy radicals)
-OOH	Lumped Hydroperoxide Group (Used to represent photolizable hydroperoxide groups formed when peroxy radicals react with HO_2)
HCHO	Formaldehyde
CCHO	Acetaldehyde
C-PAN	PAN
RCHO	Propionaldehyde and Lumped Higher Aldehydes
C2-PAN	PPN (and PAN analogues formed from higher aldehydes)
C-CO-C	Acetone
CCOCHO	Methyl Glyoxal
MEK	Methyl Ethyl Ketone and Lumped Higher Ketones
ROH	Pentanol (used in part to represent OH-substituted bi- and poly-functional compounds formed following the isomerazation of long-chain alkoxy radicals formed in the photooxidations of the higher alkanes.
HCOCHO	Glyoxal
HCO-PAN	$HCO-CO-OONO_2$ (PAN analogue formed from glyoxal)
HOCCHO	Glycolaldehyde
HOC-PAN	$HOCH_2-CO-OONO_2$ (PAN analogue formed from glycolaldehyde
C4ONO2	2-Butyl Nitrate (used with 4-heptyl nitrate to represent $\geq C_4$ alkyl nitrates)
C7ONO2	4-heptyl Nitrate
C:C	Ethene
C:CC	Propene
CC:CC	trans-2-Butene

(continued)

Table C-2 (continued) - 2

Species Name	Compound or Use
C2	Ethane
C4	n-Butane
C5	n-Pentane
ISO-C8	2,2,4-Trimethyl Pentane (iso-Octane)
C15	n-Pentadecane
TOLU	Toluene
M-XYEN	m-Xylene
BZ-CHO	Benzaldehyde
BZ-PAN	PBzN
PHENOL	Phenol
NITROPHEN	Nitrophenols
CRES	Cresols and other alkyl phenols.
TOLU-UNKN	Unknown Product(s) Formed in the Ring Opening Reactions of Toluene.
TOLU-PAN	Pan Analogue Assumed to be Formed in the Reactions of TOLU-UNKN
MXYL-UNKN	Unknown Product(s) Formed in the Ring Opening Reactions of m-Xylene.
MXYL-PAN	Pan Analogue Assumed to be Formed in the Reactions of MXYL-UNKN
2. Constant Species (Concentrations held constant during the calculations.)	
HV	Total Light Intensity. Always 1.0 in these calculations.
O2	Oxygen in Air (always 2.090E+05 PPM)
M	Total Pressure (always 1.000E+06 PPM)
H2O	Water Concentration. 2.0E+04 ppm used for ITC simulations, and 2.08E+04 used for simulations of airshed scenarios.
3. Product-Only and Counter Species (Species which are formed, but which do not react, or pseudo-species used to keep track of carbon, nitrogen, etc.)	
-C	"Lost" or Unreactive Product Carbon (used to check for carbon balance, and to determine the extent of species whose reactions are ignored.)
-N	"Lost" or Unreactive Product Nitrogen (used to check for nitrogen balance.)
NOX-WALL	NO_x Absorbed on the Walls (used primarily to check for nitrogen balance)

(continued)

Table C-2 (continued) - 3

Species Name	Compound or Use
CO2	Carbon Dioxide
CH4	Methane (reactions ignored)
H2	Hydrogen (reactions ignored)
4. Species for which the Steady State Approximation is Applied	
O	$O(^3P)$ Atoms
O*1D2	$O(^1D)$ Atoms
HO.	Hydroxyl Radicals
HOC-O2.	$HOCH_2OO.$ (peroxy radical formed from HO_2 + HCHO)
CCO-O2.	Acetyl Peroxy Radicals
C-O2.	Methyl Peroxy Radicals
C-O.	Methoxy Radicals
C2CO-O2.	Propionyl Peroxy Radicals
C2-O2.	Ethyl Peroxy Radicals
C-CO-C-O2.	CH_3-CO-$CH_2OO.$ (peroxy radical formed in the OH + acetone reaction)
MEK-O2.	50% CH_3-CO-CH(OO.)CH_3 + 50% CH_3-CO-$CH_2CH_2OO.$ (formed initially in the OH + methyl ethyl ketone reaction)
MEK(2)-O2.	$HOCH_2CH_2$-CO-$CH_2OO.$ (formed in the OH + MEK reaction)
ROH-O2.	Lumped Peroxy Species Used to Represent Species in the OH + Penataol Reactions
HCOCO.	H-CO-CO. (radical initially formed in the OH + glyoxal reaction)
HCOCO-O2.	Acyl Peroxy Radical Formed when O_2 Reacts with HCOCO.
HOCCO-O2.	$HOCH_2$-CO-OO. (acyl peroxy radical formed from glycolaldehyde)
C4ONO2-O2.	60% $CH_3CH(ONO_2)CH(OO.)CH_3$ + 40% $CH_3CH(ONO_2)CH_2CH_2OO.$ (formed in the OH + 2-butyl nitrate reaction)
C4ONO2(2)-O2.	$CH_3C(OO.)(ONO_2)CH_2CH_2OH$ (formed in the OH + 2-butyl nitrate reaction)
C7ONO2-O2.	11% $.OOC_3H_6CH(ONO_2)C_3H_7$ + 66% $CH_3CH(OO.)CH_2CH(ONO2)C_3H_7$ + 23% $C_2H_5CH(OO.)CH(ONO_2)C_3H_7$ (formed in the OH + 4-heptyl nitrate reaction)
C7ONO2(2)-O2.	$CH_3CH(OH)CH_2CH(ONO_2)CH(OO.)C_2H_5$ (formed in the OH + 4-heptyl nitrate reaction)
HOC2-O2.	$HOCH_2CH_2OO.$ (OH - ethene - O_2 adduct)
C:C-N-O2.	$.OOCH_2CH_2ONO2$ (NO_3 - ethene - O_2 adduct)
C:CC-O2.	$CH_3CH(OH)CH_2OO.$ + $CH_3CH(OO.)CH_2OH$ (OH - propene - O_2 adducts)
C:CC-N-O2.	$CH_3CH(ONO_2)CH_2OO.$ + $CH_3CH(OO.)CH_2ONO_2$ (NO_3 - propene - O_2 adducts)

(continued)

Table C-2 (continued) - 4

Species Name	Compound or Use
CC:CC-O2.	$CH_3CH(OH)CH(OO.)CH_3$ (OH - *trans*-2-butene - O_2 adduct)
CC:CC-N-O2	$CH_3CH(ONO_2)CH(OO.)CH_3$ (NO_3 - *trans*-2-Butene - O_2 adduct)
(HCHO2)	"Hot" Criegee Biradical Formed in the Reactions of Ozone with Alkenes with $=CH_2$ Groups
HCHO2	Stabilized Criegee Biradical Formed in the Reactions of Ozone with Alkenes with $=CH_2$ Groups
(CCHO2)	"Hot" Criegee Biradical Formed in the Reactions of Ozone with Alkenes with $=CHCH_3$ Groups
CCHO2	Stabilized Criegee Biradical Formed in the Reactions of Ozone with Alkenes with $=CHCH_3$ Groups
C4-O2.	$CH_3(CH_2)_3OO.$ (formed in the OH + n-butane reactions)
C3(C)-O2.	$CH_3CH(OO.)CH_2CH_3$ (formed in the OH + n-butane reactions)
HOC4-O2.	$HOCH_{24}OO.$ (formed in the OH + n-butane reactions)
C5-RO2.	Lumped Species Representing All Peroxy Radicals Formed in the OH + n-Pentane Reactions
C15-RO2.(A)	Lumped Species Representing All Peroxy Radicals Formed in the OH + n-Pentadecane Reactions for Mechanism "A"
C15-RO2.(B)	Lumped Species Representing All Peroxy Radicals Formed in the OH + n-Pentadecane Reactions for Mechanism "B"
R2O2.	Psuedo-Specie Used to Account For NO to NO_2 Conversions Caused by Subsequently Formed Peroxy Radicals in the Reactions of the $\geq C_5$ Alkanes.
C5-PROD	Temporary Pseudo-Specie (used in the n-pentane mechanism to represent the set of organic products formed. Immediately "reacts" to form those products.)
I8-RO2.	Lumped Species Representing All Peroxy Radicals Formed in the OH + iso-Octane Reactions
I8-PROD	Temporary Pseudo-Specie (used in the iso-octane mechanism to represent the set of organic products formed. Immediately "reacts" to form those products.)
HO-TOLU-O2.	Used to Represent the Peroxy Radical Intermediates Which Lead to Ring Opening in the OH + Toluene Reactions.
BZ-C-O2.	Benzyl Peroxy Radicals
TOLU-RCO3.	Used to Represent the Acyl Peroxy Radicals Assumed to be Initially Formed in the Reactions of OH Radicals with the Uncharacterized Toluene

(continued)

Table C-2 (continued) - 5

Species Name	Compound or Use
	Ring-Opening Products. (Assumed to be an analogue of H-CO-CH=CH-CO-OO..)
TOLU-R1O2.	Used to Represent the Peroxy Radicals Initially Formed from TOLU-RCO3. (Assumed to be an analogue of H-CO-CH=CHOO.)
TOLU-R2O2.	Used to Represent the Peroxy Radicals Formed from TOLU-R1O2. (Assumed to be an analogue of H-CO-CH(OO.)CHO)
MXYL-RCO3.	Used to Represent the Acyl Peroxy Radicals Assumed to be Initially Formed in the Reactions of OH Radicals with the Uncharacterized m-Xylene Ring-Opening Products. (Assumed to be an analogue of H-CO-CH=CH-CO-OO..)
MXYL-R1O2.	Used to Represent the Peroxy Radicals Initially Formed from MXYL-RCO3. (Assumed to be an analogue of H-CO-CH=CHOO.)
MXYL-R2O2.	Used to Represent the Peroxy Radicals Formed from MXYL-R1O2. (Assumed to be an analogue of H-CO-CH(OO.)CHO)
BZ-CO-O2.	Benzoyl Peroxy Radical
BZ-O2.	Phenyl Peroxy Radical
BZ-O.	Phenoxy Radical
BZ(NO2)-O.	Nitro-Substituted Phenoxy Radicals
HO-PHEN-O2.	Lumped Peroxy Radical Used in the Emperical Representation of the OH + Phenol Reactions
HO-CRES-O2.	Lumped Peroxy Radical Used in the Emperical Representation of the OH + Cresol Reactions

Table C-3. Absorption Coefficient x Quantum Yield Products Used to Calculate the Rate Constants for Photolysis Reactions in Table C-1 (From Carter et al. 1986b)

PHOT. Name	(Wavelength, Absorption Coefficient x Quantum Yield) (microns) (cm^2 molec^{-1}, base e)		
NO2	(0.250 2.830E-20)	(0.255 1.450E-20)	(0.260 1.900E-20)
	(0.265 2.010E-20)	(0.270 3.130E-20)	(0.275 4.020E-20)
	(0.280 5.540E-20)	(0.285 6.990E-20)	(0.290 8.180E-20)
	(0.295 6.970E-20)	(0.300 1.156E-19)	(0.305 1.619E-19)
	(0.310 1.695E-19)	(0.315 2.137E-19)	(0.320 2.383E-19)
	(0.325 2.581E-19)	(0.330 2.730E-19)	(0.335 3.105E-19)
	(0.340 3.445E-19)	(0.345 3.561E-19)	(0.350 3.538E-19)
	(0.355 4.361E-19)	(0.360 3.779E-19)	(0.365 4.768E-19)
	(0.370 4.406E-19)	(0.375 3.906E-19)	(0.380 4.852E-19)
	(0.385 4.158E-19)	(0.390 4.440E-19)	(0.395 4.771E-19)
	(0.400 4.394E-19)	(0.405 2.022E-19)	(0.410 8.078E-20)
	(0.415 4.221E-20)	(0.420 1.433E-20)	(0.425 0.000E-01)
NO3NO	(0.585 0.000E-01)	(0.590 1.285E-18)	(0.595 1.632E-18)
	(0.600 7.075E-19)	(0.605 6.900E-19)	(0.610 2.960E-19)
	(0.615 1.960E-19)	(0.620 3.580E-19)	(0.625 4.625E-19)
	(0.630 2.830E-19)	(0.635 4.350E-20)	(0.640 0.000E-01)
NO3NO2	(0.400 0.000E-01)	(0.405 3.000E-20)	(0.410 4.000E-20)
	(0.415 5.000E-20)	(0.420 8.000E-20)	(0.425 1.000E-19)
	(0.430 1.300E-19)	(0.435 1.800E-19)	(0.440 1.900E-19)
	(0.445 2.200E-19)	(0.450 2.800E-19)	(0.455 3.300E-19)
	(0.460 3.700E-19)	(0.465 4.300E-19)	(0.470 5.100E-19)
	(0.475 6.000E-19)	(0.480 6.400E-19)	(0.485 6.900E-19)
	(0.490 8.800E-19)	(0.495 9.500E-19)	(0.500 1.010E-18)
	(0.505 1.100E-18)	(0.510 1.320E-18)	(0.515 1.400E-18)
	(0.520 1.450E-18)	(0.525 1.480E-18)	(0.530 1.940E-18)
	(0.535 2.040E-18)	(0.540 1.810E-18)	(0.545 1.810E-18)
	(0.550 2.360E-18)	(0.555 2.680E-18)	(0.560 3.070E-18)
	(0.565 2.530E-18)	(0.570 2.540E-18)	(0.575 2.740E-18)
	(0.580 3.050E-18)	(0.585 2.770E-18)	(0.590 3.855E-18)
	(0.595 2.448E-18)	(0.600 1.556E-18)	(0.605 1.380E-18)
	(0.610 4.350E-19)	(0.615 4.900E-19)	(0.620 7.160E-19)
	(0.625 1.388E-18)	(0.630 2.830E-19)	(0.635 0.000E-01)
O3O3P	(0.260 1.070E-08)	(0.270 7.740E-19)	(0.280 3.790E-19)
	(0.290 1.340E-19)	(0.300 3.160E-20)	(0.310 4.341E-20)
	(0.320 2.600E-20)	(0.330 6.700E-21)	(0.340 1.700E-21)
	(0.350 4.000E-22)	(0.355 0.000E-01)	(0.400 0.000E-01)
	(0.450 1.600E-22)	(0.500 1.340E-21)	(0.550 3.320E-21)
	(0.600 5.060E-21)	(0.650 2.450E-21)	(0.700 8.700E-22)
	(0.750 3.200E-22)	(0.800 1.600E-22)	(0.900 0.000E-01)

(continued)

Table C-3 (continued) - 2

PHOT. Name	(Wavelength, (microns)	Absorption Coefficient x Quantum Yield) (cm^2 molec^{-1}, base e)	
O3T300	(0.260 9.630E-18)	(0.270 6.966E-18)	(0.280 3.411E-18)
	(0.290 1.206E-18)	(0.300 3.420E-19)	(0.305 1.673E-19)
	(0.310 5.488E-20)	(0.313 1.950E-20)	(0.315 6.760E-21)
	(0.317 2.080E-21)	(0.320 0.000E-01)	
HONO	(0.311 0.000E-01)	(0.312 2.000E-21)	(0.313 4.200E-21)
	(0.314 4.600E-21)	(0.315 4.200E-21)	(0.316 3.000E-21)
	(0.317 4.600E-21)	(0.318 3.600E-20)	(0.319 6.100E-20)
	(0.320 2.100E-20)	(0.321 4.270E-20)	(0.322 4.010E-20)
	(0.323 3.930E-20)	(0.324 4.010E-20)	(0.325 4.040E-20)
	(0.326 3.130E-20)	(0.327 4.120E-20)	(0.328 7.550E-20)
	(0.329 6.640E-20)	(0.330 7.290E-20)	(0.331 8.700E-20)
	(0.332 1.380E-19)	(0.333 5.910E-20)	(0.334 5.910E-20)
	(0.335 6.450E-20)	(0.336 5.910E-20)	(0.337 4.580E-20)
	(0.338 1.910E-19)	(0.339 1.630E-19)	(0.340 1.050E-19)
	(0.341 8.700E-20)	(0.342 3.350E-19)	(0.343 2.010E-19)
	(0.344 1.020E-19)	(0.345 8.540E-20)	(0.346 8.320E-20)
	(0.347 8.200E-20)	(0.348 7.490E-20)	(0.349 7.130E-20)
	(0.350 6.830E-20)	(0.351 1.740E-19)	(0.352 1.140E-19)
	(0.353 3.710E-19)	(0.354 4.960E-19)	(0.355 2.460E-19)
	(0.356 1.190E-19)	(0.357 9.350E-20)	(0.358 7.780E-20)
	(0.359 7.290E-20)	(0.360 6.830E-20)	(0.361 6.900E-20)
	(0.362 7.320E-20)	(0.363 9.000E-20)	(0.364 1.210E-19)
	(0.365 1.330E-19)	(0.366 2.130E-19)	(0.367 3.520E-19)
	(0.368 4.500E-19)	(0.369 2.930E-19)	(0.370 1.190E-19)
	(0.371 9.460E-20)	(0.372 8.850E-20)	(0.373 7.440E-20)
	(0.374 4.770E-20)	(0.375 2.700E-20)	(0.376 1.900E-20)
	(0.377 1.500E-20)	(0.378 1.900E-20)	(0.379 5.800E-20)
	(0.380 7.780E-20)	(0.381 1.140E-19)	(0.382 1.400E-19)
	(0.383 1.720E-19)	(0.384 1.990E-19)	(0.385 1.900E-19)
	(0.386 1.190E-19)	(0.387 5.650E-20)	(0.388 3.200E-20)
	(0.389 1.900E-20)	(0.390 1.200E-20)	(0.391 5.000E-21)
	(0.392 0.000E-01)		
H2O2	(0.250 8.300E-20)	(0.255 6.700E-20)	(0.260 5.200E-20)
	(0.265 4.200E-20)	(0.270 3.200E-20)	(0.275 2.500E-20)
	(0.280 2.000E-20)	(0.285 1.500E-20)	(0.290 1.130E-20)
	(0.295 8.700E-21)	(0.300 6.600E-21)	(0.305 4.900E-21)
	(0.310 3.700E-21)	(0.315 2.800E-21)	(0.320 2.000E-21)
	(0.325 1.500E-21)	(0.330 1.200E-21)	(0.335 9.000E-22)
	(0.340 7.000E-22)	(0.345 5.000E-22)	(0.350 3.000E-22)
	(0.355 0.000E-01)		

(continued)

Table C-3 (continued) - 3

PHOT. Name	(Wavelength, Absorption Coefficient x Quantum Yield) (microns) (cm^2 molec^{-1}, base e)		
CO2H	(0.210 3.750E-19)	(0.220 2.200E-19)	(0.230 1.380E-19)
	(0.240 8.800E-20)	(0.250 5.800E-20)	(0.260 3.800E-20)
	(0.270 2.500E-20)	(0.280 1.500E-20)	(0.290 9.000E-21)
	(0.300 5.800E-21)	(0.310 3.400E-21)	(0.320 1.900E-21)
	(0.330 1.100E-21)	(0.340 6.000E-22)	(0.350 4.000E-22)
	(0.360 0.000E-01)		
HCHOR	(0.240 6.300E-23)	(0.250 3.120E-22)	(0.260 1.410E-21)
	(0.270 3.440E-21)	(0.280 1.097E-20)	(0.290 1.782E-20)
	(0.300 2.044E-20)	(0.310 1.886E-20)	(0.320 1.147E-20)
	(0.330 5.456E-21)	(0.340 0.000E-01)	
HCHOM	(0.240 1.260E-22)	(0.250 5.980E-22)	(0.260 2.256E-21)
	(0.270 3.956E-21)	(0.280 6.510E-21)	(0.290 6.526E-21)
	(0.300 5.764E-21)	(0.310 5.635E-21)	(0.320 7.030E-21)
	(0.330 1.214E-20)	(0.340 8.142E-21)	(0.350 1.680E-21)
	(0.360 7.200E-23)	(0.370 0.000E-01)	
CCHOR	(0.260 6.696E-21)	(0.270 1.315E-20)	(0.280 2.549E-20)
	(0.290 2.618E-20)	(0.295 2.181E-20)	(0.300 1.672E-20)
	(0.305 1.111E-20)	(0.310 6.392E-21)	(0.315 3.135E-21)
	(0.320 1.200E-21)	(0.325 3.390E-22)	(0.330 0.000E-01)
RCHO	(0.280 5.260E-20)	(0.290 5.770E-20)	(0.300 5.050E-20)
	(0.310 3.680E-20)	(0.320 1.660E-20)	(0.330 6.490E-21)
	(0.340 1.440E-21)	(0.345 0.000E-01)	
KETONE	(0.210 1.100E-21)	(0.220 1.200E-21)	(0.230 4.600E-21)
	(0.240 1.300E-20)	(0.250 2.680E-20)	(0.260 4.210E-20)
	(0.270 5.540E-20)	(0.280 5.920E-20)	(0.290 5.160E-20)
	(0.300 3.440E-20)	(0.310 1.530E-20)	(0.320 4.600E-21)
	(0.330 1.100E-21)	(0.340 0.000E-01)	
GLYOXAL	(0.230 2.867E-21)	(0.235 2.867E-21)	(0.240 4.301E-21)
	(0.245 5.735E-21)	(0.250 8.602E-21)	(0.255 1.147E-20)
	(0.260 1.434E-20)	(0.265 1.864E-20)	(0.270 2.294E-20)
	(0.275 2.581E-20)	(0.280 2.867E-20)	(0.285 3.298E-20)
	(0.290 3.154E-20)	(0.295 3.298E-20)	(0.300 3.584E-20)
	(0.305 2.724E-20)	(0.310 2.724E-20)	(0.312 2.867E-20)
	(0.315 2.294E-20)	(0.320 1.434E-20)	(0.325 1.147E-20)
	(0.327 1.434E-20)	(0.330 1.147E-20)	(0.335 2.867E-21)
	(0.340 0.000E-01)	(0.355 0.000E-01)	(0.360 2.294E-21)
	(0.365 2.867E-21)	(0.370 8.029E-21)	(0.375 1.004E-20)
	(0.380 1.720E-20)	(0.382 1.577E-20)	(0.384 1.491E-20)
	(0.386 1.491E-20)	(0.388 2.867E-20)	(0.390 3.154E-20)

(continued)

Table C-3 (continued) - 4

PHOT. Name	(Wavelength, Absorption Coefficient x Quantum Yield) (microns) (cm^2 molec^{-1}, base e)		
	(0.391 3.242E-20)	(0.392 3.040E-20)	(0.393 2.229E-20)
	(0.394 2.634E-20)	(0.395 3.040E-20)	(0.396 2.634E-20)
	(0.397 2.432E-20)	(0.398 3.242E-20)	(0.399 3.040E-20)
	(0.400 2.837E-20)	(0.401 3.242E-20)	(0.402 4.458E-20)
	(0.403 5.269E-20)	(0.404 4.255E-20)	(0.405 3.040E-20)
	(0.406 3.040E-20)	(0.407 2.837E-20)	(0.408 2.432E-20)
	(0.409 2.837E-20)	(0.410 6.079E-20)	(0.411 5.066E-20)
	(0.412 6.079E-20)	(0.412 4.863E-20)	(0.413 8.308E-20)
	(0.414 6.484E-20)	(0.414 7.497E-20)	(0.414 8.105E-20)
	(0.415 8.105E-20)	(0.415 6.890E-20)	(0.416 4.255E-20)
	(0.417 4.863E-20)	(0.418 5.876E-20)	(0.419 6.687E-20)
	(0.420 3.850E-20)	(0.421 5.674E-20)	(0.421 4.458E-20)
	(0.422 5.269E-20)	(0.423 1.054E-19)	(0.423 8.511E-20)
	(0.424 6.079E-20)	(0.425 7.295E-20)	(0.426 1.175E-19)
	(0.426 1.297E-19)	(0.427 1.074E-19)	(0.428 1.662E-19)
	(0.429 4.053E-20)	(0.430 5.066E-20)	(0.431 4.863E-20)
	(0.432 4.053E-20)	(0.433 3.647E-20)	(0.434 4.053E-20)
	(0.435 6.079E-20)	(0.435 5.066E-20)	(0.436 8.105E-20)
	(0.437 1.135E-19)	(0.437 5.269E-20)	(0.438 1.013E-19)
	(0.438 1.378E-19)	(0.439 7.700E-20)	(0.440 2.472E-19)
	(0.441 8.105E-20)	(0.442 6.079E-20)	(0.443 7.497E-20)
	(0.444 9.321E-20)	(0.445 1.135E-19)	(0.446 5.269E-20)
	(0.447 2.432E-20)	(0.448 2.837E-20)	(0.449 3.850E-20)
	(0.450 6.079E-20)	(0.451 1.094E-19)	(0.451 9.321E-20)
	(0.452 1.216E-19)	(0.453 2.391E-19)	(0.454 1.702E-19)
	(0.455 3.404E-19)	(0.456 4.053E-19)	(0.456 1.013E-19)
	(0.457 1.621E-20)	(0.458 1.216E-20)	(0.458 1.418E-20)
	(0.459 4.053E-21)	(0.460 4.053E-21)	(0.461 6.079E-21)
	(0.461 2.026E-21)	(0.462 0.000E-01)	
MEGLYOX	(0.220 2.103E-21)	(0.225 2.103E-21)	(0.230 4.206E-21)
	(0.235 7.570E-21)	(0.240 9.252E-21)	(0.245 8.411E-21)
	(0.250 9.252E-21)	(0.255 9.252E-21)	(0.260 9.673E-21)
	(0.265 1.051E-20)	(0.270 1.262E-20)	(0.275 1.430E-20)
	(0.280 1.514E-20)	(0.285 1.430E-20)	(0.290 1.472E-20)
	(0.295 1.178E-20)	(0.300 1.136E-20)	(0.305 9.252E-21)
	(0.310 6.308E-21)	(0.315 5.467E-21)	(0.320 3.365E-21)
	(0.325 1.682E-21)	(0.330 8.411E-22)	(0.335 0.000E-01)
	(0.350 0.000E-01)	(0.354 4.206E-22)	(0.358 1.262E-21)
	(0.360 2.103E-21)	(0.362 2.103E-21)	(0.364 2.944E-21)
	(0.366 3.365E-21)	(0.368 4.206E-21)	(0.370 5.467E-21)
	(0.372 5.888E-21)	(0.374 7.570E-21)	(0.376 7.991E-21)
	(0.378 8.832E-21)	(0.380 1.009E-20)	(0.382 1.093E-20)
	(0.384 1.346E-20)	(0.386 1.514E-20)	(0.388 1.724E-20)
	(0.390 2.061E-20)	(0.392 2.103E-20)	(0.394 2.313E-20)

(continued)

Table C-3 (continued) - 5

PHOT. Name	(Wavelength, Absorption Coefficient x Quantum Yield) (microns) (cm^2 molec^{-1}, base e)		
	(0.396 2.481E-20)	(0.398 2.607E-20)	(0.400 2.776E-20)
	(0.402 2.986E-20)	(0.404 3.196E-20)	(0.406 3.785E-20)
	(0.408 3.953E-20)	(0.410 4.332E-20)	(0.412 4.710E-20)
	(0.414 4.794E-20)	(0.416 4.879E-20)	(0.418 5.047E-20)
	(0.420 5.215E-20)	(0.422 5.299E-20)	(0.424 5.173E-20)
	(0.426 5.299E-20)	(0.428 5.215E-20)	(0.430 5.551E-20)
	(0.432 5.131E-20)	(0.434 5.678E-20)	(0.436 6.224E-20)
	(0.438 6.056E-20)	(0.440 5.467E-20)	(0.441 6.140E-20)
	(0.442 5.467E-20)	(0.443 5.551E-20)	(0.433 6.813E-20)
	(0.444 5.972E-20)	(0.445 5.131E-20)	(0.446 4.879E-20)
	(0.447 5.720E-20)	(0.448 5.467E-20)	(0.449 6.561E-20)
	(0.450 5.047E-20)	(0.451 3.028E-20)	(0.452 4.290E-20)
	(0.453 2.776E-20)	(0.454 2.271E-20)	(0.456 1.766E-20)
	(0.458 8.411E-21)	(0.460 4.206E-21)	(0.464 1.682E-21)
	(0.468 0.000E-01)		
BZCHO	(0.299 1.776E-19)	(0.304 7.400E-20)	(0.306 6.910E-20)
	(0.309 6.410E-20)	(0.313 6.910E-20)	(0.314 6.910E-20)
	(0.318 6.410E-20)	(0.325 8.390E-20)	(0.332 7.650E-20)
	(0.338 8.880E-20)	(0.342 8.880E-20)	(0.346 7.890E-20)
	(0.349 7.890E-20)	(0.354 9.130E-20)	(0.355 8.140E-20)
	(0.364 5.670E-20)	(0.368 6.660E-20)	(0.369 8.390E-20)
	(0.370 8.390E-20)	(0.372 3.450E-20)	(0.374 3.210E-20)
	(0.376 2.470E-20)	(0.377 2.470E-20)	(0.380 3.580E-20)
	(0.382 9.900E-21)	(0.386 0.000E-01)	
AROMUNKN	(0.200 3.950E-20)	(0.350 3.950E-20)	(0.360 0.000E-01)

Table C-4. Photolysis Rate Constants Calculated for the Indoor Teflon Chamber (ITC), and for Sunlight at Zenith Angles of 0, 40, and 70 Degrees. Solar Photolysis Rate Constants are Calculated Theoretically for Ground Level and Clear Sky Conditions Using the Actinic Irradiances Given by Peterson (1976) Based on his "Best Estimate" Surface Albitos

PHOT. Name	ITC[a]	Z=0	Z=40	Z=70
NO2	0.3250	0.4619	0.3939	0.1819
NO3NO	0.0000	1.118	1.028	0.6563
NO3NO2	1.1771E-02	10.14	9.301	5.841
O3O3P	1.6323E-03	2.9380E-02	2.6306E-02	1.5835E-02
O3T300	3.9572E-04	2.2697E-03	1.2080E-03	1.1356E-04
HONO	0.1052	9.7642E-02	8.2447E-02	3.6201E-02
H2O2	2.8194E-04	4.5195E-04	3.3534E-04	9.9236E-05
CO2H	2.9431E-04	4.4349E-04	3.3122E-04	1.0015E-04
HCHOR	7.5764E-04	1.8149E-03	1.3175E-03	3.4878E-04
HCHOM	2.4025E-03	2.7772E-03	2.1990E-03	7.7194E-04
CCHOR	6.9815E-05	2.9228E-04	1.8452E-04	3.1146E-05
RCHO	1.2111E-03	2.9553E-03	2.1058E-03	5.3319E-04
KETONE	2.9935E-04	9.5019E-04	6.3979E-04	1.3684E-04
GLYOXAL	1.1795E-02	0.1362	0.1217	6.8407E-02
MEGLYOX	7.7226E-03	7.9919E-02	7.1476E-02	3.9912E-02
BZCHO	5.4901E-02	5.1595E-02	4.2310E-02	1.7011E-02
AROMUNKN	1.6213E-02	1.5856E-02	1.2627E-02	4.5734E-03

[a] ITC Photolysis rates shown are those used in ITC scenario simulations discussed in Section IV.C. The values used in the simulations of the ITC experiments carried out in this study, discussed in Section IV.B, are obtained by multiplying these values by a factor of 0.9538, to yield the measured NO_2 photolysis rate of 0.310 min^{-1}.